Algorithms and Subsystems for Next Generation Optical Networks

Milen PLAMENOV PASKOV

A thesis submitted to the University College London (UCL) for the degree of Doctor of Philosophy

Optical Networks Group
Department of Electronic and Electrical Engineering
University College London (UCL)

September 2015

I, Milen Plamenov Paskov, confirm that the work presented in this thesis is my own. Where information has been derived from other sources, I confirm that this has been indicated.

Abstract

THIS thesis investigates algorithms and subsystems for digital coherent optical networks to alleviate system requirements and enable spectrally efficient systems.

Spectral shaping of individual channel is investigated to mitigate backreflections in bi-directional Passive Optical Network (PON) enabling more than 1000 users operating at 10 Gbit/s. It is then shown that temporal delay skews, caused by misalignment in the coherent receiver, induce a large penalty for Nyquist filtered signals. An adaptive 4×4 equaliser is developed to compensate the imperfections dynamically. This is subsequently demonstrated experimentally with Polarisation Division Multiplexed (PDM) Quadrature Phase Shift Keying (QPSK) and 16-level Quadrature Amplitude Modulation (QAM). Furthermore, a modified blind equaliser is designed to adaptively compensate for unknown amount of Chromatic Dispersion (CD). The equaliser is demonstrated experimentally using 10.7 GBd PDM-QPSK transmission over 5,200 km. To simplify the computational complexity of the equalisers a multiplier free update scheme is explored in simulations.

Optical frequency combs are investigated as phase and frequency synchronised sub-carrier sources for Dense Wavelength Division Multiplexing (DWDM) systems. The effect of phase synchronisation between sub-channels of a superchannel is examined in simulations without showing performance deviation when no additional optical or digital processing is applied. Afterwards, the transmission performance of two generation techniques implementing 400 Gbit/s superchannels, utilising PDM-16QAM, is evaluated. Although, the average performance of the two combs is identical sub-channel fluctuations are observed due to uneven spectral profile.

Carrier Phase Estimation (CPE) is explored for both single channel and superchannels systems. An equaliser interleaved with CPE, is explored for PDM-64QAM with minor improvement. Alternatively, Digital Coherence Enhancement (DCE) allowed the detection of 6 GBd PDM-64QAM with a 1.4 MHz linewidth laser, an order of magnitude improvement in linewidth tolerance. Finally, a joint CPE across a comb superchannel is demonstrated with a factor of 5 tolerance improvement.

Acknowledgements

FIRST and foremost I want to thank my supervisors Professor Seb J. Savory and Professor Alwyn Seeds for giving me the opportunity to pursue a PhD at UCL. I would especially like to thank Professor Savory for sharing his knowledge while supporting and guiding me to become a better researcher, it has truly been a unique and wonderful experience.

I would like to thank Professor Polina Bayvel for welcoming me the Optical Networks Group (ONG), which was my home for the last few years. Next, I want to thank Dr. Martyn Fice for being the first one to show me around an optical lab and point me in the right direction and Dr. Benn C. Thomsen for always being willing to share his time to explain any issues from simulations to lab experiments.

I am grateful to Dr. Domanic Lavery for everything from research advice, reading numerous drafts, to everyday discussions of any topic that we could think of (there simply is too many to mention here). Next, I would like thank Dr. Robert Maher for introducing me to experimental part of work and proper lab etiquette, an art of its own. I would also like to thank some of the fellow PhD students Hou-Man Chin, Gabriele Liga, David J. Ives, postdocs Drs. Kai Shi and Alex Alvarado as well as all the other ONG members (current and former) for the stimulating everyday discussions in addition to making my PhD years a fantastic experience. I also have to thank Dr. Jose M. D. Mendinueta for the beautiful thesis template.

Additionally, I would like to acknowledge the funding from the Engineering and Physical Sciences Research Council (EPSRC) under the COSINE project for the financial support during my PhD.

Finally, I have to thank my parents Tanya and Plamen for supporting and believing in me as well as my sister Gabi for always being there when I needed her. Special thanks go to my wonderful girlfriend, Vanya, who has been next to me during my entire studies to support and encourage me, without her I would not have come this far.

Contents

List of Figures

List of Tables

Abbreviations

ADC	Analogue-to-Digital Converter
AOM	Acoustic Optic Modulator
ASE	Amplified Spontaneous Emission
AWG	Arbitrary Waveform Generator
AWGN	Additive White Gaussian Noise
BER	Bit Error Rate
BPSK	Binary Phase Shift Keying
CD	Chromatic Dispersion
CMA	Constant Modulus Algorithm
CPE	Carrier Phase Estimation
DAC	Digital-to-Analogue Converter
DCE	Digital Coherence Enhancement
DCF	Dispersion Compensating Fibre
DD	Decision Directed
DD-MZM	Dual-Drive Mach-Zehnder Modulator
DSP	Digital Signal Processing
DWDM	Dense Wavelength Division Multiplexing
ECL	External Cavity Laser
EDFA	Erbium Doped Fibre Amplifier
ENOB	Effective Number of Bits
EOM	Electro-Optic Modulator
FEC	Forward Error Correction
FIR	Finite Impulse Response
FFT	Fast Fourier Transform

FPGA Field-Programmable Gate Array

FWM Four Wave Mixing

HNLF Highly Non-Linear Fibre

ICI Inter-Channel Interference

IM-DD Intensity-Modulation and Direct-Detection

IP Internet Protocol

LMS Least Mean Squares

LO Local Oscillator

LP Low Pass Filter

MAP Maximum *a posteriori* Probability

MIMO Multiple Input Multiple Output

MMA Multiple Modulus Algorithm

MZI Mach-Zehnder Interferometer

MZM Mach-Zehnder Modulator

NOLM Non-linear Optical Loop Mirror

NALM Non-linear Amplified Loop Mirror

OIF Optical Internetwork Forum

OFCG Optical Frequency Comb Generator

OLT Optical Line Terminal

ONU Optical Network Unit

OSNR Optical Signal-to-Noise Ratio (in 0.1 nm bandwidth)

PBS Polarisation Beam Splitter

PDE Phase Directed Equalizer

PDM Polarisation Division Multiplexed

PM Power Meter

PMD Polarisation Mode Dispersion

PON Passive Optical Network

PPG Pulse Pattern Generator

PRBS Pseudo-Random Binary Sequence

PSK	Phase Shift Keying
QAM	Quadrature Amplitude Modulation
QPSK	Quadrature Phase Shift Keying
RF	Radio Frequency
RRC	Root-Raised Cosine
SE	Spectral Efficiency
SMF	Single Mode Fibre
SNR	Signal-to-Noise Ratio
SSF	Split Step Fourier
TDM	Time Division Multiplexing
TIA	Trans-Impedance Amplifier
VOA	Variable Optical Attenuator
WDM	Wavelength Division Multiplexed
WSS	Wavelength Selector Switch

1

Introduction

EVER since the commercialisation of the internet at the end of last century the demand for data distribution has increased dramatically. The internet underpins our daily life with ever evolving applications, from video-on-demand to newly emerging services associated with the 'Internet of Things', resulting in an exponential growth of the internet traffic. Current predictions suggest that the global annual Internet Protocol (IP) traffic will increase from 523 exabytes to 1440 exabytes from 2012 to 2017 [1]. To put this into perspective 1 exabyte = 10^{18} bytes $\approx$ 250 million high-definition movies; 42,000 years of continuous watching.

Initially global communications were underpinned by copper undersea cables and satellites originally designed for voice transmission. However, these have been displaced by optical fibre due to its advantages; including increased bandwidth, lower loss and reduced latency. Historically optical fibres were considered to have 'infinite' bandwidth [2], where digital data was transmitted using binary intensity modulation, where a ONE is encoded by the presence of light and a ZERO by the absence of light. This

simple but robust transmission scheme supported the growth of global communications, however, in the last decade the short comings of this approach which results in inefficient utilisation of the finite fibre bandwidth has been realised. This has prompted the need to research in new technologies, such as digital coherent systems, to further meet data demands, by improving the utilisation.

1.1 Coherent systems

In the 1980's systems were loss limited and so coherent detection was investigated to improve receiver sensitivity and overcome this limit. While significant improvements were demonstrated at this time, research was also conducted in a competing technology, the Erbium Doped Fibre Amplifier (EDFA). It offered the same receiver sensitivity as coherent detection [3], but with significantly reduced complexity and the potential for multi-channel systems through Wavelength Division Multiplexed (WDM). When the EDFA was combined with optical dispersion compensating fibre, transmission over transoceanic distances could be achieved. However, over these long distances Polarisation Mode Dispersion (PMD) became the limiting factor requiring significantly more complex receivers to achieve reliable communication. The limitation due to PMD together with advances in silicon processing prompted a renewed research interest in coherent detection. By detecting and digitising the full optical field the complexity of the original coherent receivers is shifted into the digital domain, where Digital Signal Processing (DSP) can be used to compensate PMD, Chromatic Dispersion (CD) and demodulate arbitrary modulation formats.

While digital coherent system have now been adopted, as data demand grows, further increases in fibre capacity are required. There are two main methods to increase the capacity; to employ more of the optical bandwidth (which is outside the scope of this work) or to utilise the existing bandwidth more efficiently. One approach is to increase the data rate per channel by adopting modulation formats, such as Quadrature Amplitude Modulation (QAM), that are more spectrally efficient and carry several bits/s/Hz. However, there are both electrical and optical restrictions on spectrally efficient modulation formats. The electrical limitation is achieving high Signal-to-Noise Ratio (SNR), from the Analogue-to-Digital Converters (ADCs) and Digital-to-Analogue

Converters (DACs), at the symbol rates required for optical systems. One possible method for tackling high frequency requirements is to use multiple lower symbol rate channels. However, the optical limitation of spectrally efficient formats is the phase margin, phase stability between the transmitter and receiver lasers, which is exacerbated with low symbol rates. An alternative approach, to increasing bandwidth utilisation, is to space the WDM channels closer together, potentially at the symbol (Nyquist) rate and eliminate the guardbands. This would then allow for more channels to be transmitted through the same total bandwidth. This, however, imposes frequency stability on the channels, as any drift will cause overlap with adjacent channels, resulting in destructive crosstalk.

The aim of this work is to investigate and develop techniques and subsystems to tackle some of the issues mentioned above. The main aspects will focus on DSP algorithms for equalisation of Nyquist shaped signals and phase estimation techniques to enable spectrally efficient formats. Additional, optical frequency combs are investigated to facilitate Dense Wavelength Division Multiplexing (DWDM) systems. There are a variety of optical fibre systems ranging from short reach networks within a data centre, spanning hundreds of meters, to transoceanic point-to-point connections of tens of thousands kilometres. Naturally, those systems have very different constraints such as cost, power consumption and reliability. The subsystems investigated in this work are applicable to multiple systems or can be adapted to the requirements of the system of interest.

1.2 Thesis outline

This Ph.D. thesis is organised as follows. Chapter 2 introduces the theory for digital coherent detection, modulation formats, optics and DSP. Chapter 3 concentrates on single channel systems and details DSP that has been developed and optimised to tackle some of the challenges of higher order modulation formats. Chapter 4 focus on WDM systems by investigating existing methods for generating optical frequency combs and verifying their use for telecommunications. A study of the effects frequency and phase synchronisation is presented before developing a DSP technique that utilises those properties. Finally chapter 5 discusses potential future directions of DSP techniques

and WDM systems, before chapter 6 concludes the thesis.

1.3 Key contributions

The main original contributions in this thesis are summarized as follows:

- Development and testing, in simulation and experiment, of a new type of digital equaliser which is able to dynamically compensate for temporal misalignment within the coherent receiver without introducing additional complexity. This work resulted in a journal publication [4], chapter 3, section 3.2.
- Development of a modified equaliser which is able to adaptively compensate for chromatic dispersion in systems utilising PDM-QPSK. The compensation is blind and does not require look-up tables or training symbols. This work resulted in a conference publication [5] and is outlined in chapter 3, section 3.3.
- Demonstration of how digital coherence enhancement (a technique for estimating the phase noise of a laser and compensating it digitally) can be used to enable higher order modulation formats with high linewidth lasers. One order of magnitude higher linewidth tolerance for PDM-64QAM and burstmode switching using PDM-16QAM are experimentally demonstrated for the first time. This work resulted in two journal publications [6; 7], chapter 3, section 3.5.2.
- Demonstrations and validation of optical frequency combs as optical sources for DWDM systems, for PON, metro back-haul and longhaul applications. This work resulted in the following publications [8; 9; 10; 11; 12; 13; 14]. Parts of these works are outlined in chapter 4.

1.4 List of publications

The following list cites the publications originated from the work described in this document,

1. D. Lavery, **M. Paskov**, R. Maher, B. C. Thomsen, S. J. Savory, P. Bayvel, "Low Complexity Multichannel Nonlinear Predistortion for Passive Optical Networks,"

Signal Processing in Photonic Communications (SPPCom) 2015, SpS2C.5, June 2015.

2. D. Millar, R. Maher, D. Lavery, T. Koike-Akino, A. Alvarado, **M. Paskov**, K. Kojima, K. Parsons, B.C. Thomsen, S. J. Savory, P. Bayvel, "Transceiver-Limited High Spectral Efficiency Nyquist-WDM-System," *Proceedings of the Optical Fiber Communication Conference and Exhibition (OFC) 2015*, Th2A.13, March 2015.

3. **M. Paskov**, D. Lavery, S. J. Savory, "Blind Adaptive Equalization of Chromatic Dispersion for PDM-QPSK," *OptoElectronics and Communication Conference and Australian Conference on Optical Fibre Technology 2014*, Th11B-4, July 2014.

4. P. Rosa, M. S. Erkilinc, R. Maher, **M. Paskov**, S. Kilmurray, M. Tan, P. Harper, I. D. Philips, A. D. Ellis, J.D. Ania-Castanon, B. C. Thomsen, S. J. Savory, R. I. Killey, P. Bayvel, "Nyquist-WDM PDM-QPSK transmission over SMF-28 fibre using URFL amplification," *16th International Conference on Transparent Optical Networks (ICTON)*, Tu.D1.5, 2014.

5. P. M. Anandarajah, R. Zhou, V. Vujicic, M. D. G. Pascual, R. Maher, D. Lavery, **M. Paskov**, B. C. Thomsen, S. J. Savory, L. P. Barry, "Long reach UDWDM PON with direct and coherent detection", *16th International Conference on Transparent Optical Networks (ICTON)*, Mo.C3.2, 2014,

6. M.S. Erkilinc, S. Kilmurray, R. Maher, **M. Paskov**, R. Bouziane, S. Pachnicke, H. Griesser, B.C. Thomsen, P. Bayvel, R.I. Killey, "Nyquist-shaped dispersion-precompensated subcarrier modulation with direct detection for spectrally-efficient WDM transmission," *Optics Express*, Vol. 22, Issue 8, 2014.

7. D. Millar, T. Koike-Akino, R. Maher, D. Lavery, **M. Paskov**, K. Kojima, K. Parsons, B.C. Thomsen, S. J. Savory, P. Bayvel, "Experimental Demonstration of 24-Dimensional Extended Golay Coded Modulation with LDPC," *Proceedings of the Optical Fiber Communication Conference and Exhibition (OFC) 2014*, M3A.5, March 2014.

8. R. Maher, D. Lavery, **M. Paskov**, P. Bayvel, S. J. Savory, B. C. Thomsen, "Fast Wavelength Switching 6 GBd Dual Polarization 16QAM Digital Coherent Burst Mode Receiver," *IEEE Photonics Technology Letters*, Vol. 26, Issue 3, 2014.

9. R. Zhou, P. M. Anandarajah, R. Maher, **M. Paskov**, D. Lavery, B. C. Thomsen, S. J. Savory, L. P. Barry, "80-km Coherent DWDM-PON on 20-GHz Grid With Injected Gain Switched Comb Source," *IEEE Photonics Technology Letters*, Vol. 26, Issue 4, 2014.

10. **M. Paskov**, D. Lavery, S. J. Savory, "Blind Equalization of Receiver In-Phase/Quadrature Skew in the Presence of Nyquist Filtering," *IEEE Photonics Technology Letters* Vol. 25, Issue 22, 2013.

11. D. Lavery, R. Maher, **M. Paskov**, B. C. Thomsen, P. Bayvel, S. J. Savory, "Digital Coherence Enhancement Enabling Coherent Detection of 6 GBd DP-64QAM Using a 1.4 MHz Linewidth Tunable Laser," *IEEE Photonics Technology Letters*, Vol. 25, Issue 22, 2013.

12. H.M. Chin, K. Shi, R. Maher, **M. Paskov**, B. C. Thomsen, S. J. Savory, "Fast Optical Spectrum Estimation Using a Digital Coherent Receiver," *Proceedings of European Conference and Exhibition on Optical Communications (ECOC) 2013*, London, UK, P.3.23, September 2013.

13. M. S. Erkilinc, R. Maher, **M. Paskov**, S. Kilmurray, S. Pachnicke, H. Griesser, B. C. Thomsen, P. Bayvel, R. I. Killey, "Spectrally-Efficient Single-Sideband Subcarrier-Multiplexed Quasi-Nyquist QPSK with Direct Detection," *Proceedings of European Conference and Exhibition on Optical Communications (ECOC) 2013*, London, UK, Tu.3.C.4, September 2013.

14. M. V. Ionescu, M. S. Erkilinc, **M. Paskov**, S. J. Savory, B. C. Thomsen, "Novel Baud-Rate Estimation Technique for M-PSK and QAM Signals based on the Standard Deviation of the Spectrum," *Proceedings of European Conference and Exhibition on Optical Communications (ECOC) 2013*, London, UK, P.3.1, September 2013.

15. P. M. Anandarajah, R. Zhou, R. Maher, D. Lavery, **M. Paskov**, B. C. Thomsen, S. J. Savory, L. P. Barry, "Gain Switched Multi-Carrier Transmitter in a Long Reach

UDWDM PON with a Digital Coherent Receiver," *Optics Letters*, Vol. 38, Issue 22, 2013

16. K. Shi, G. Gordon, **M. Paskov**, J. Carpenter, T.D. Wilkinson, B. C. Thomsen, "Degenerate Mode-Group Division Multiplexing using MIMO Digital Signal Processing," in *Photonics Society Summer Topical Meeting Series, 2013 IEEE*, Hawaii, USA, WC4.4 July 2013

17. R. I. Killey, S. Erkilinc, R. Maher, **M. Paskov**, S. Kilmurray, R. Bouziane, B. C. Thomsen, P. Bayvel, "Nyquist-WDM-based system performance evaluation," *15th International Conference on Transparent Optical Networks (ICTON), 2013*, We.D3.2, 2013.

18. D. Lavery, **M. Paskov**, S. J. Savory, "Spectral shaping for mitigating backreflections in a bidirectional 10 Gbit/s coherent WDM-PON," *Proceedings of the Optical Fiber Communication Conference and Exhibition (OFC) 2013*, Anaheim CA, USA, OM2A.6, March 2013.

Papers Accepted for Publication:

1. D. Lavery, **M. Paskov**, R. Maher, S. J. Savory, P. Bayvel, "Modified Radius Directed Equaliser for High Order QAM," To be presented at European Conference on Optical Communications 2015.

2. M. Pajovic, D. S. Millar, T. Koike-Akino, R. Maher, D. Lavery, A. Alvarado, **M. Paskov**, K. Kojima, K. Parsons, B. C. Thomsen, S. J. Savory, P. Bayvel, "Experimental Demonstration of Multi-Pilot Aided Carrier Phase Estimation for DP-64QAM and DP-256QAM," To be presented at European Conference on Optical Communications 2015.

3. D. S. Millar, R. Maher, D. Lavery, T. Koike-Akino, M. Pajovic, A. Alvarado, **M. Paskov**, K. Kojima, K. Parsons, B. C. Thomsen, S. J. Savory, P. Bayvel, "Detection of a 1 Tb/s Superchannel with a Single Coherent Receiver," To be presented at European Conference on Optical Communications 2015.

4. M. S. Erkilinc, D. Lavery, R. Maher, **M. Paskov**, B. C. Thomsen, P. Bayvel, R. I. Killey, S. J. Savory, "Polarization-Insensitive Single Balanced Photodiode

Coherent Receiver for Passive Optical Networks," To be presented at European Conference on Optical Communications 2015.

2

Background theory

COHERENT detection was first investigated during the 1980's [15] because it offered higher receiver sensitivity and extending the transmission distances. However, during the same time the EDFA [16] was developed allowing practical amplification which alleviated receiver sensitivity limitations. Recent development of CMOS technology enables high speed ADCs/DACs and DSP which facilitates digital coherent detection offering higher spectral efficiency and flexibility than existing Intensity-Modulation and Direct-Detection (IM-DD) systems. This chapter presents some of the fundamental aspects of digital coherent optical communications and associated DSP which are essential in realizing high capacity optical transmission.

2.1 Coherent detection

Although coherent detection offers advantages over the traditional IM-DD system it still suffers from effects such as CD and PMD. However, through the use of DSP those

impairments can be mitigated. Digital coherent systems are a vital technology for future high spectrally efficient systems that have to meet increased demands for data.

2.1.1 Phase- and polarisation-diverse coherent receiver

Using a single photodiode the envelope of the optical field can be detected, $i \propto |E|^2$, where i is the photocurrent and the E is the electrical field. Using such a receiver only information about the amplitude is captured. By mixing the incoming optical signal with a Local Oscillator (LO), laser, the incoming signal is converted to a baseband frequency, which can be subsequently be detected. Using a second photodiode which detects the field with a 90° phase shift both the in-phase and quadrature components (amplitude and phase) are captured. Additionally, by using a Polarisation Beam Splitters (PBSs) both polarisations of the signal can be captured, covering all four dimensions of the optical signal (amplitude and phase across two polarisations). The behaviour of a phase- and polarisation-diverse coherent receiver can be described with equation (2.1). X and Y represent the two polarisations of the optical field, I and Q are the in-phase and quadrature components, while E_{LO} is the field of the LO and * denotes complex conjugate. The second term on the right hand side represents the desired coherently detected terms, while the first term represents the direct detection terms.

$$\begin{pmatrix} X_I \\ X_Q \\ Y_I \\ Y_Q \end{pmatrix} \propto \frac{1}{4} \begin{pmatrix} 2|E_X|^2 + |E_{LO}|^2 \\ 2|E_X|^2 + |E_{LO}|^2 \\ 2|E_Y|^2 + |E_{LO}|^2 \\ 2|E_Y|^2 + |E_{LO}|^2 \end{pmatrix} + \begin{pmatrix} \Re(E_X E_{LO}^*) \\ \Im(E_X E_{LO}^*) \\ \Re(E_Y E_{LO}^*) \\ \Im(E_Y E_{LO}^*) \end{pmatrix} \tag{2.1}$$

A DC block can be used to remove the $|E_{LO}|^2$, however, the AC component of the $|E_X|^2$ term, which cannot be removed, can influence the performance of the coherent receiver. To avoid this effect the power of LO can be increased, making the $|E_X|^2$ significantly smaller than the coherent terms. However, intensity fluctuations of the LO will also effect the performance, so the ratio needs to be optimised. Another approach, used when the optical complexity of the receiver is not limited, is to double the photodiodes and implement a balanced detection. The 90° phase shift is accomplished using a optical hybrid, which can have secondary output 180° out of phase compared to the original one. By detecting those outputs with a second photodiode and using a differential amplifier

the direct detection terms can be suppressed more effectively. Equation (2.2) shows the two detected signal from two balanced diodes, while equation (2.3) demonstrated the operation of the differential amplifier.

$$\begin{aligned} X_{I+} &\propto \frac{1}{4}(2|E_X|^2 + |E_{LO}|^2) + \Re(E_X E_{LO}^*) \\ X_{I-} &\propto \frac{1}{4}(2|E_X|^2 + |E_{LO}|^2) - \Re(E_X E_{LO}^*) \end{aligned} \tag{2.2}$$

$$X_{I+} - X_{I-} \propto 2\Re(E_X E_{LO}^*) \tag{2.3}$$

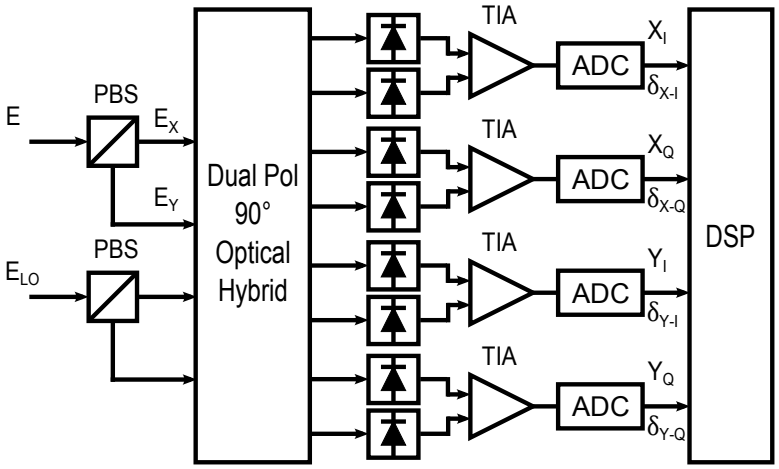

Figure 2.1: Phase- and polarisation diverse coherent receiver, with balanced detection.

Figure 2.1 illustrates a phase- and polarisation-diverse coherent receiver. PBSs are used for both the input signal and LO to detect both polarisations. The optical hybrid provides four outputs, for the four dimensions of the optical field, and secondary outputs phase shifted by 180°. The outputs of the optical hybrid are then detected with eight photodiodes. Afterwards, the signals are amplified using Trans-Impedance Amplifiers (TIAs) to amplify the difference between the inputs, before being digitised by the ADC. The use of balanced detection leads to equation (2.4), where only the coherent terms are left.

$$\begin{pmatrix} X_I \\ X_Q \\ Y_I \\ Y_Q \end{pmatrix} \propto \begin{pmatrix} \Re(E_X E_{LO}^*) \\ \Im(E_X E_{LO}^*) \\ \Re(E_Y E_{LO}^*) \\ \Im(E_Y E_{LO}^*) \end{pmatrix} \tag{2.4}$$

2.1.2 Analogue-to-digital conversion

Once the signal has been detected and amplified it is digitized using ADCs. It is conventional to use 2 Sa/symbol when digitizing the signal to allow for easier anti-aliasing filtering, timing recovery and compensation for frequency offset between the signal and LO. Higher oversampling is advantageous for anti- aliasing, however, it requires ADCs to operate at higher clock frequencies. When operating at high frequency even small imperfections or timing jitter will cause performance degradation. Additionally, the limited number of levels, that can be represented from the ADC, cause quantisation noise that can be described by as additive noise with uniform distribution and nearly white spectrum. Once the quantisation noise is filtered by a linear filter it can be modelled as Additive White Gaussian Noise (AWGN), due to the central limit theorem. Effective Number of Bits (ENOB) encompasses both noise effects and is used as a performance metric for ADC, where each effective bit is equivalent to approximately 6 dB of SNR [17]. Additionally, if the length of each individual signal path, figure 2.1, $\delta_{X\_I} = \delta_{X\_Q} = \delta_{Y\_I} = \delta_{Y\_Q}$, are not the same or are not compensated correctly within the DSP, the performance of the system can be further degraded.

2.2 Modulation

In order to be able to transmit data a common alphabet must be chosen in advance. Modulation formats are alphabets, sets of pre-determined symbols which represent a specific bit or bit-sequence. The modulation format can span multiple dimensions, such as amplitude, phase, polarisation or time. In direct detection systems only the amplitude dimension is used, because only that is the only dimension recovered. As previously mentioned a phase- and polarisation-diverse coherent receiver recovers all four dimensions of the optical signal, therefore multiple dimensions can be utilised. Optical systems traditionally used two dimensional formats (amplitude and phase) which is the same for both polarisation states, this is referred to as Polarisation Division Multiplexed (PDM). Each symbol encodes $\log_2(M)$ bits where M is total number of unique symbols in the two dimensional alphabet. More recently, however, 4D-formats (4 dimensional) that encode each symbol in amplitude and phase across both polarisations have been investigated [18]. By designing carefully the modulation format across

all four dimension it is possible to achieve a system that performs better in certain operational regimes. Spectral Efficiency (SE) is a metric used to compare modulation formats, for two dimensional formats it can be calculated as $2\log_2(M)$ (two polarisations are used) and has a unit of b/s/Hz, for 4D-formats the $\log_2(M_{4D})$, where M_{4D} is the number of constellation points in four dimensions. In this work only two dimensional modulation formats are considered, however, four and higher dimensional are discussed for future systems, section 5.3. Although it is beneficial to use a large alphabet, M, in order to increase the SE it means that at the receiver it is harder to distinguish between symbols, potentially resulting in more errors and lower performance. Therefore, the modulation formats need to be chosen carefully based on the system specifications. This section presents some of the most commonly used modulation formats for optical transmission and the devices that can be used to modulate them onto an optical carrier.

Phase shift keying

Modulation formats where only the phase of the signal is used to encode data are called M-*ary* Phase Shift Keying (PSK), where M refers to the number of symbols; allowed phase states. The optical signal has the form of equation (2.5), where $|\mathbf{E}(t)|$ represents the time dependent amplitude of the signal and $\theta(t)$ is the time dependent phase.

$$\mathbf{E}(t) = |\mathbf{E}(t)| \exp\left(j\theta(t)\right) \tag{2.5}$$

For PSK modulation formats only the phase is varied depending on the data, which can be represented with equation (2.6). Where $\mathbf{D}$ represents one of the possible phase states, which corresponds to $\log_2(M)$ bits.

$$\mathbf{E}(t) = |\mathbf{E}(t)| \exp\left(j\left(\theta(t) + \mathbf{D}\frac{2\pi}{M}\right)\right) \qquad \mathbf{D} \in 1...M \tag{2.6}$$

In this work only $M = 4$, Quadrature Phase Shift Keying (QPSK), is investigated, however, systems utilising higher order have been considered for optical communications systems; $M = 2,\ 8$ [19]. Modulation formats are often visualised using constellation diagrams where the symbols are plotted on the complex plane; QPSK is shown in figure 2.2(a). The limitation of M-PSK modulation formats is that as the number of symbols are increased the phase difference between them decreases, which poses

stricter requirements on the linewidth (phase noise) of the optical carrier.

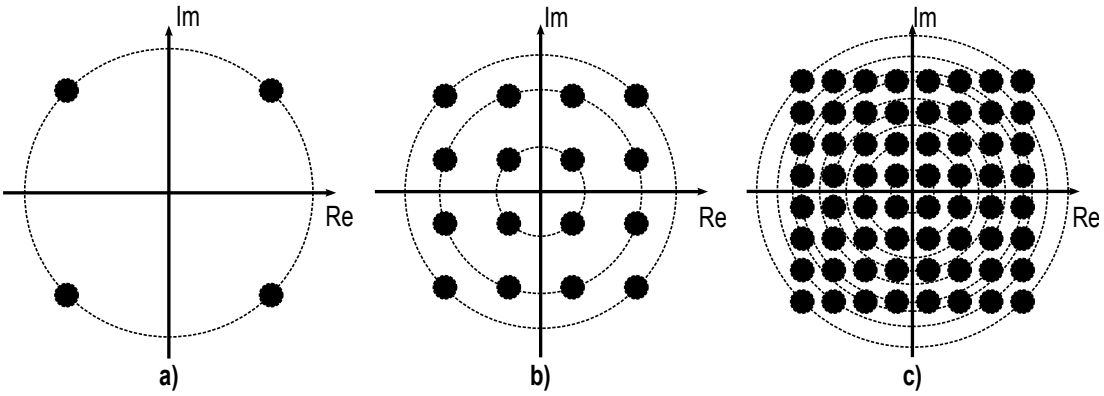

Figure 2.2: Modulation formats: **a)** QPSK **b)** 16QAM **c)** 64QAM

Quadrature Amplitude Modulation (QAM)

An alternative way of modulating data is to encode information both in the phase and amplitude, if this is done in a symmetrical pattern it is referred to as M-QAM. This can be done by amplitude modulating two independent carriers at the same frequency but with the phase difference of $\pi/2$ (90°), in-phase and quadrature. If the two carriers are modulated with the same one dimensional alphabet the resulting constellation will be square, figure 2.2. The modulation format can be represented using equation (2.7), where $\mathbf{D}_I$ and $\mathbf{D}_Q$ represents N possible amplitude states from the one dimensional alphabet. The constellation will then have $M = N^2$ symbols each representing $\log_2(M) = 2\log_2(N)$ bits of data.

$$\mathbf{E}(t) = \left[\mathbf{D}_I - \frac{N+1}{2}\right] + j\left[\mathbf{D}_Q - \frac{N+1}{2}\right] \qquad \mathbf{D}_I, \mathbf{D}_Q \in 1...N \tag{2.7}$$

In this work $M = 16,\ 64$ are investigated. It should be noted that QPSK can also be seen as QAM format where $M = 4$. Table 2.1 summarises the modulation formats that are investigated in this work.

2.2.1 Optical modulators

Optical modulators are an essential part in optical communications systems as they are used to convert any electrical baseband signal to an optical carrier, normally operating

Modulation Format	Spectral Efficiency (b/symbol)
PDM-QPSK (PDM-4QAM)	4
PDM-16QAM	8
PDM-64QAM	12

Table 2.1: Modulation formats.

around 193 THz (1550 nm). This can be used both for modulating data as well as generating additional wavelengths.

Phase modulator

The phase modulator is the simplest form of modulator, where the optical signal passes through the an Electro-Optic Modulator (EOM), figure 2.3. When a voltage is applied to the EOM material its refractive index is changed, which effects the speed of the propagating light. The small changes in speed manifests as phase modulation. The output of the modulator can be described using equation (2.8). The V_π is the voltage that is required to change the phase of the signal by π (180°) and $\mathbf{V}$ is the electrical field applied to the modulator. Phase modulator can be used to generate any M-PSK.

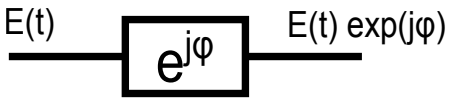

Figure 2.3: Phase modulator schematic.

$$\mathbf{E}_{Out} = \mathbf{E}_{In} \exp\left(j\frac{\pi}{V_\pi}\mathbf{V}\right) \tag{2.8}$$

Intensity modulator

An intensity modulator or Mach-Zehnder Modulator (MZM) splits the optical signal into two paths. In each path there is an EOM which changes the phase of the optical signal in opposite directions forming a so called Push-Pull configuration, figure 2.4. Afterwards when the optical signal is recombined there is a constructive or destructive interference depending on the relative phase between the two paths, this leads to an amplitude change. The output of the modulator can be described using equation (2.9). The V_{Bias} is a simple DC-term which is used to bias the modulator along the transfer function and

determines the output of the modulator when $\mathbf{V} = 0$. An intensity modulator can be used for intensity modulation and 2-PSK (Binary Phase Shift Keying (BPSK)) depending on the V_{Bias}.

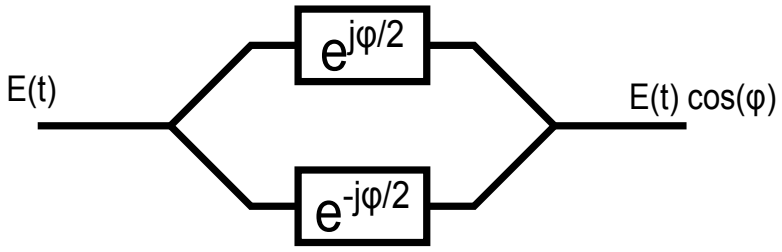

Figure 2.4: Intensity modulator schematic.

$$\begin{aligned}\mathbf{E}_{Out} &= \mathbf{E}_{In}\left[\exp\left(j\frac{\pi}{V_\pi}\left(V_{Bias}+\frac{\mathbf{V}}{2}\right)\right)+\exp\left(-j\frac{\pi}{V_\pi}\left(V_{Bias}+\frac{\mathbf{V}}{2}\right)\right)\right] \\ &= \mathbf{E}_{In}\cos\left(\frac{\pi}{V_\pi}\left(V_{Bias}+\frac{\mathbf{V}}{2}\right)\right)\end{aligned} \tag{2.9}$$

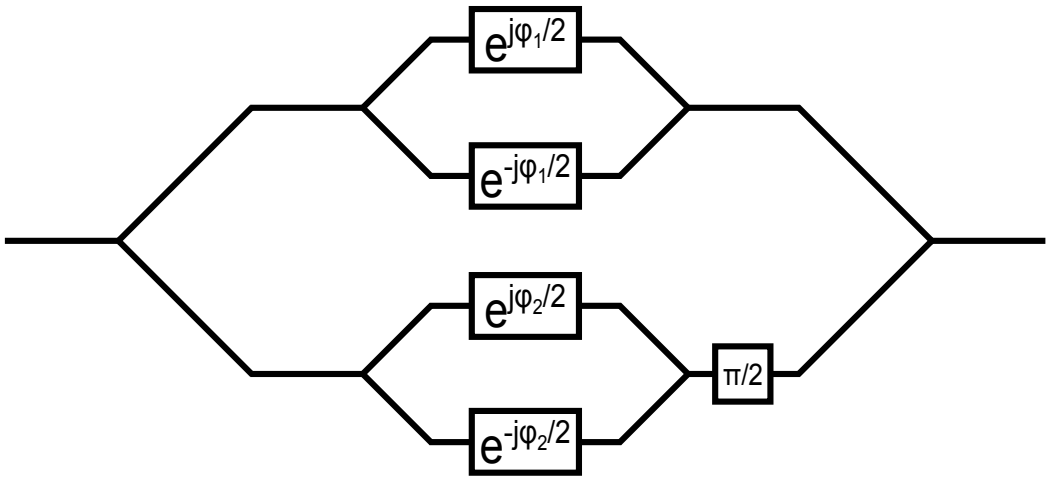

Figure 2.5: IQ modulator schematic.

In-phase and quadrature modulator

The in-phase and quadrature modulator (IQ Modulator), combines two MZMs together with a phase shift, figure 2.5; it is also known as a nested MZM. A phase shift of $\pi/2$ (90°) allows the two MZMs to operate on two orthogonal phases. This enables the modulator to recreate any two dimensional constellation spanning in-phase and quadrature (not limited to M-QAM).

2.3 Impairments in optical systems

The impairments that this work will focus on are Chromatic Dispersion (CD) and phase noise. Although optical communications is associated with other impairments such as PMD and Kerr non-linearity they are not investigated in detail.

2.3.1 Chromatic dispersion

Different wavelengths travel through the optical fibre with different velocities which leads to the effect called chromatic dispersion. The effect can be expressed using equations (2.10) [20]. **E** represents the electrical field along the fibre at a distance z, β is the propagation constant, β_2 is the dispersion parameter of the fibre and ω is the angular frequency.

$$\begin{aligned} \frac{\partial \mathbf{E}}{\partial z} &= j\frac{\beta_2}{2}\frac{\partial^2}{\partial t^2}\mathbf{E} \\ \beta_2 &= \frac{\partial^2 \beta}{\partial \omega^2} \end{aligned} \tag{2.10}$$

The dispersion parameter is more often expressed as equation (2.11), where c is the speed of light and λ is the reference wavelength, the units for dispersion is ps/nm/km. For a standard Single Mode Fibre (SMF) the dispersion is about 17 ps/nm/km at wavelength 1550 nm.

$$D = -\frac{2\pi c \beta_2}{\lambda} \tag{2.11}$$

Chromatic dispersion effects all transmission systems, however, systems that operate over large distance are particularly sensitive due to the accumulated dispersion. Additionally, channels that utilise high symbol rates are especially susceptible because they carry more frequency components.

2.3.2 Additive noise

As the optical signal propagates through the fibre part of it is absorbed by the medium or scattered by imperfections in the material, which ultimately leads to power loss. Typical losses for SMF are approximately 0.2 dB/km or lower. To overcome these losses the optical signal is periodically amplified using EDFAs which introduce additive noise in a process called Amplified Spontaneous Emission (ASE). The noise contribution cause by ASE is modelled as AWGN. As the signal is amplified repeatedly the noise

is accumulated, which leads to a degraded Optical Signal-to-Noise Ratio (in 0.1 nm bandwidth) (OSNR). This affects primarily transmission system over long distances or short shorter distances where the launch power is low.

2.3.3 Frequency and phase noise

Although lasers are designed to produce a single frequency they have a finite phase variation. The phase of the laser is fluctuating over time which causes the laser to change frequency around its original wavelength, this is mainly caused by imperfections in the resonator cavity and is referred to as phase noise or linewidth. The random process of the laser phase noise is described with a 'random walk' (Wiener process [21]) where the difference between two time consecutive points is Gaussian distributed with a variance proportional to the laser linewidth and the time between observations, equation (2.12). The Δv represents the 3 dB Lorentzian bandwidth of the linewith and T is the time between consecutive time samples (equivalent to the symbol period).

$$\sigma^2 = 2\pi\Delta v T \tag{2.12}$$

This effect limits the performance of all systems, however, systems with lower symbol rates and higher order modulation formats are particularly vulnerable. Passive Optical Networks (PONs) are susceptible to this because they use utilise low symbol rates as well as try to use cheaper lasers which often have higher linewidth. Additionally, systems that use higher order modulation formats are sensitive to phase noise due to the dense constellations and lower phase margin between symbols, as illustrated in figure 2.6. Using equation (2.13), the phase margin can be calculated for arbitrary M-QAM formats. The phase margin for the modulation formats that are investigated in this work are presented in table 2.2.

$$\theta = \arccos\left(\frac{x-1}{x\sqrt{2}}\right) - 45^\circ \tag{2.13}$$

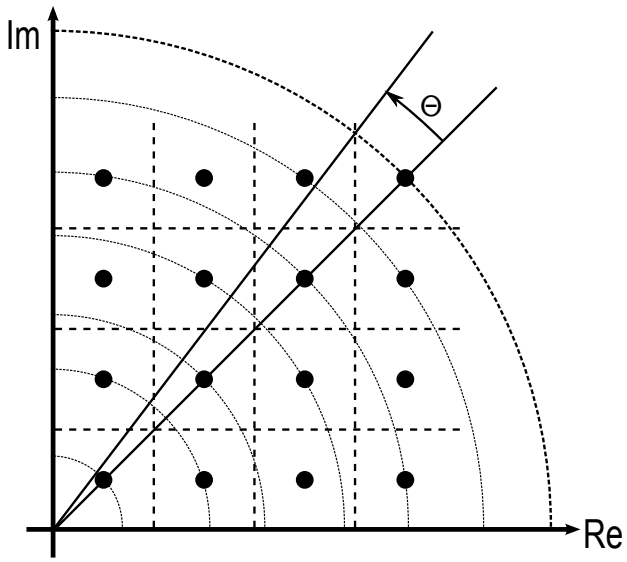

Figure 2.6: QAM phase margin illustrated.

Modulation Format	Phase Margin
PDM-QPSK (PDM-4QAM)	45°
PDM-16QAM	16.9°
PDM-64QAM	7.7°

Table 2.2: Phase margin for QAM modulation formats.

2.4 Digital signal processing

Once the incoming optical signal has been detected and digitized by the phase- and polarisation-diverse coherent receiver (section 2.1.1) and the ADCs (section 2.1.2) the signal can be processed by DSP. Using specific DSP algorithms the constraints of optical components can be alleviated. Additionally, the linear distortions (CD and phase noise) mentioned in the previous (section 2.3) can be mitigated by inverting their effects on the signal. As the full optical field is captured the full channel response can be calculated and then applied inversely to the signal. However, this is not practical as the operation is computationally intensive and the optical channel is time dependent, requiring constant adaptation. It is, however, possible compensate the channel effects separately because they are linear, this work utilises this modular approach.

The effects of conventional DSP blocks is shown in figure 2.7. After sampling at 2 Sa/symbol any DC offset is removed and the signal is normalised to unit power. If the initial sampling is higher then 2 Sa/symbol, as is often the case in experiments, the

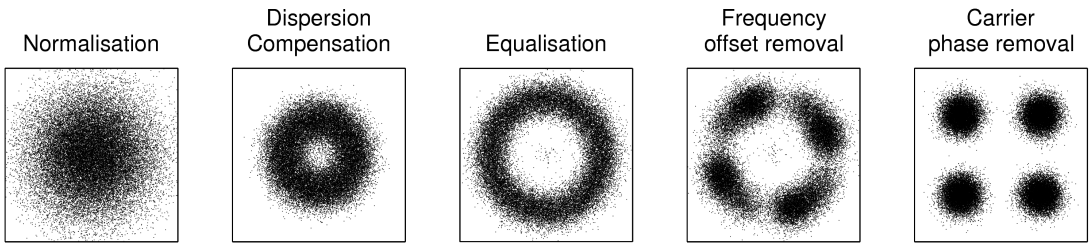

Figure 2.7: DSP blocks and their effect on the digitized signal. For demonstration a 6 GBd PDM-QPSK is transmitted over 2000 km of SMF with 20 dB OSNR in simulations.

signal would be down sampled. When the signal is transmitted and CD is present it is compensated using a Finite Impulse Response (FIR) filter, as described in section 2.4.1. Once the static effects of the channel are compensated the signal is equalised to mitigate time dependent polarisation rotations and optimize the sampling instant, section 2.4.2. Afterwards, the frequency offset (the difference in frequency between the optical carrier and the LO) is removed and the phase noise is tracked and compensated as described in section 2.4.3. Finally symbol decisions are made to extract the information stream. Although not implemented or investigated in detail the use of hard decision Forward Error Correction (FEC) is assumed in this work. At a specific Bit Error Rate (BER) threshold it is assumed that the signal can be recovered to an error free performance (BER below 10^{-15}) after a particular FEC implementation with a specific coding overhead.

2.4.1 Chromatic dispersion compensation

Chromatic dispersion (CD) as previously explained in section 2.3.1 is the effect of wavelength dependent velocity through the optical fibre. This effect is time independent and can therefore be compensated by using a linear non adaptive filter, [22]. The filter response can be calculated by solving equation (2.10) using a Fourier transform, equation (2.14).

$$G(z,\omega) = \exp\left(-j\frac{D\lambda^2}{4\pi c}z\omega^2\right) \tag{2.14}$$

By taking the inverse Fourier transform of the filter response and truncating at the Nyquist frequency, to avoid aliasing and non-causality. The time domain implementation is then described by equations (2.15). Where N is the number of filter taps, n is the tap index, $\mathbf{a}(n)$ is the tap values of the FIR and T is the sampling period. It is

clear from the formulae that larger distances required longer filters, which is logical as the wavelengths have spread over a longer time period during the transmission. Additionally, the number of filter taps are proportional to the symbol rate and inversely proportional to the sampling period.

$$\begin{aligned} N &= 2\left\lfloor \frac{|D|\lambda^2 z}{2cT^2} \right\rfloor + 1 \\ -\left\lfloor \frac{N}{2} \right\rfloor &\leq n \leq \left\lfloor \frac{N}{2} \right\rfloor \\ \mathbf{a}(n) &= \sqrt{\frac{jcT^2}{D\lambda^2 z}} \exp\left(-j\frac{\pi cT^2}{D\lambda^2 z} n^2\right) \end{aligned} \tag{2.15}$$

$$\mathbf{y}(k) = \mathbf{a}^T \cdot \mathbf{x} = \sum_{n=0}^{N-1} \mathbf{a}(n)\, \mathbf{x}(k-n) \tag{2.16}$$

$$\mathbf{y}_k = \mathbf{a}^T \cdot \mathbf{x} = \mathcal{F}\left\{\mathcal{F}\{\mathbf{a}\}\mathcal{F}\{\mathbf{x}_k\}\right\}^{-1} \tag{2.17}$$

This truncated filter can be implemented in both time and frequency domain. For longer distances and high symbol rates, when the number of taps is increased the complexity of the frequency domain implementation is significantly lower compared to the time domain implementation. A FIR is implemented as a convolution in the time domain, where the multiplications scale are in $O(N^2)$[1] per N samples, equation (2.16), where $\mathbf{x}$ is the input vector and k is the output sample. In the frequency domain a FIR can be implemented as overlap-add multiplication, equation (2.17), Fast Fourier Transforms (FFTs) are used for the conversion from the time domain to the frequency domain, the total the number of multiplications are in $O(N\log_2(N))$ per N samples. Note that the time domain implementation operates on a single sample while in the frequency domain operates on blocks.

2.4.2 Equalisation

After the time independent channel response has been compensated equalisation is performed to compensate for time dependent polarisation rotations. Additionally, because the signal is sampled at 2 Sa/symbol it is possible to recover the optimal sampling instant as well. The following class of adaptive filter is called Multiple

[1] Big O notation, expresses the bounded complexity.

Input Multiple Output (MIMO), as it treats the two polarisations as independent input signals and tries to separate any mixing due to polarisation rotations caused by the fibre transmission. Figure 2.8 illustrates the structure of a 2×2 equaliser, where $\mathbf{x}_{in}$ and $\mathbf{y}_{in}$ represent the two input polarisations, which are mixed together, $\mathbf{x}_{out}$ and $\mathbf{y}_{out}$ are then the separated polarisations and **h** are the different adaptive filters.

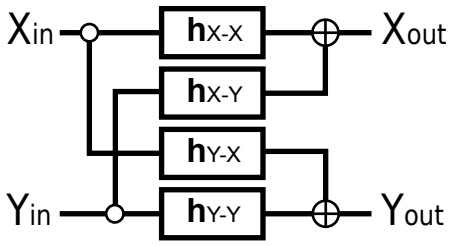

Figure 2.8: Equaliser structure for 2×2 MIMO.

Here the adaptive equalisers is separated into of three stages, the first one to apply the filters to the input signal, as described by equations (2.18). In the time domain this is implemented as convolution, equation (2.19), where N are the number of filter taps and k is the output sample.

$$\begin{aligned} \mathrm{X}_{out} &= \mathbf{h}_{XX}^{T}\mathbf{X}_{in} + \mathbf{h}_{XY}^{T}\mathbf{Y}_{in} \\ \mathrm{X}_{out} &= \mathbf{h}_{YX}^{T}\mathbf{X}_{in} + \mathbf{h}_{YY}^{T}\mathbf{Y}_{in} \end{aligned} \tag{2.18}$$

$$\mathbf{h}_{XX}^{T}\mathbf{X}_{in} = \sum_{n=0}^{N-1} \mathbf{h}_{XX}(n)\ \mathbf{X}_{in}(k-n) \tag{2.19}$$

The equalisers described here are of the class of blind and adaptive. They are trying to restore a property of the signal which is known in advance and is dependent on modulation format. In the following equaliser the property of interest is the amplitude. The modulation format QPSK has only one possible amplitude therefore the algorithm is called Constant Modulus Algorithm (CMA) [23]. However, for modulation formats such as 16QAM and 64QAM which have multiple possible amplitudes, the algorithm is called Multiple Modulus Algorithm (MMA). The second stage of equalisation is to calculate the error term by compare the amplitude of the output with the expected output (for MMA the closest amplitude is chosen) as described by equations (2.20),

where R is the radius of the closest amplitude level and $\leftarrow$ indicates an update.

$$\begin{aligned} \varepsilon_x &\leftarrow R^2 - |\mathrm{X}_{out}|^2 \\ \varepsilon_y &\leftarrow R^2 - |\mathrm{Y}_{out}|^2 \end{aligned} \tag{2.20}$$

The final stage of equalisation is to update the initial filter coefficient based on the error term, equations (2.21). The μ is called the convergence parameter which affects the convergence speed.

$$\begin{aligned} \mathbf{h}_{XX} &\leftarrow \mathbf{h}_{XX} + \mu\varepsilon_x \mathrm{X}_{out}\mathbf{X}^*_{in} \\ \mathbf{h}_{XY} &\leftarrow \mathbf{h}_{XY} + \mu\varepsilon_x \mathrm{X}_{out}\mathbf{Y}^*_{in} \\ \mathbf{h}_{YX} &\leftarrow \mathbf{h}_{YX} + \mu\varepsilon_y \mathrm{Y}_{out}\mathbf{X}^*_{in} \\ \mathbf{h}_{YY} &\leftarrow \mathbf{h}_{YY} + \mu\varepsilon_y \mathrm{Y}_{out}\mathbf{Y}^*_{in} \end{aligned} \tag{2.21}$$

Another method to equalise the signal is to decompose the signal into in-phase and quadrature parts (real and imaginary) and then try to restore the properties of those components amplitude. This method is suitable for M-QAM which have the same in-phase and quadrature components. This is equivalent to making decisions on the symbol and therefore it is called Decision Directed (DD) algorithm. Unlike the CMA and MMA the DD algorithm takes into account the phase of the signal and therefore the frequency offset and phase noise need to be removed prior to equalisation. Because of this DD algorithms are usually only used when the initial convergence of the signal has been achieved.

2.4.3 Frequency offset and carrier recovery

Once the signal has been equalised the frequency offset caused by the difference in wavelength of the sub-carrier and the LO has to be removed. To estimate the frequency offset the modulation has to be removed, otherwise the phase variations across symbols will cause false estimation. For QPSK there is a simple way of removing the modulation by raising the signal to the 4^{th} power, this maps all the symbols to the same point. Afterwards, by taking the Fourier transform of the signal and locating the peak of the signal in the frequency domain the frequency offset can be estimated, equation (2.22). By taking the 4^{th} power of other M-QAM formats, the symbols are mapped to a large cloud of points around the point of interest, this cloud can be considered as noise.

Locating the peak power of the signal in the frequency domain is still possible even through the higher noise, making this algorithm effective for arbitrary M-QAM [24].

$$\begin{aligned} \mathbf{X}(f) &= FFT(\mathbf{x}^4) \\ \mathbf{X}(f_0) &= max(\mathbf{X}(f)) \\ \phi &= \frac{2\pi f_0}{T}\frac{1}{4} \\ \mathbf{y}(k) &= \mathbf{x}(k)\exp(-jk\phi) \end{aligned} \tag{2.22}$$

By removing the frequency offset the mean of the phase difference between the carrier and the LO is removed. However, because two independent lasers are used and their phases are not synchronized, there will be small phase variation over time, this is caused by the phase noise of the lasers. An approach developed by Viterbi & Viterbi [25], which is similar to the frequency removal algorithm, can be utilised, The difference is that phase is estimated over a sliding window in order to capture time dependent effects while averaging additive noise, equation (2.23), where $2w+1$ is the window size. Note that as the angle is calculated it is also unwrapped to allow for continuously varying phase noise.

$$\phi(k) = \frac{1}{4}\left[\angle\left(\sum_{n=k-w}^{k+w}\mathbf{x}(n)^4\right)\right] \tag{2.23}$$

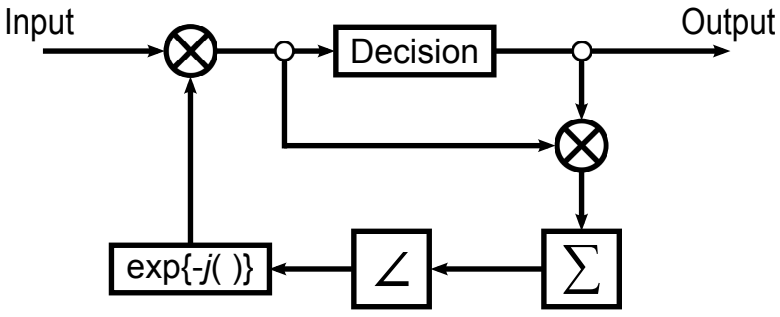

Figure 2.9: Schematic diagram of the DD-CPE algorithm.

This approach is only applicable to QPSK as raising 16QAM and 64QAM to the 4^{th} power does not remove the modulation entirely, instead a DD approach needs to be employed. For each symbol $\mathbf{x}(n)$ the closest, minimum distance, symbol is chosen (decision is made), and then the phase deviation is calculated using the decision as reference [26]. The algorithm is illustrated in figure 2.9 and is expressed mathematically

using equation (2.24), where D denotes the decision. For QPSK the algorithm is the same as the Viterbi & Viterbi described above. The maximum linewidth tolerance for higher symbol rates is larger because the 'random walk' process is sampled more frequently, which allows faster changes to be tracked. Table 2.3 lists the maximum tolerable (linewidth) $\times$ (symbol period) product for a OSNR penalty of 1 dB at a BER of 10^{-3} [26].

$$\phi(k) = \angle \left(\sum_{n=k-w}^{k+w} D[\mathbf{x}(n)]\mathbf{x}(n) \right) \tag{2.24}$$

Modulation Format	$\Delta v \times T$ for 1 dB Penalty @ BER = 10^{-3}
PDM-QPSK (PDM-4QAM)	4.1×10^{-4}
PDM-16QAM	1.4×10^{-4}
PDM-64QAM	4.0×10^{-5}

Table 2.3: Phase noise tolerance for modulation formats.

3

Single channel subsystems

In the previous chapter the basic concepts of digital coherent optical systems were discussed; this chapter will focus on extending the basic DSP blocks to achieve higher data throughput and allow dynamic networking for next generation networks. The two key techniques to achieve higher data throughput investigated in this work are DWDM and high order modulation formats. Nyquist filtering is vital for DWDM networks where the guardbands are minimised or fully discarded. The effect and constraints that the sharp filtering imposed on the digital coherent system are explored and tackled. Phase noise compensating techniques are also investigated because of the constraint phase noise imposes on the cardinality of the modulation formats. As previously discussed (chapter 2, section 2.4.1) CD can be compensated, however, the characteristics of the fibre and the transmitted distance need to be known in advance. For dynamic networks the signal can use different routes that might not be known in advance, therefore this work investigates a technique for dynamic compensation of CD.

3.1 Nyquist filters for Passive Optical Networks (PONs)

3.1.1 Passive Optical Networks (PONs)

The individual users are connected to the access network which in turn is connected to the larger metro network at a point of presence. For future optical access networks two main architectures could be considered: an Active Optical Network (AON) and a Passive Optical Network (PON). The active optical network has active components such as EDFAs and Optical-Electrical-Optical components to allow reconfigurable routing through the network. PON, as the name suggests, use only passive components such Arrayed Waveguide Gratings and power splitters. Although PONs have fewer functionalities the lower component and operational costs makes them ideal for access networks.

Different variations of PON have been standardized and are being deployed [27; 28; 29; 30], they scale with the data per channel with the latest generation, NG-PON2, reaching up to 40 Gbit/s. With the current designs the systems have a splitting ratio from 16 up to 128 for NG-PON2. Each of those fibre connection ends at a hub where the optical signal is converted to the electrical domain and is transported to the user premises via copper cable. At the hub the optical channels split between multiple users utilising Time Division Multiplexing (TDM), where each user is allocated a time slot effectively resulting in lower data rate per user. Research has recently focused on a full WDM PON with digital coherent detection, where each user receives an individual WDM channel carrying 1 Gbit/s [31], or 10 Gbit/s [32; 33].

To accommodate and reach more users these new architectures would have to utilise additional WDM channels while the signal is split to more users, potentially up to 1024. Due to the high splitting ratio there will be significant power loss leading to a stricter loss budget for the whole system, and ultimately limiting the maximum reach of the network. To simplify the network and avoid extra costs associated with additional fibres and splitters bi-direction transmission could be employed. A single laser can be utilised at the user premises, Optical Network Unit (ONU), by tuning to match the frequency of the downstream channel and act as a LO, while the upstream channel is generated digitally with a fixed offset frequency. This means that by using a fixed grid for the downstream channel the grid for the upstream channels would be automatically set

as well. Although this would require a tight frequency grid it will avoid the need for additional laser for upstream at the ONU.

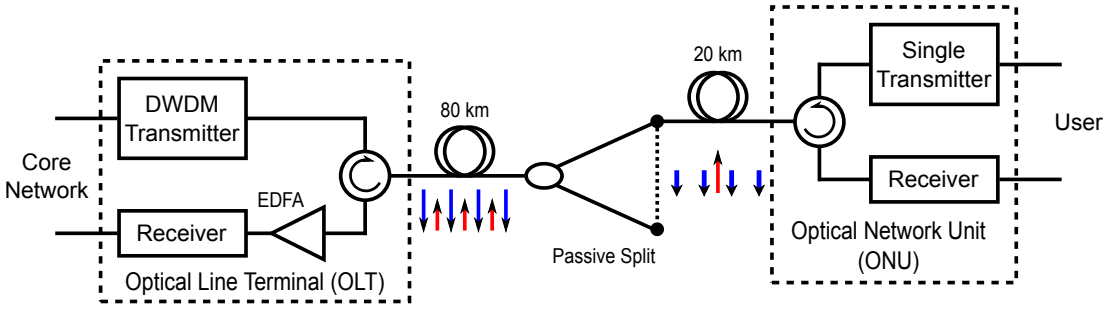

Figure 3.1: Bi-directional PON. Blue and red arrows represent downstream and upstream respectively while their heights demonstrate their relative power.

The PON considered in this work is illustrated in figure 3.1. At the Optical Line Terminal (OLT) a DWDM transmitter is used to modulate channels that are spaced at 10 GHz. The signal is then transmitted through a backhaul link before being passively split and directed to the ONUs. The coherent receiver is then used to select and detect a dedicated channel. The upstream channel is transmitted through the same fibre with a 5 GHz offset to the downstream channel. Note that this is only one possible PON configuration that suitable for 3 GBd PDM-QPSK.

Although there are many challenges with this architecture the use of coherent detection and DSP alleviate some of the requirements on the optical component by increasing receiver sensitivity, eliminating the need for optical filters.

One particular problem that is associated with bi-directional access networks is backreflections. They arise as a transmitted channel, from the ONU, is reflected backwards from; connectors, power splitters, fibre splices and Rayleigh scattering, towards the co-located receiver. Although the power for N-splitter is attenuated by at least $10\log_{10}(N)$ dB, if they are close to the receiver the powers can even be 10 dB higher than the channel of interest. Furthermore, if the power of the aggressor channel is not fully contained in its nominal bandwidth, and is spilling into the channel of interest, this will cause penalty due to crosstalk [33; 34]. This work will investigate the backreflections that are seen at the ONU. By spectrally shaping the down and upstream channels digitally with Nyquist filters or utilising low pass Bessel filters backreflections can effectively be mitigated.

3.1.2 Experimental configuration

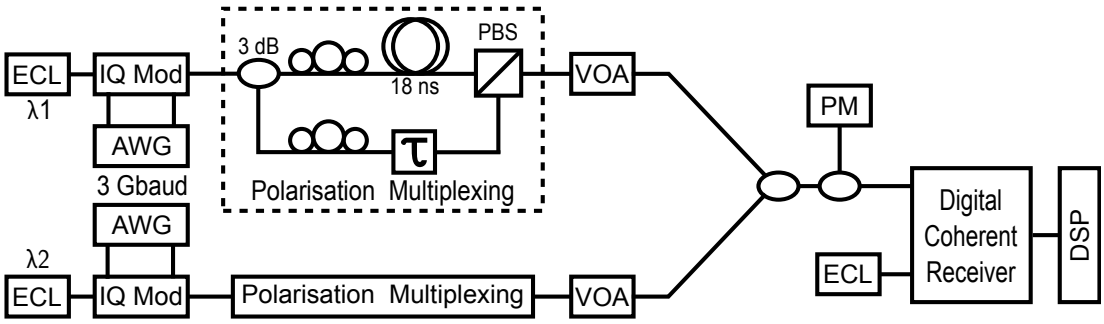

Figure 3.2: Experimental configuration used to emulate backreflections.

This section will cover the experimental configuration used to spectrally shape the channels and evaluate their performance in the presence of backreflections in a DWDM PON system.

Backreflections at the ONU are emulated by generating two 3 GBd PDM-QPSK. The net data rate per channel is 10 Gbit/s after including a 20% for FEC. The FEC considered in this part of the work is a hard decision code with a BER limit of 1.5×10^{-2} [35].

Figure 3.2 illustrates the configuration used to collect data. The channel of interest (downstream) was generated by an External Cavity Laser (ECL) operating at 1550 nm, λ_1. The laser was modulated with an IQ modulator driven by an Arbitrary Waveform Generator (AWG) operating at 12 GSa/s to produce 3 GBd QPSK signal, at 4 Sa/symbol. The waveforms were filtered digitally with chosen spectral shape before uploaded to the AWG. The aggressor channel, upstream, was generated with a 5 GHz frequency offset, λ_2, with an independent AWG and IQ modulator. PDM was emulated by passing the two signal through independent polarisation multiplexing stages.

The two channels were attenuated with two Variable Optical Attenuators (VOAs) before being combined and detected by a digital coherent receiver. The LO was a third independent ECL operating at λ_1. After detection the signal was digitally sampled and down sampled to 6 GSa/s, 2 Sa/symbol. The signal was equalised with a 5 tap filter, while frequency offset and phase recovery were performed as described in section 2.4.

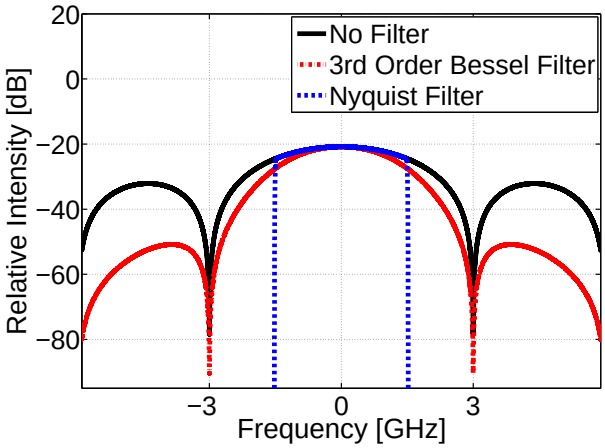

Figure 3.3: RF spectra with; no filtering, 1.5 GHz 3^{rd} order Bessel filter and RRC with a rolloff of 0.

3.1.3 Spectral shaping

Before uploading the waveforms onto the AWGs they were digitally filtered to achieve the investigated spectra shapes. The initial waveforms where generated using Pseudo-Random Binary Sequences (PRBSs) of length $2^{15} - 1$, the in-phase and quadrature components were decorrelated by half of the pattern length to avoid any false convergence of the equaliser. Two different filter options were considered and were benchmarked against a scenario where no spectral shaping was used, except for the bandwidth limitation from the AWG which is 6 GHz. At the ONU where resources are sparse, so a simple 3^{rd} order Bessel filter was considered. This can be achieved either by using low bandwidth electrical components or using off the shelf filters. At the OLT it can be assumed that the transmitter could use a DAC to generate the Radio Frequency (RF) waveforms, thus Nyquist filtering, Root-Raised Cosine (RRC), with a rolloff of 0 is possible[1]. Figure 3.3 illustrates the spectral shapes for the three scenarios considered.

When RRC filtering is used it customary to use a matched filter at the receiver, ONU, to improve performance. However, to keep the DSP at the ONU as simple as possible and because only the spectral shape is of interest, in this scenario the matched filter was been omitted. Instead the adaptive equaliser was used to converge and apply the optimal matched filter. This leads to an implementation penalty due to non-optimally matched filtering. The performance is evaluated by measuring the required received

[1]The complexity for implementing this rolloff in the transmitter might be prohibitive. Therefore, a trade-off between complexity and filter rolloff could be investigated in future works.

optical power, this is also known and receiver sensitivity. Figure 3.4(a) illustrates that the penalty was decreased as the equaliser taps are increased. This allows the equaliser to approximate the channel response more accurately. By using 5 taps for the adaptive equaliser there was a penalty of less than 1.5 dB compared to the asymptomatic performance.

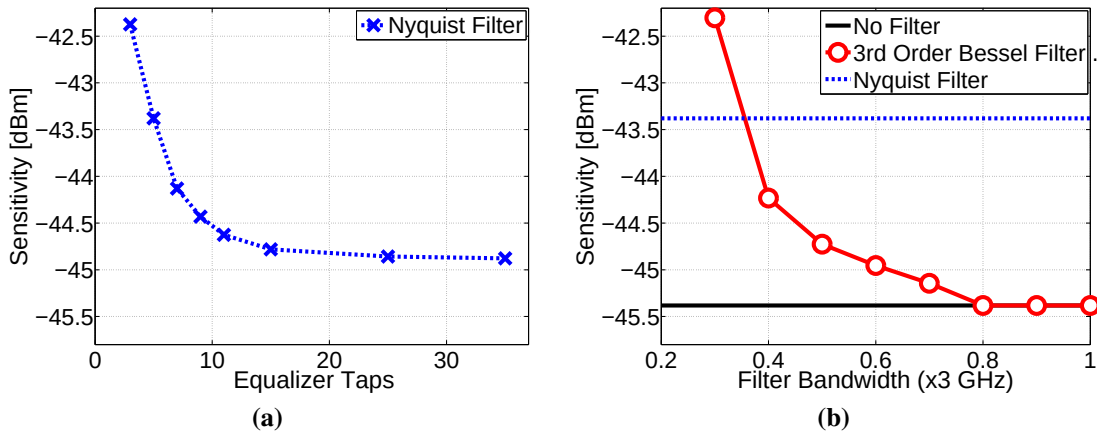

Figure 3.4: 3 GBd PDM-QPSK **a)** Sensitivity vs number of equaliser taps when no matched filter is used. **b)** Sensitivity for different pulse shaping schemes.

The single channel performance for the three scenarios; no filter, Bessel filter and RRC filter, were compared with respect to their sensitivity at the FEC limit, figure 3.4(b). The RRC filtering exhibits a penalty compared to no filtered regime due to non-optimal matched filtering previously discussed. The Bessel filter performance improves as the bandwidth of the filtered is increased towards the full bandwidth of the signal. For a penalty no larger than 1 dB, compared to no filtering, a Bessel filter with a 50% bandwidth can be utilised to reduce the bandwidth of the upstream channel.

3.1.4 Experimental results and discussion

Once the single channel performance, for the different spectral shapes, was established backreflection emulation was performed as illustrated in figure 3.2 and previously discussed. The results are illustrated in figure 3.5. When no additional spectral shaping is applied the penalty from crosstalk increases continuously with the power of the backreflected channel. When the power of the aggressor channel is at -25 dB there is a penalty of about 4 dB. This penalty drops to 0.5 dB, when Nyquist filtering is used for the downstream channel and a Bessel filter is used for the upstream channel, although

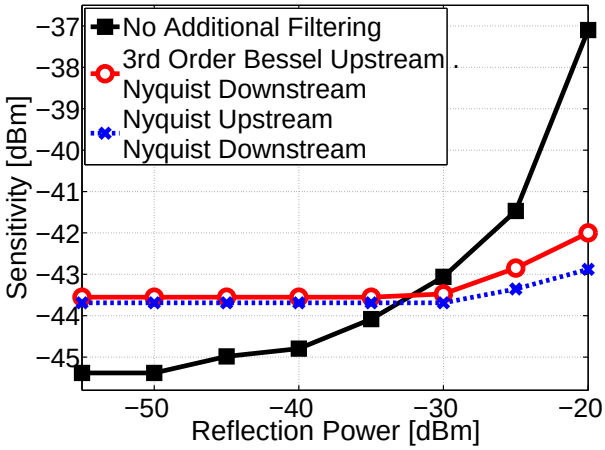

Figure 3.5: Impact of backreflections on receiver sensitivity.

with penalty offset as in figure 3.4(b). Nyquist filtering was also applied to the upstream, to investigate the ultimate performance limit when spectral shaping is used. In that scenario the penalty dropped to less than 0.2 dB.

In the architecture that is considered here the backreflections accumulated from the first splitter, 20 km from the ONU as well as Rayleigh backscattering. Assuming that either FC-PC or FC-APC connector, which have return loss of -35 dB and -50 dB, would result in -30 dB and -32 dB respectively reflected loss after 20 km [36]. By utilising the spectral shaping technique presented in this work a reflected power of -25 dBm can be tolerated at the ONU without significant penalties. This means that if FC-PC connectors are used a maximum of 5 dBm can be launched into the fibre to have a reflected power no larger than -25 dBm. This would then allow for a 512-way split over 100 km. However, by replacing the connectors with FC-APC the upstream launch power can be increased to 7 dBm and which would enable a split ratio of 1024 to reaching twice the amount of users.

Nyquist filtering is a key subsystem that allows the implementation of next generation DWDM-PON delivering 10 Gbit/s to the end user while still maintaining more than 1000 users. By spectrally shaping the channels the excess bandwidth can be constraints and the effects of backreflections alleviated. Additionally, Nyquist filtering has since also been used to allow a bi-directional DWDM PON with 2.5 GBd 16QAM channels spaced at the Nyquist rate for a total data rate of more than 1 Tbit/s [34]. With 16QAM the SE is increased and the symbol rate can be lowered, however, the sensitivity tolerance is lower compared to QPSK and phase noise tolerance can be limiting especially

with the lower symbol rate.

3.2 Equalisation for Nyquist filtering

Any imperfection in the optical front-end and the ADC, figure 3.9(a), can severely limit the channel performance; especially if high symbol rates are used (shorter symbol period). The Optical Internetwork Forum (OIF) states that a coherent receiver for PDM-QPSK with symbol rates up to 32 GBd should have a maximum delay skew of 10 ps [37]; 32% of the symbol period. Current state of the art phase and polarisation diverse coherent receivers can achieve delay skews below 5 ps [38] which corresponds to 28% of a 56 GBd symbol period, which is in agreement with OIF. There are calibration techniques that compensate for those misalignments [39], however, they all require additional DSP blocks which may lead to higher cost and power consumption. The main purpose of equalisers is to compensate PMD, however they are also used to apply an inverse of the channel response such as filter response and residual CD. In this section a blind equaliser is investigated to mitigate the timing skew as well and effectively relax constraints on optical components. A similar structure using training sequences and decision directed equalisation has previously been proposed [40]. However, decision directed equalisation requires frequency offset removal and Carrier Phase Estimation (CPE) to be carried out simultaneously or prior to equalisation, otherwise symbol decisions will be incorrect. In the following section it is demonstrated that an adaptation can be achieved without the need for training sequences, which lower the SE, or decision directed equalisation, which require large feedback loops.

Future systems with data rates of 400 Gbit/s, could utilise higher order QAM as well as high symbol rates. One option currently being explored is to use 56 GBd PDM-16QAM [41], achieving 448 Gbit/s (400 Gbit/s with 12% coding overhead). Furthermore, for compatibility with the ITU standard, 100 GHz frequency grid, Nyquist filtering would be required. However, with Nyquist filtering the eye opening of each symbol is shorter, making the systems even more sensitive to potential delay skew caused by the coherent receivers and can lead to severe performance degradation. Investigation through simulation and experiments of the proposed equaliser demonstrate how potential delays can be compensated.

3.2.1 Equaliser structure

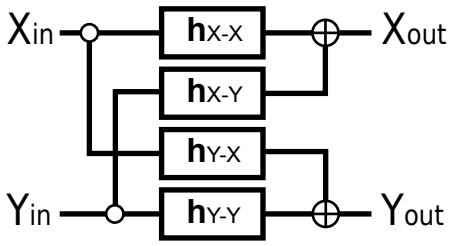

Figure 3.6: Equaliser structure for 2×2 MIMO.

In a conventional butterfly equaliser, figure 3.6 (section 2.4.2), the in-phase and quadrature components for each polarisation are treated together as one complex-valued input. This is a valid assumption because the in-phase and quadrature component interact together only through CD (section 2.3.1), a deterministic effect which is compensated prior the equaliser. This equaliser has two complex inputs and two complex outputs and is often referred to as 2×2 MIMO. The modified equaliser structure, figure 3.7, separates in- phase and quadrature for each polarisation, having four real-valued inputs and four real-valued outputs, 4×4 MIMO.

Because the 2×2 equaliser structure enforces joint filtering of the in- phase and quadrature signal components and has only 4 complex-valued independent filters it is not able to compensate for any imbalance between the in-phase and quadrature components. The constraints of the 2×2 MIMO, equation (3.1), are valid only when there is no delay skew; $\delta_{X\_I} = \delta_{X\_Q} = \delta_{Y\_I} = \delta_{Y\_Q} = 0$, with respect to figure 3.9(a) (detailed derivation in appendix A.1). By removing the constraints and using 16 real- valued independent filters, each of the four (in-phase and quadrature across two polarisations) input components can have a different transfer function through the equaliser; this allows for tracking and compensation of any imbalance.

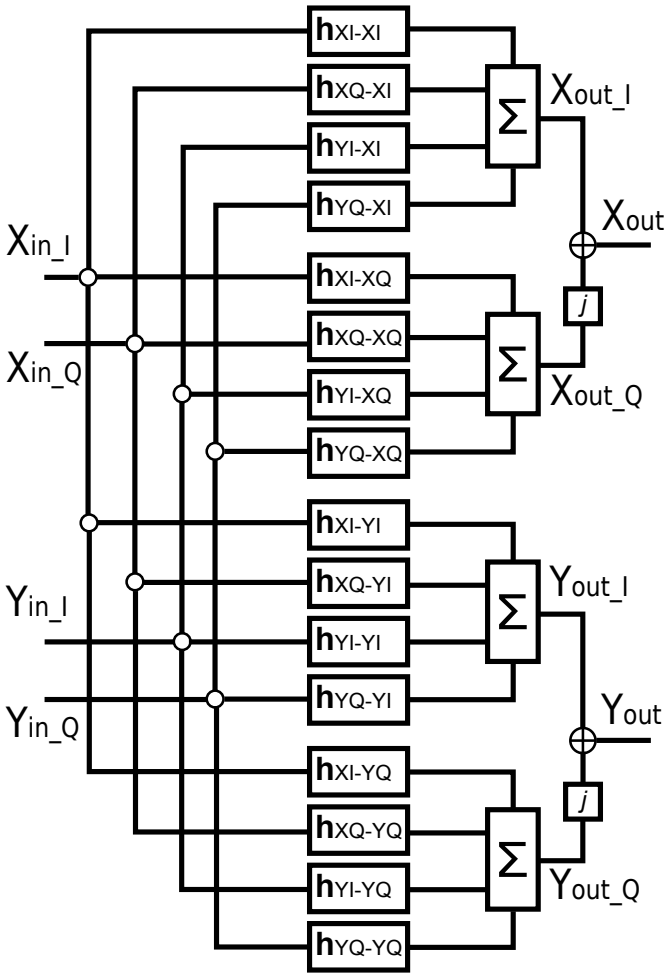

Figure 3.7: Equaliser structure for 4×4 MIMO.

$$
\begin{aligned}
\Re\{\mathbf{h}_{XX}\} &\Longrightarrow \mathbf{h}_{XI\_XI} = \mathbf{h}_{XQ\_XQ} \\
\Im\{\mathbf{h}_{XX}\} &\Longrightarrow \mathbf{h}_{XI\_XQ} = -\mathbf{h}_{XQ\_XI} \\
\Re\{\mathbf{h}_{XY}\} &\Longrightarrow \mathbf{h}_{YI\_XI} = \mathbf{h}_{YQ\_XQ} \\
\Im\{\mathbf{h}_{XY}\} &\Longrightarrow \mathbf{h}_{YI\_XQ} = -\mathbf{h}_{YQ\_XI} \\
\Re\{\mathbf{h}_{YX}\} &\Longrightarrow \mathbf{h}_{XI\_YI} = \mathbf{h}_{XQ\_YQ} \\
\Im\{\mathbf{h}_{YX}\} &\Longrightarrow \mathbf{h}_{XI\_YQ} = -\mathbf{h}_{XQ\_YI} \\
\Re\{\mathbf{h}_{YY}\} &\Longrightarrow \mathbf{h}_{YI\_YI} = \mathbf{h}_{YQ\_YQ} \\
\Im\{\mathbf{h}_{YY}\} &\Longrightarrow \mathbf{h}_{YI\_YQ} = -\mathbf{h}_{YQ\_YI}
\end{aligned}
\tag{3.1}
$$

To update the taps of the filter a CMA is implemented for QPSK and a MMA for higher order QAM, which does not require training symbols and can be updated using a blind algorithm (section 2.4.2). Although false locking (equaliser convergence on only

one polarisation) is possible, it was not observed during experiments and simulations. Initial simulations shown in figure 3.8 illustrate that the probability of false locking is lower than for 2×2 MIMO. The errors and filter tap update calculations are shown in equations (3.2) and (3.3); where R is the radius of the nearest constellation ring, ε_x and ε_y are the errors in X and Y polarisations respectively and μ is the convergence parameter and $\leftarrow$ indicates an update.

$$\begin{aligned} \varepsilon_x &\leftarrow R^2 - (\mathrm{X}_{out\_I}^2 + \mathrm{X}_{out\_Q}^2) \\ \varepsilon_y &\leftarrow R^2 - (\mathrm{Y}_{out\_I}^2 + \mathrm{Y}_{out\_Q}^2) \end{aligned} \tag{3.2}$$

$$\begin{aligned} \mathbf{h}_{XI\_XI} &\leftarrow \mathbf{h}_{XI\_XI} + \mu\varepsilon_x \mathrm{X}_{out\_I}\mathbf{X}_{in\_I} \\ \mathbf{h}_{XQ\_XI} &\leftarrow \mathbf{h}_{XQ\_XI} + \mu\varepsilon_x \mathrm{X}_{out\_I}\mathbf{X}_{in\_Q} \\ \mathbf{h}_{YI\_XI} &\leftarrow \mathbf{h}_{YI\_XI} + \mu\varepsilon_x \mathrm{X}_{out\_I}\mathbf{Y}_{in\_I} \\ \mathbf{h}_{YQ\_XI} &\leftarrow \mathbf{h}_{YQ\_XI} + \mu\varepsilon_x \mathrm{X}_{out\_I}\mathbf{Y}_{in\_Q} \\ \\ \mathbf{h}_{XI\_XQ} &\leftarrow \mathbf{h}_{XI\_XQ} + \mu\varepsilon_x \mathrm{X}_{out\_Q}\mathbf{X}_{in\_I} \\ \mathbf{h}_{XQ\_XQ} &\leftarrow \mathbf{h}_{XQ\_XQ} + \mu\varepsilon_x \mathrm{X}_{out\_Q}\mathbf{X}_{in\_Q} \\ \mathbf{h}_{YI\_XQ} &\leftarrow \mathbf{h}_{YI\_XQ} + \mu\varepsilon_x \mathrm{X}_{out\_Q}\mathbf{Y}_{in\_I} \\ \mathbf{h}_{YQ\_XQ} &\leftarrow \mathbf{h}_{YQ\_XQ} + \mu\varepsilon_x \mathrm{X}_{out\_Q}\mathbf{Y}_{in\_Q} \end{aligned} \tag{3.3}$$

$$\begin{aligned} \mathbf{h}_{XI\_YI} &\leftarrow \mathbf{h}_{XI\_YI} + \mu\varepsilon_y \mathrm{Y}_{out\_I}\mathbf{X}_{in\_I} \\ \mathbf{h}_{XQ\_YI} &\leftarrow \mathbf{h}_{XQ\_YI} + \mu\varepsilon_y \mathrm{Y}_{out\_I}\mathbf{X}_{in\_Q} \\ \mathbf{h}_{YI\_YI} &\leftarrow \mathbf{h}_{YI\_YI} + \mu\varepsilon_y \mathrm{Y}_{out\_I}\mathbf{Y}_{in\_I} \\ \mathbf{h}_{YQ\_YI} &\leftarrow \mathbf{h}_{YQ\_YI} + \mu\varepsilon_y \mathrm{Y}_{out\_I}\mathbf{Y}_{in\_Q} \\ \\ \mathbf{h}_{XI\_YQ} &\leftarrow \mathbf{h}_{XI\_YQ} + \mu\varepsilon_y \mathrm{Y}_{out\_Q}\mathbf{X}_{in\_I} \\ \mathbf{h}_{XQ\_YQ} &\leftarrow \mathbf{h}_{XQ\_YQ} + \mu\varepsilon_y \mathrm{Y}_{out\_Q}\mathbf{X}_{in\_Q} \\ \mathbf{h}_{YI\_YQ} &\leftarrow \mathbf{h}_{YI\_YQ} + \mu\varepsilon_y \mathrm{Y}_{out\_Q}\mathbf{Y}_{in\_I} \\ \mathbf{h}_{YQ\_YQ} &\leftarrow \mathbf{h}_{YQ\_YQ} + \mu\varepsilon_y \mathrm{Y}_{out\_Q}\mathbf{Y}_{in\_Q} \end{aligned}$$

It should be noted that both equaliser structures have the same computational com-

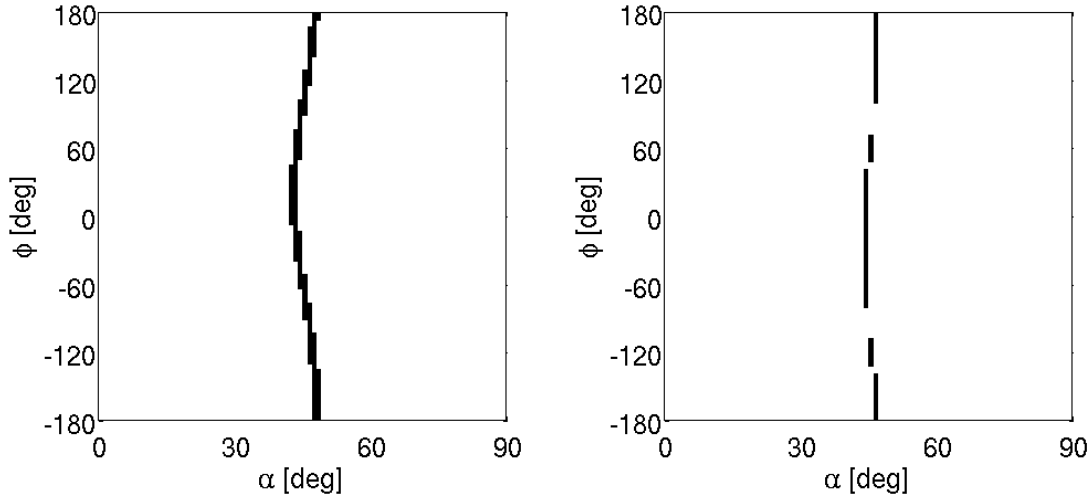

Figure 3.8: False locking for different rotation angles: **a)** 2×2 equaliser **b)** proposed 4×4 equaliser.

plexity. This is because the 2×2 MIMO structure requires complex multiplications, where each complex multiplication consists of four real multiplications and two additions, while the 4×4 MIMO structure is using only real multiplications. It is also possible to implement complex multiplications using three real multiplications and five additions [42], however, in some scenarios this might increase latency because of the extra additions. In either case, the hardware memory is doubled for the 16 real filters (4×4) versus the four complex filters (2×2), however for relatively short filter lengths the memory increase is small compared to other hardware resources.

3.2.2 Simulation and experimental configuration

In simulation a 448 Gbit/s (56 GBd) PDM-16QAM signal was generated. Nyquist filtering was implemented using a RRC filter with a rolloff of 0.01; when Nyquist filtering was not used this filter was omitted. The signal was then detected using a coherent receiver. A LO with a 100 kHz linewidth and a frequency offset of 200 MHz was used to simulate what can be achieved in the lab using free running lasers. The delay skews were added in the frequency domain before down sampling to 2 Sa/symbol. The delays were set as follows; δ_{X_I} was kept at zero, $0 \leq \delta_{X\_Q} \leq 0.5T$, $\delta_{Y\_I} = -0.5\delta_{X\_Q}$ and $\delta_{Y\_Q} = 0.25\delta_{X\_Q}$, with respect to figure 3.9(a) and T representing the symbol period. This is forcing the equaliser to compensate for multiple different delays. When

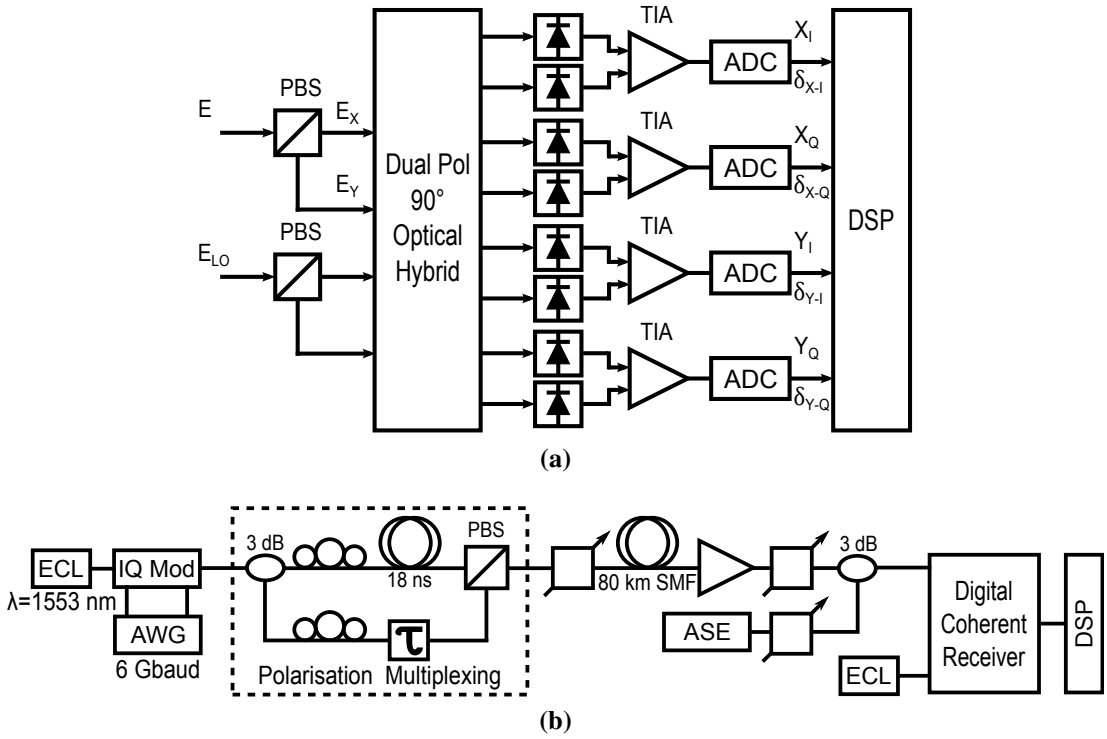

Figure 3.9: a) Optical Front End. X and Y represent each of the two polarisations while I and Q represent the in-phase and quadrature components. **b)** Experimental configuration used to test adaptive 4×4 equaliser structure for in-phase/quadrature skew.

using Nyquist filters the same filter can be applied at the receiver side as a matched filter. This can be done by using a FIR with precomputed taps, however, any imbalance between the in-phase and quadrature components needs to be corrected before the matched filtering. An alternative approach is to increase the number of equaliser taps and allow the equaliser to converge to the matched filter while also compensating for any imbalance. Either a conventional 2×2 or the proposed 4×4 equaliser were used for this. Afterwards, frequency offset removal was performed before CPE using DD phase estimator [26] (section 2.4.3). Finally hard decisions were made using the maximum likelihood algorithm k-means clustering [43] before symbol decoding and BER estimation.

The configuration used to collect the data is displayed in figure 3.9(b). An ECL with a linewidth of 20 kHz was modulated using an IQ modulator, driven by an AWG operating at 12 GSa/s to produce 6 GBd QPSK and 16QAM. The signals were pre-filtered with the same RRC filter as in simulations. PDM was emulated by passing the signal through a polarisation multiplexing stage. Afterwards, the signal peak power was set to 0 dBm, to minimize any non-linear effects during the transmission through

80 km of SMF. At the receiver the signal was first pre-amplified using an EDFA and noise-loaded before detection by a phase- and polarisation-diverse digital coherent receiver. The LO laser was another ECL with a linewidth of 100 kHz. After sampling the signal at 50 GSa/s, PDM-16QAM was processed as previously described, while for PDM-QPSK a 4^{th} power Viterbi & Viterbi phase estimator [25] (section 2.4.3) and simple hard decisions were used instead.

3.2.3 Results and discussion

In simulations, before the delay skew was applied the signal was noise loaded to a BER of 3.8×10^{-3} [44]. To determine the number of taps required for the equaliser to approximate the matched filter 1.8 ps (about 10% of the symbol period) of delay skew was added to the signal and the number of taps was varied. Figure 3.11(a) shows that the performance for both equalisers improves as the number of taps is increased until 31 taps with no significant gain afterwards. Therefore the number of taps used for the equaliser was set to 31. In figure 3.11(b) the delay skew was varied from 0% to 50% of the symbol period. As the delay skew increases the penalty for using the 2×2 equaliser increases rapidly as it is not able to compensate for the delays. The Nyquist filtered signal suffers more severely from delay skew therefore this section will focus on this case. The proposed 4×4 equaliser has a constant performance for all the delays up to 50% of the symbol period (9 ps) with and without Nyquist filtering. When the delay is 30% of the symbol period, as recommended by OIF for PDM-QPSK, the gain for using the 4×4 equaliser is more than 5 dB with respect to required OSNR.

Verification of the simulation was done experimentally with 6 GBd PDM-QPSK and PDM-16QAM. The signals were noise loaded at the receiver before detection, as in simulations. The delays added to the signals were proportional to the symbol period for a valid comparison between the 6 GBd signals and the simulated 56 GBd.

Similarly to the simulation the number of taps required for a matched filter approximation, in the presence of 17 ps delay (10% of the symbol period), was investigated. The results for PDM-QPSK, shown in figure 3.12(a), demonstrate that 25 taps are required. The delay skew was then varied from 0% to 50% of the symbol period, figure 3.12(b). The same procedure was then applied to PDM-16QAM; determining that 31 taps would be required for saturation and then varying the delays, figure 3.12(c) and (d). At a delay

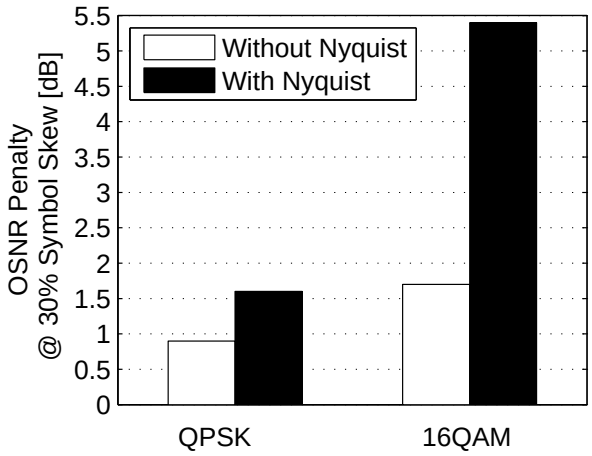

Figure 3.10: OSNR penalty at a skew of 30% symbol period (as recommended by OIF) for different configurations.

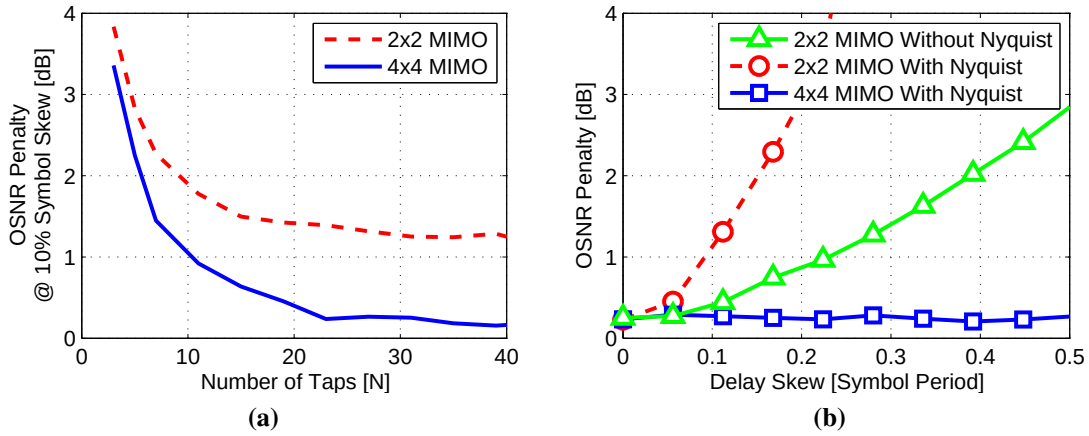

Figure 3.11: Simulation results for 56 GBd PDM-16QAM: **a)** OSNR penalty vs. number of equaliser taps in the presence of 1.8 ps delay skew (about 10% of the symbol period). **b)** OSNR penalty vs. delay skew, using 31 equaliser taps. The 4×4 MIMO has the same performance with and without Nyquist filtering.

of 30%, as recommended by OIF the penalty for PDM-QPSK is about 1.6 dB, while for PDM-16QAM is larger than 5 dB, figure 3.10.

There is excellent agreement between the simulation results, figure 3.11(b), and the experimental results, figure 3.12(d). The experimental results for PDM-QPSK, figure 3.12(b), exhibit the same trend, although the penalty for the 2×2 equaliser is smaller compared to PDM-16QAM. In all three scenarios the 4×4 equaliser was able to compensate for delay skews up to half a symbol period with no extra penalty. While the 2×2 equaliser was not able to compensate for the delay skew and the performance was severely degraded.

As a narrow frequency grid is one of the way to improve the total capacity of

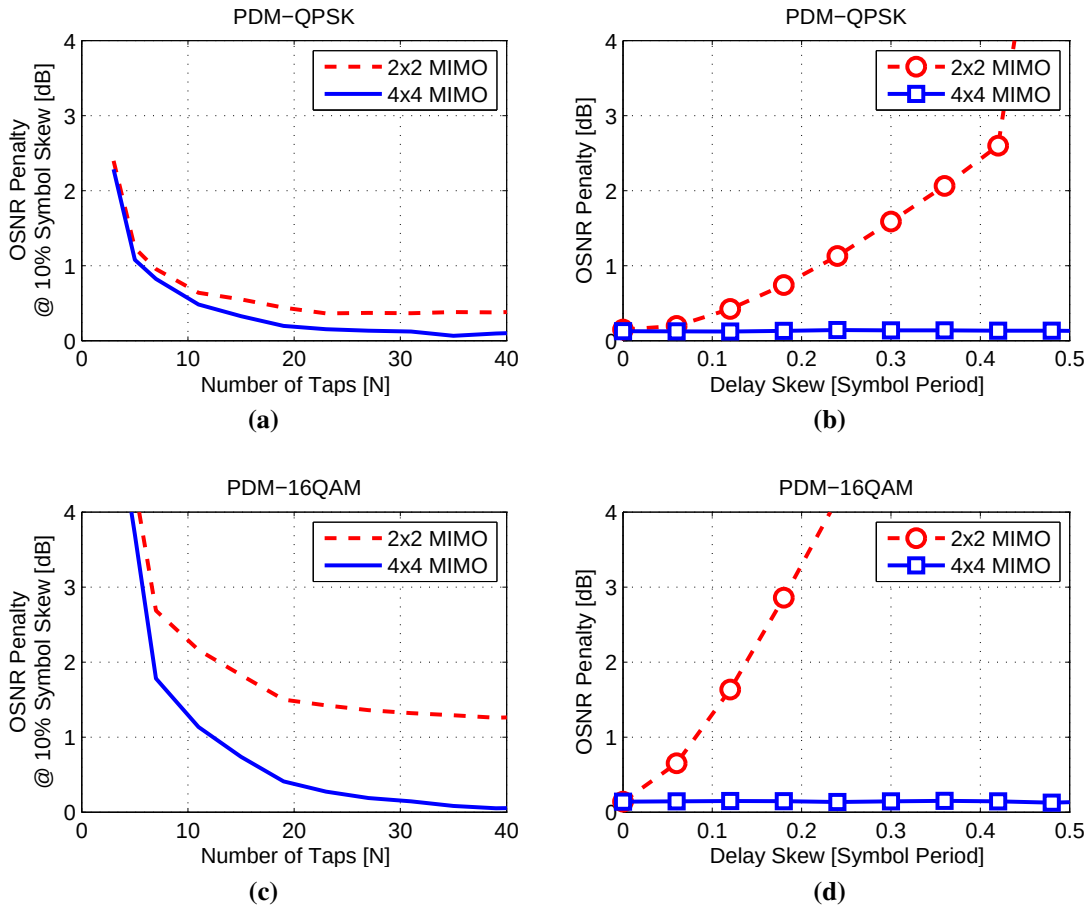

Figure 3.12: Experimental results for Nyquist filtered 6 GBd signals. OSNR penalty vs. number of equaliser taps in the presence of 17 ps delay skew (about 10% of the symbol period): **a)** PDM-QPSK, **c)** PDM-16QAM. OSNR penalty vs. delay skew: **b)** PDM-QPSK using 25 equaliser taps, **d)** PDM-16QAM using 31 equaliser taps.

future networks Nyquist filtering is a key subsystem that needs to be incorporated into current systems without placing unnecessary constraints on the optical components. Furthermore, as shown in this section higher order modulation formats are significantly less tolerant to delay skew imperfections. Therefore this adaptive equaliser is an essential technology which can enable next generation optical systems.

3.3 Adaptive Chromatic Dispersion (CD) compensation

As previously discussed, coherent detection has proven to be a very attractive prospect for next generation optical networks because, when aided by high speed ADC, the entire optical field is translated into the digital domain. This enables DSP to be used to compensate the impairments of the optical channel. Methods to compensate linear

impairments such as PMD and CD are well known [22]. In practice optical networks are not static and a signal between two nodes can take different routes through the system. The receiving node does not know a priori which path has been traversed, which means that the transmission distance and the accumulated channel impairments are unknown. Although, CD can easily be compensated the total accumulated amount needs to be known in advance for accurate compensation. Having a system that can adaptively compensate for CD without knowing the transmission distance would then ease routing constraints and allow for high reconfigurability within the network without considering which path was used between two nodes. There are techniques that attempt to estimate the CD but they have shortcomings. Look-up tables require additional logic and often have large feedback loops delaying convergence [45; 46]. It is possible to use training symbols, however, they lower the SE and the training sequence length needs to be proportional to the accumulated CD [47]. Finally, brute force algorithms, which test an array of dispersion values have a trade-off between accuracy and convergence speed [48].

It is well known that conventional 2×2 equalisers can compensate for a small amounts of CD; such as in short reach transmission systems or in the case of residual dispersion after a discrete (non-adaptive) CD compensator. However, they are unsuitable for compensating large amounts of dispersion as they become unstable when the number of taps is increased to accommodate the increased channel memory. This section investigates a modified blind equaliser which overcomes this problem and is able to adaptively estimate the filter coefficients for CD compensation. The equaliser is used for pre-convergence before switching to the conventional equaliser. The performance is demonstrated through simulations and experiment using 10.7 GBd PDM-QPSK compensating for 88,000 ps/nm CD (5,240 km).

3.3.1 Adaptive CD equalisation algorithm

Conventional 2×2 equalisers, figure 3.13(a), are used primarily to track time dependent polarisation rotations. To compensate for CD, the length of the equaliser has to be larger than the memory of channel, however, this leads to unstable behaviour. By using an equaliser dedicated to estimating the CD for pre-convergence, additional constraints can be applied to improve stability.

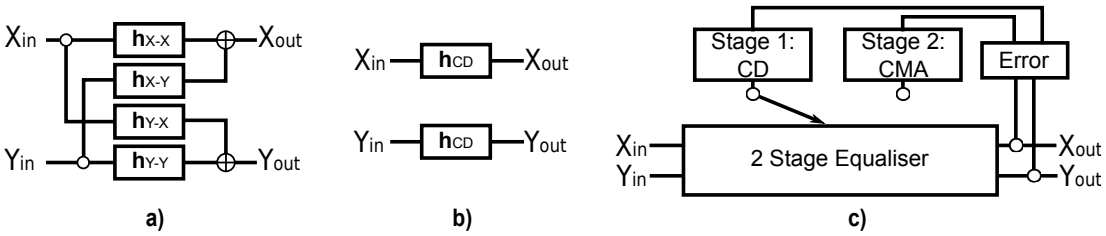

Figure 3.13: a) Equaliser structure for 2×2 MIMO **b)** Modified equaliser for adaptive CD compensation. **c)** Proposed two stage equaliser.

CD is a phase shift with a quadratic frequency dependence, which affects both polarisations equally. Therefore, a CD equaliser should apply the same filter on both polarisations and there should be no power exchange between the polarisations. The proposed equaliser structure can be seen in figure 3.13(b). The error terms for the equaliser can be calculated using a CMA, equation (3.4). The update can be averaged over the two polarisations, equation (3.4), to get a better estimate. While the approach presented here tries to achieve constant power per polarisation, a modified approach where constant power across both polarization is considered was later developed and is detailed in appendix A.2. Once convergence has been achieved the equaliser is switched to the conventional update scheme, figure 3.13(c). The filters $\mathbf{h}_{X-X}$ and $\mathbf{h}_{Y-Y}$ are initialised as $\mathbf{h}_{CD}$, while $\mathbf{h}_{X-Y}$ and $\mathbf{h}_{Y-X}$ are initialised to zero. In a hardware implementation, $\mathbf{h}_{CD}$ can use the same resources as $\mathbf{h}_{X-X}$ and $\mathbf{h}_{Y-Y}$.

$$\begin{aligned} \varepsilon_x &\leftarrow 1-|\mathrm{X}_{out}|^2 \qquad \varepsilon_y \leftarrow 1-|\mathrm{Y}_{out}|^2 \\ \mathbf{h}_{CD} &\leftarrow \mathbf{h}_{CD}+\mu(\varepsilon_x \mathrm{X}_{out}\mathbf{X}^*_{in}+\varepsilon_y \mathrm{Y}_{out}\mathbf{Y}^*_{in})/2 \end{aligned} \tag{3.4}$$

For any given network, the range of link lengths would be known in advance and it will determine the range over which the dispersion will vary in the network. To improve equaliser convergence speed, a fixed CD filter can be used to compensate 50% of the maximum CD in the network, followed by an equaliser to adaptively compensate up to a further ±50%. Alternatively, the equaliser can be initialised with tap weights equal to 50% of the maximum CD; the approach taken herein. The initial taps are calculated using the algorithm in [22]. After the modified equaliser has converged, the taps are passed to the conventional equaliser which is able to fine tune the CD compensation and additionally compensate for other channel impairments. Although the equaliser requires more taps than conventional systems, by using a frequency domain implementation

[49] the complexity can be reduced significantly while the potential for a reconfigurable network is tremendous. Additionally, having a longer equaliser allows fixed filters for CD compensation and matched filtering, when Nyquist pulse shaping is used, to be omitted.

3.3.2 Simulation and experimental configuration

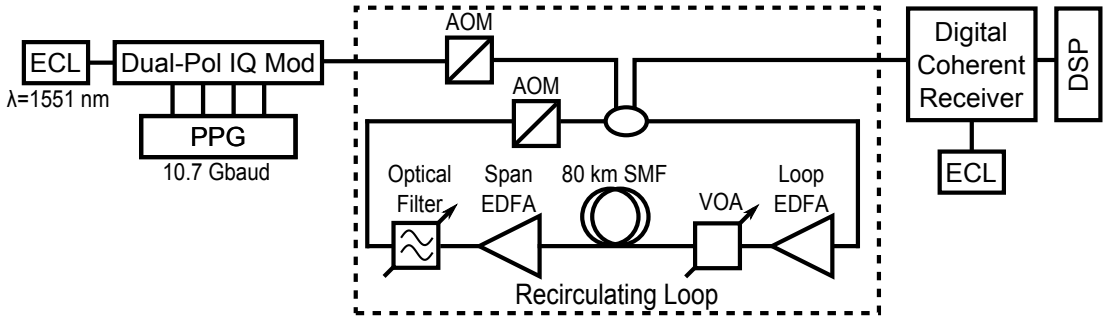

Figure 3.14: Experimental configuration used to test adaptive CD compensation.

In simulations 42.8 Gbit/s (10.7 GBd) PDM-QPSK was generated before CD was added to the signal and detected using a coherent receiver. A linewidth of 300 kHz and a frequency offset of 200 MHz was used to simulate realistic conditions. The signal was quantised and a polarisation rotation of $\pi/9$ was included to avoid potential performance enhancement from ideal alignment. The signal was then down sampled to 2 Sa/symbol; from 4 Sa/symbol. The equaliser length was set to the required number of taps to compensate the CD [22]. The equaliser was initialised with the filter coefficients for a CD filter compensating for 50% of the total dispersion. After pre-convergence using the modified equaliser the taps were passed to a conventional equaliser to undo the polarisation rotation. A 4^{th} power frequency offset removal and CPE [25] were applied (section 2.4.3). Finally, hard decisions, symbol decoding and BER estimation were performed over 2^{17} symbols.

The experimental configuration is shown in figure 3.14. An ECL with a linewidth of 20 kHz was modulated using a Dual-Polarisation IQ modulator, driven by four random binary streams (8192 bits decorrelation), from a pulse pattern generator, to produce 10.7 GBd PDM-QPSK. The signal power was set to -6 dBm, the optimal launch power [50]. A single-span recirculating loop with 80.7 km of standard SMF was used for transmission. Each iteration through the recirculating loop accumulated a dispersion

of 1,354 ps/nm. Two EDFAs with noise figures of 5 dB were used, one to set the launch power into each span and the other to compensate the loss due to connecting components. A tunable optical filter was used to reject out of band noise. At the receiver the signal was detected by a phase- and polarisation-diverse coherent receiver. The LO laser was an ECL with a 100 kHz linewidth. After sampling the signal at 50 GSa/s, the signal was down sampled to 2 Sa/symbol and processed as previously described.

3.3.3 Results and discussion

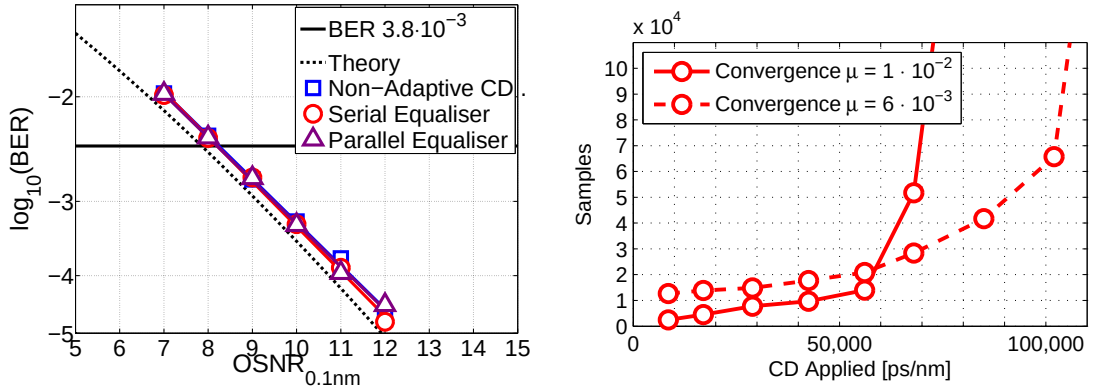

Figure 3.15: Simulation results: **a)** Different methods for compensating 50,000ps/nm CD. **b)** Convergence rate using different μ values.

In simulations the signal was noise loaded and 50,000 ps/nm CD (3000 km with 10.7 GBd) were added to evaluate the performance of the equaliser. In figure 3.15(a) the results are compared to CD compensation using a non-adaptive CD filter with 187 taps (the required number of taps to compensate the CD) and conventional equalisation with 15 taps. The modified equaliser using 187 taps was initialised with 25,000 ps/nm CD, as previously described. Both a serial implementation and a parallel implementation using a bus width of 256 samples are shown. This demonstrates that there is no performance degradation for using the equaliser to compensate for the CD and that a parallel [51] or frequency domain implementation with lower computational complexity could be used.

Equaliser convergence is defined as $\pm 1\%$ of the applied CD, estimated from the equaliser taps [52]. For consistency, the convergence speed of the equaliser was investigated using the serial implementation for all cases. The results are displayed in figure 3.15(b). Using a μ of 1×10^{-2} (equation (3.4)) enables faster convergence in the

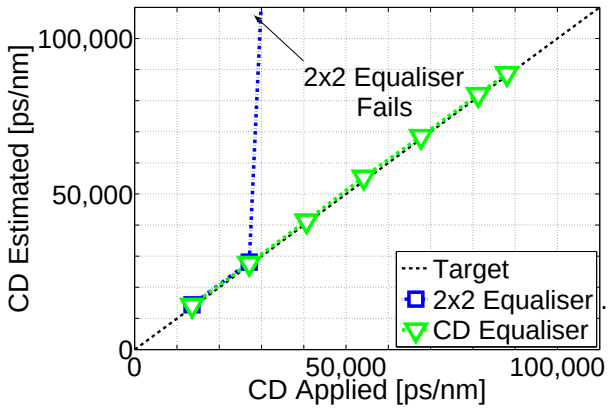

Figure 3.16: Experimental results CD applied versus CD estimated from equaliser taps.

presence of smaller CD, however, the equaliser converges less reliably for larger CD. When the μ factor is lowered to 6×10^{-3} a slower but more consistent convergence can be observed. This suggests that, with sufficient time and judicious selection of the convergence parameter, μ, the equaliser could compensate for arbitrarily large CD.

After convergence of the equaliser, the compensated CD was estimated from the equaliser taps to verify that the correct CD was compensated. In figure 3.16 experimental results are shown where the signal was transmitted up to distances of 5,240 km. It is clear that there is excellent agreement between the amount of CD that is applied and the compensated CD for dispersion, up to 88,000 ps/nm. When using the conventional 2×2 equaliser, only CD up to 30,000 ps/nm could be compensated; beyond this it fails to converge even as the convergence parameter, μ, was decreased.

Although, the technique is demonstrated with 10.7 GBd signal it can equally be applied a different symbol rates. The total dispersion of 88,000 ps/nm, which was experimentally demonstrated, will, however, be accumulated after a different distance; for 6 GBd a distance of 16,700 km can be propagated while for 28 GBd only 760 km is required. The network size limits the maximum applicable symbol rate, one potential network where this can be applied to is the German national network DTAG/T-Systems [53] where the longest shortest path is 1000 km which would allow for 24 GBd. However, the algorithm can further be optimised based on the minimum shortest distance, which would define the smallest accumulated dispersion. By knowing the range of possible dispersions the initialisation can be tailored (unlike in this section where the initialisation is set to half of the total dispersion) to allow for a convergence

within this smaller region.

Dynamic networking, based on the traffic demand, is a promising way to better utilise the capacity of a network. However, the transceivers in the network will need to be able to handle data from different location sources. This section has introduced an algorithm that can adaptively compensate CD in a network scenario without prior knowledge of signal's origin. It would enable high reconfigurability and ease the routing constraints. However, the algorithm will have to be optimised for a specific network to allow for reliable and fast convergence.

3.4 Low complexity equalisation

In section 3.1 digital spectral shaping was used to limit the bandwidth of the channel and reduce guardbands between channels. However, as shown in section 3.2 this increased the sensitivity to imperfection in the coherent receiver, most notably to receiver delay skew between the in- phase and quadrature components, especially for higher order modulation formats such as 16QAM. However, as matched filtering cannot be applied before the delay skews are compensated the equaliser was modified to be able to adaptively compensate for delay skews and apply the matched filter. Additionally, the equaliser was further modified in section 3.3 to adaptively compensate for chromatic dispersion as well. While those changes allow for flexible and adaptive compensation, to achieve optimal performance the number of equaliser taps would have to be increased; leading to higher computational complexity. This section investigates how the complexity of the equaliser can be decreased without losing any of the benefit previously demonstrated.

Complexity of the DSP is directly related to the power consumption, because multiplications consume more power [54] than additions[2] computational complexity is often expressed in terms of number of real-valued multiplications. By reducing or eliminating the multiplications the complexity and the total power consumption can be decreased, making the DSP subsystem more attractive for power restricted applications.

The equaliser can be broken down into two components; filtering (applying the FIR) and updating the filter coefficients. Using a direct implementation, in the time

[2]As the number of bits used to represent a number is decreased the power consumption for additions and multiplications become comparable.

domain, the complexity of the two components is the same [55] with respect to real multiplications. The complexity of first component, filtering, can be decreased by applying the filter in the frequency domain. As the number of taps, N, is increased filtering in the frequency domain scales as $O(N\log_2(N))$ compared to $O(N^2)$ in the time domain. This section addresses the complexity of the second component of the equaliser; updating the filter coefficients, by using a simplified update algorithms [54; 55], of the 4×4 equaliser discussed in section 3.2. The 4×4 equaliser maintains the ability to compensate the receiver skew, while also applying the matched filter and compensating for chromatic dispersion. Transmission of 15 GBd PDM-16QAM (100 Gbit/s) over 500 km with no dedicated chromatic dispersion compensation, is demonstrated as a metro scale application of this equaliser although the update scheme can be used for all previously mentioned applications of the equaliser. Afterwards this technique is experimentally verified using 6 GBd Nyquist PDM-16QAM over 1,600 km.

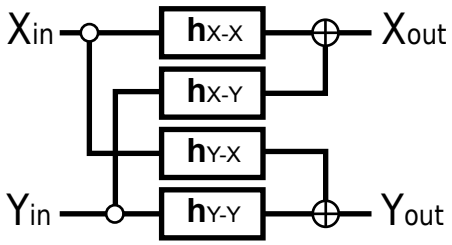

Figure 3.17: equaliser structure for 2×2 MIMO.

3.4.1 Equaliser update algorithm

The 2×2 and 4×4 equaliser structures are again shown here in figures 3.17 and 3.18 respectively, while the update algorithms are summarized in equations (3.7), (3.8), and (3.9). Equation (3.7) (original equation (2.20)) represents the general error term for a MMA, where R is the amplitude of the constellation ring closest to the point k_{out}. Equation (3.8) (original equation (2.21)) is the update algorithm for the four complex-valued FIRs of the 2×2 equalisers, where μ is the convergence parameter while n and m are respectively the inputs and outputs of the equaliser. Finally, equation (3.9) (original equation (3.2)) represents the update for of the 16 real-valued FIRs of the 4×4 equaliser.

For each tap of each FIR filter there is a multiplication of the form $\varepsilon_k\ \mathrm{n}_{out}\ \mathrm{m}_{in}$. By discarding the amplitude information of the gradient term, and only keeping the

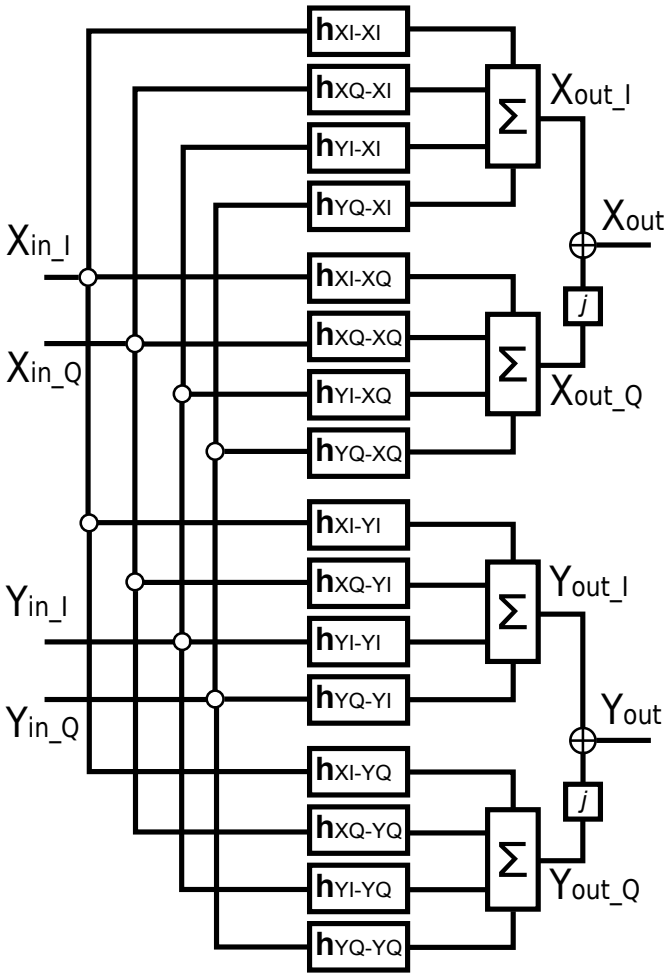

Figure 3.18: Equaliser structure for 4×4 MIMO.

sign, multiplications can be replaced with inverters[3], which require fewer hardware resources. In this work, two alternatives were investigated; Sign-Data: ε_k csgn(n_{out}) m_{in} and Sign-Sign: sgn(ε_k) csgn(n_{out}) m_{in}. Where sgn and csgn are the real and the complex signum functions respectively, equations (3.5, 3.6), where a and z are real and complex number respectively, [56]. The simplified update schemes applied to the 4×4 equaliser are shown in equation (3.10).

$$\text{sgn}(a) = \begin{cases} -1 & \text{if } a < 0 \\ 0 & \text{if } a = 0 \\ 1 & \text{otherwise} \end{cases} \tag{3.5}$$

$$\text{csgn}(z) = \text{sgn}(\Re(z)) + j\text{sgn}(\Im(z)) \tag{3.6}$$

[3]Inverters change the sign of the number, multiplication with -1. If numbers are represented with two's complement inversion is implemented by flipping all bits and adding 1.

$$\varepsilon_k \leftarrow R^2 - |\mathrm{k}_{out}|^2 \qquad k \in \{X,Y\} \tag{3.7}$$

$$\mathbf{h}_{mn} \leftarrow \mathbf{h}_{mn} + \mu\, \varepsilon_k\, \mathrm{n}_{out}\, \mathbf{m}_{in}^* \qquad m,n \in \{X,Y\} \tag{3.8}$$

$$\mathbf{h}_{mn} \leftarrow \mathbf{h}_{mn} + \mu\, \varepsilon_k\, \mathrm{n}_{out}\, \mathbf{m}_{in} \qquad m,n \in \{XI,XQ,YI,YQ\} \tag{3.9}$$

$$\left.\begin{aligned} \mathbf{h}_{mn} &\leftarrow \mathbf{h}_{mn} + \mu\, \varepsilon_k\, \mathrm{sgn}(\mathrm{n}_{out})\, \mathbf{m}_{in} \\ \mathbf{h}_{mn} &\leftarrow \mathbf{h}_{mn} + \mu\, \mathrm{sgn}(\varepsilon_k)\, \mathrm{sgn}(\mathrm{n}_{out})\, \mathbf{m}_{in} \end{aligned}\right\} \quad m,n \in \{XI,XQ,YI,YQ\} \tag{3.10}$$

The computational complexity for the different update schemes is summarized in table 3.1, and is extended in appendix A.3. It should be noted that four real-valued multiplications and two real-valued additions per complex multiplication are assumed. The number of multiplications for the 2×2 and 4×4 equalisers using the conventional update scheme is the same while for the Sign-Data and Sign-Sign algorithms the multiplications are replaced by inverters.

	Real Multiplications	Real Additions	Inverters
2×2 Conventional	16N + 4	16N	4N+2
4×4 Conventional	16N + 4	16N	0
4×4 Sign-Data	8N	16N	16N
4×4 Sign-Sign	0	16N	16N+8

Table 3.1: Computational implementation complexity for different update schemes.

3.4.2 Simulation and experimental configuration

In simulations 120 Gbit/s (15 GBd) PDM-16QAM was generated, assuming 20% hard-decision FEC, with a BER limit of 1.5×10^{-2} [35]. Nyquist filtering was implemented using a RRC filter with a rolloff of 0.01. The signal was then detected with a coherent receiver and down sampled to 2 Sa/symbol before adding the delay skews. The delays were set as follows; δ_{X_I} was fixed to zero, δ_{X_Q} was varied from zero to a quarter of the symbol period, $\delta_{Y\_I} = -0.5 \cdot \delta_{X\_Q}$ and $\delta_{Y\_Q} = 0.25 \cdot \delta_{X\_Q}$, with respect to figure 3.9(a), forcing the equaliser to compensate for multiple different delays. The equaliser was used to apply the matched filter and compensate the chromatic dispersion as no dedicated filters were used, however, it was initialised with the filter coefficients necessary to compensate the chromatic dispersion, as in section 3.3. Afterwards, frequency offset removal was performed before a CPE using DD phase estimator [26] (section 2.4.3).

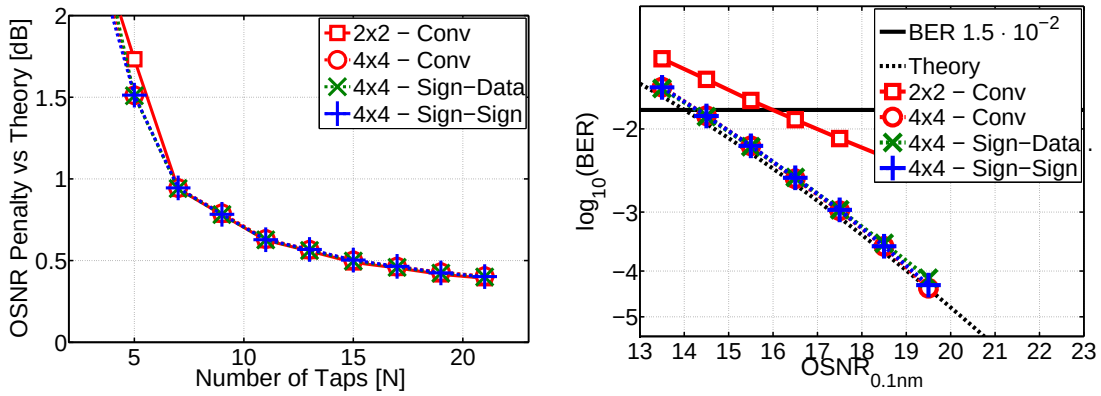

Figure 3.19: Simulation results for Nyquist 15 GBd PDM-16QAM: **a)** OSNR penalty vs. number of equaliser taps. This result is independent of the symbol rate. **b)** BER vs. OSNR for different update schemes at 15% IQ delay skews.

Finally hard decisions were made using the maximum likelihood algorithm k-means clustering [43] before symbol decoding and BER estimation.

Experimentally, an ECL with 100 kHz linewidth was modulated with 6 GBd 16QAM using an AWG operating at 12 GSa/s. PDM was emulated by passing the signal through a polarisation multiplexing stage. A single-span recirculating loop with 80.7 km of standard single mode fibre was used for transmission. At the receiver the signal was detected by a phase- and polarisation-diverse coherent receiver. The local oscillator laser was an ECL with a 100 kHz linewidth. The signal was sampled at 50 GSa/s and processed as previously described.

3.4.3 Results and discussion

Applying a matched filter before delays are compensated can introduce a penalty, therefore the matched filter was applied as part of the equaliser. The number of taps required to achieve less than 0.5 dB implementation penalty was verified in simulation. Figure 3.19(a) indicates that at least 15 taps are required. In these simulations no time dependent elements were included making the results independent of symbol rate.

Afterwards, 15 GBd PDM-16QAM was simulated, chromatic dispersion equivalent to 500 km of SMF (8,500 ps/nm) was added before the signal was detected and delay skews were introduced. No dedicated chromatic dispersion compensation was used instead the equaliser used 61 taps which were initialised with the dispersion coefficients. Instead of using separate filters for chromatic dispersion compensation, matched filtering

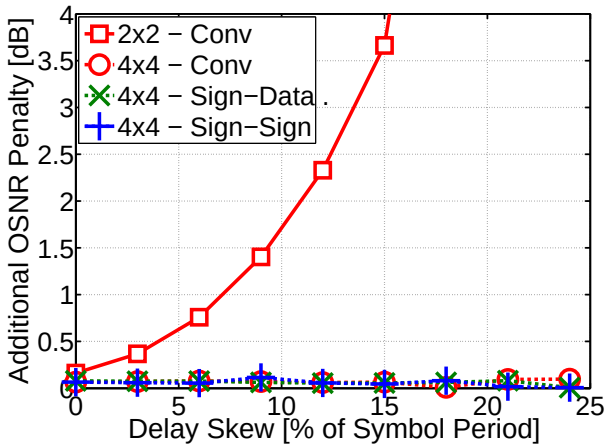

Figure 3.20: Experimental results for 6 GBd PDM-16QAM transmission over 1600 km; additional OSNR penalty vs. delay skews for different update schemes.

and equalisation, all linear filters were merged into a single adaptive equaliser saving DSP resources. Usually, the larger number of adaptive equaliser taps would require more computational resources, however, by using the simplified update algorithms, the computational complexity of the updates is made negligible compared to the FIR filter. Figure 3.19(b) shows that, when a IQ delay skew of 15% was introduced, the 2×2 equaliser exhibits an additional OSNR penalty of 1.7 dB, compared to the 4×4 equaliser, which was able to fully compensate the delay skew. Additionally, it can be seen that the low complexity update schemes, including the multiplier free Sign-Sign, have the same performance as the conventional 4×4 equaliser. These simulations did not include frequency offset and phase noise, which operate both on I and Q components, resulting in an underestimation of the penalty from IQ skew.

To verify the equaliser experimentally 6 GBd PDM-16QAM was transmitted over 1600 km and noise loaded before digitally adding delay skew. The equaliser used 15 taps; initialisation with chromatic dispersion coefficients was not required in this case as the equaliser was able to fully adapt. Figure 3.20 shows the penalty at the BER limit of 1.5×10^{-2} [35] as the delays are increased. The 4×4 equaliser was able to track the delays independently of the update algorithm in contrast to the 2×2 equaliser, which exhibits large OSNR penalties as the delays are increased. At a delay skew of 15% of the symbol period a penalty of 3.5 dB is observed.

The multiplier free update scheme for a 4×4 equaliser shown can compensate for IQ delay skew while applying a matched filter as well as compensate for chromatic dispersion. This is demonstrated in simulations using 15 GBd PDM-16QAM over

500 km and experimentally verified with 6 GBd PDM-16QAM over 1600 km. The 4×4 equaliser exhibits no additional penalty from the delay skews while significant performance degradation is observed for the conventional 2×2 equaliser.

This technique is very useful for system where there are power constraints on the DSP or there are limited computational resources. A 2×2 equaliser with the simplified update algorithm has been proposed for PON [55] and 4×4 could be used similarly for the delay skew compensation. Additionally, due to the resistance to CD, the technique could be applied to future low cost coherent metro scale networks where the CD can easily be compensated by the equaliser.

3.5 Phase noise compensation for higher order Quadrature Amplitude Modulation (QAM)

An alternative method for increasing capacity rather than decreasing channel spacing is to use higher order modulation formats which carry more information in the same spectral bandwidth. However, those modulation formats have stricter requirements such as; higher SNR and lower phase noise because the constellation points are closer together and the decision regions are smaller. The SNR can be increased by using EDFAs with lower noise figure and/or using ADC and DAC with higher resolution, however, those techniques are outside the scope of this work. This section will focus on how the phase noise tolerance can be increased with optical techniques and specialised DSP.

3.5.1 Phase directed equaliser (PDE)

Equalisation for 64QAM has previously been investigated to tackle low frequency distortions. A two stage approach has been previously used [57], where after initial equalisation, frequency offset and carrier phase estimation a second stage of equalisation with a long filter was carried out. This second filter is then able to compensate for low frequency distortions.

An alternative approach is to adopt an equaliser which is interleaved with DD-CPE (section 2.4.3), to do both equalisation and carrier phase recovery. Although the use of

this technique has previously been reported [58], this section evaluates the performance of this equaliser.

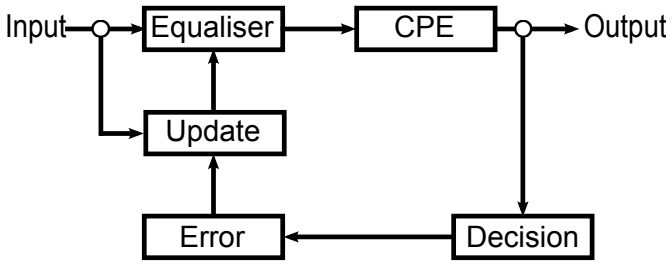

Figure 3.21: A DD equaliser interleaved with a CPE.

The joined algorithm is illustrated in figure 3.21. Frequency offset needs to be performed prior to equalisation otherwise the CPE will not be able to compensate the fast phase rotations and correct decision will not be possible. An equal number if symbols is equalised around the symbol of interest in order to provide a symmetrical window around the symbol of interest for the CPE. The phase is estimated and removed before a DD error is calculated. This error is then used to update the equaliser.

Simulation configuration

In simulations 72 Gbit/s (6 GBd) PDM-64QAM was generated and detected using a phase- and polarisation-diverse coherent receiver. A frequency offset of 200 MHz and a variable linewidth was used to investigate the performance of the equaliser. The signal was low pass filtered with a 5^{th} order Bessel filter to include the effect of electronics with bandwidth of 70% of the symbol rate. After detection the signal was down sampled to 2 Sa/symbol and normalised to unit power. An initial stage of equalisation was performed using a MMA with 25 taps, pre-converged with a CMA. Afterwards a 4^{th} power frequency offset removal was applied, section 2.4.3. Carrier phase removal was performed either by a DD phase estimator or by the interleaved equaliser, Phase Directed Equalizer (PDE). Finally, hard decisions, symbol decoding and BER counting were performed over 2^{17} symbols.

Results and discussion

The linewidth of the LO was set to 10 kHz and the signal was noise loaded to evaluate the performance of the equaliser[4]. Figure 3.22(a) shows the performance compared to using a MMA equaliser followed by a separate stage for carrier phase removal. In both scenarios the window length over which the phase was estimated was set to 32 symbols (in each direction of the symbol). It can be seen that there is a minor gain of 0.2 dB at a BER limit of 10^{-2}, however, there is no gain at higher OSNR where the two techniques perform equally. This indicates that if a different FEC code is employed with a higher BER limit the interleaved equaliser would be more beneficial.

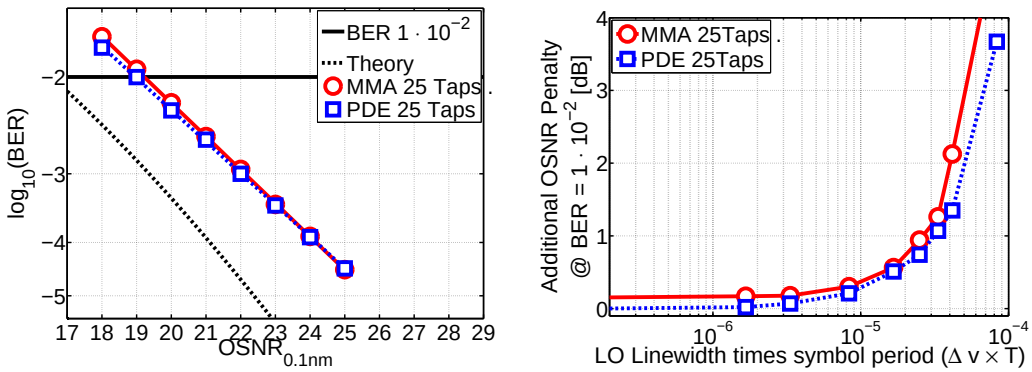

(a) **(b)**

Figure 3.22: Simulations results, for 6 GBd PDM-64QAM, comparing MMA to PDE. **a)** OSNR vs BER. **b**) (linewidth) $\times$ (symbol period) product ($\Delta\nu \times T$) vs additional OSNR penalty at a BER of 10^{-2}.

Furthermore, the phase noise tolerance was investigated, where the phase noise of the LO was varied, for each linewidth the phase estimate window was optimised (between 8 and 40 symbols, in each direction of the symbol). The results are displayed in figure 3.22(b), where additional OSNR penalty (at a BER limit of 10^{-2}) is plotted against the (linewidth) $\times$ (symbol period) product ($\Delta\nu \times T$) to make the results independent of symbol rate. It can be observed that both methods follow the same trajectory, the non-interleaved method has the 0.2 dB penalty (as previously observed) and smaller phase noise tolerance. At a 1 dB penalty the difference between the two approaches is 5×10^{-6} (linewidth) $\times$ (symbol period) product. For the channel under investigation that results in 30 kHz increased linewidth tolerance, a change from 150 kHz to 180 kHz.

[4]An additional 1.8 dB implementation penalty was added to be consistent with the experimental results, section 3.5.2.

The simulation results indicate that although the complexity of the interleaved equaliser is significantly higher there is a potential gain in linewidth tolerance which might enable the use of even higher order QAM such 256 or 1024, where the phase noise tolerance is even lower. Although further simulation would be required to optimise the length of the nested equaliser and CPE window under those configuration.

3.5.2 Digital coherence enhancement

A different method of improving the phase noise estimation is to send the unmodulated carrier along with the channel, detect and estimate the phase noise from it before removing it from the channel. This estimation is, however, impaired by any noise from the channel over which the signal was transmitted. Another method known as 'Coherent Enhancement' can be used where the phase noise of the carrier laser is measured and inversely applied back to the carrier during modulation [59]. This method effectively compensates for the phase noise of the carrier but not any phase noise from the LO. In systems where the signal accumulates large amount of dispersion the phase noise of the LO alone can cause significant penalties to the channel [60]. A similar method for compensating phase noise of the LO exists and is called Digital Coherence Enhancement (DCE), [61]. This section will focus on applying DCE at the receiver, the benefits are demonstrated utilising a high linewidth laser as a LO to detect 6 GBd PDM-64QAM.

Phase noise measurement technique

The technique is used to measure the phase noise of the LO, as described in [61], is illustrated in figure 3.23(a) and (b). The LO laser is split into three paths one is used as a LO for the coherent receiver while the other two are used for the phase noise measurement. For the phase noise measurement one of the signals is delayed by a time, τ to creating an interferometer with a bandwidth of $1/\tau$. The two versions of the high linewidth laser are then feed into a single polarisation receiver, the detected terms can be expressed using equation (3.11). Because balanced detection is utilised the direct

detection terms are omitted.

$$\begin{pmatrix} X_I(t) \\ X_Q(t) \end{pmatrix} \propto \begin{pmatrix} Re(E(t)E^*(t-\tau)) \\ Im(E(t)E^*(t-\tau)) \end{pmatrix} \tag{3.11}$$

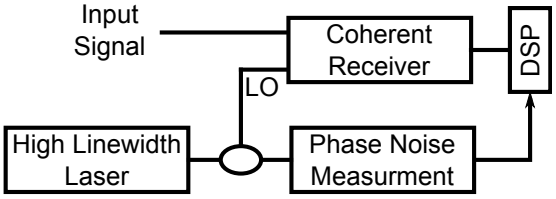

(a)

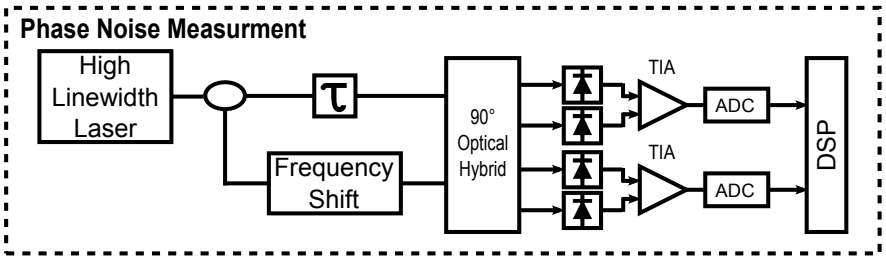

(b)

Figure 3.23: Experimental configuration used for phase compensation technique. **a)** Receiver. **b)** Phase noise measurement technique.

The detected signal of the phase measurement is $E(t)E^*(t-\tau)$. If τ is small then the differential phase can be expressed as the phase difference between the two time instances divided by the time duration, equation (3.12). By numerically integrating the differential phase the phase can be extracted, equation (3.13).

$$\frac{d\phi(t)}{dt} \approx \frac{1}{\tau}[\phi(t) - \phi(t-\tau)] = \frac{1}{\tau}\angle[E(t)E^*(t-\tau)] \tag{3.12}$$

$$\phi(t) = \frac{1}{\tau}\int_0^t \angle[E(x)E^*(x-\tau)] \quad (mod\ 2\pi) \tag{3.13}$$

It should be noted that the measurement is independent of the phase noise distribution and is only limited by the interferometer bandwidth. Once measured, the phase can be applied inversely to the data signal detected by the main coherent receiver to remove the effects of phase noise.

To investigate the phase noise measurement technique a high linewidth laser was emulated. An ECL with an intrinsic linewidth of 10 kHz modulated with pre-computed phase noise using an AWG operating at 12 GSa/s [62]. The bandwidth of the interferometer was set to 550 MHz which could be digitized in practice with 1.1 GSa/s ADC.

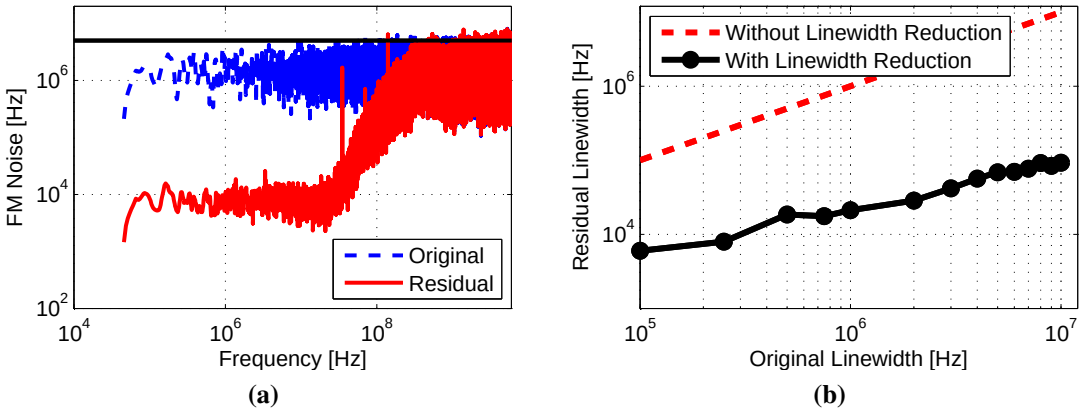

Figure 3.24: a) FM Noise spectrum of 10 MHz laser before and and after compensation. **b)** Residual linewidth after compensation in the compensation bandwidth.

A frequency shift of 35 MHz was applied in one of the arms of the interferometer to overcome AC-coupling of the balanced TIA. This frequency shift was removed digitally after detection. In the configuration illustrated in figure 3.23(a) an unmodulated signal was used as an input signal. The phase was estimated as described and applied to the signal detected by the main coherent receiver. Figure 3.24(a) shows the FM noise spectrum of a laser with 10 MHz linewidth (emulated), as detected by the coherent receiver before and after compensation. Although the interferometer bandwidth is 550 MHz the FM noise is only flat up to 30 MHz where the linewidth is well below 100 kHz. The performance of the compensation technique was the verified by varying the emulated linewidth, figure 3.24(b). For the linewidths up to 10 MHz the technique achieves a consistent reduction of more than one order of magnitude.

Simulation and experimental configuration

Experimentally, an ECL with 10 kHz linewidth was modulated by a 12 GSa/s AWG operating at 2 Sa/symbol to produce 6 GBd 64-QAM. PDM was emulated by passing the signal through a polarisation multiplexing stage, figure 3.25. The LO was a DS-DBR laser with an estimated 1.4 MHz Lorentzian linewidth. The phase noise of the LO was measured synchronously with the detection of the PDM-64QAM signal.

To quantify the benefit of DCE on communication systems 72 Gbit/s (6 GBd) PDM-64QAM was simulated with varying linewidth. The simulation configuration was the same as described section 3.5.1. The phase noise measurements were emulated by applying equations (3.12), (3.13) to the simulated LO signal and applying the inverse

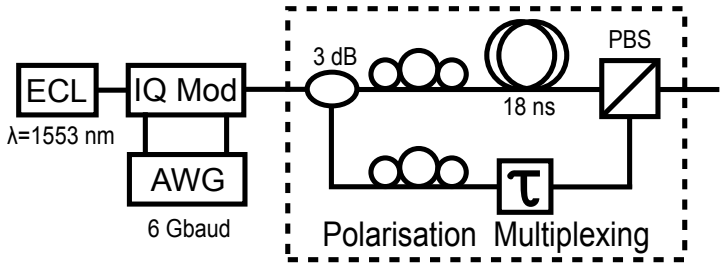

Figure 3.25: Experimental configuration for the transmitter used to phase compensation technique.

phase noise before the QAM signal was equalised.

Results and discussion

Experimentally noise loading at the receiver was performed to demonstrate the performance of the technique. Figure 3.26(a) illustrated the performance for both homodyne detection (where the transmitter laser is used as LO to remove any phase noise dependence) and when the DS-DBR was used as LO. An additional penalty of 0.6 dB is observed at a BER of 1×10^{-2} due to the uncompensated phase noise which falls outside of the interferometer bandwidth. If the phase compensation technique was omitted it was not possible to recover the signal at all as the phase noise was too large.

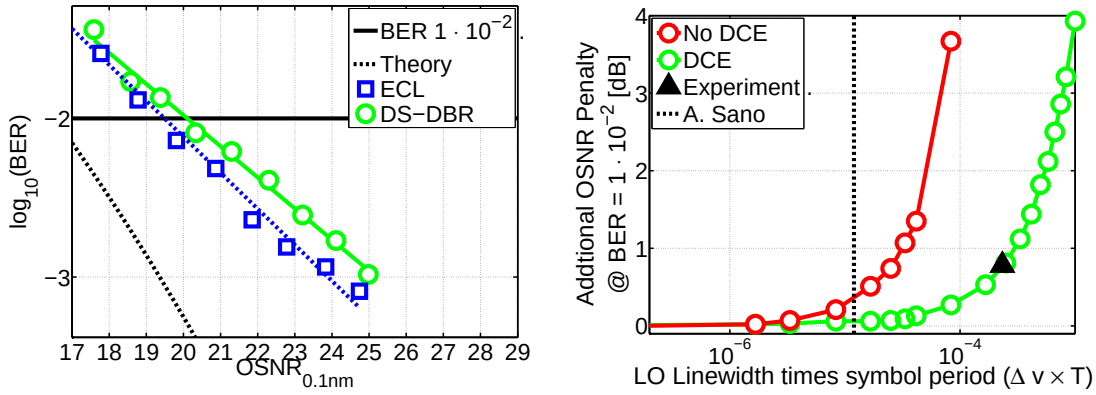

Figure 3.26: Experimental verification of 6 GBd PDM-64QAM. **a)** OSNR vs BER with different LO. **b**) (linewidth) $\times$ (symbol period) product ($\Delta\nu \times T$) vs additional OSNR penalty at a BER of 10^{-2}. A. Sano is the performance demonstrated in reference [63].

To investigate the effects of the high frequency components which fall outside of the interferometer bandwidth simulations were performed. Figure 3.26(b) shows the phase noise tolerance as additional OSNR penalty against (linewidth) $\times$ (symbol period) product ($\Delta\nu \times T$). The results show that, using this technique, one order of

magnitude higher linewidth can be tolerated for the same OSNR penalty. Additionally, figure 3.26(b) shows the highest reported linewidth symbol period product achieved so far [63] together with the experimental results which verify the simulations from figure 3.26(a).

This technique improves the phase noise tolerance of QAM formats significantly, although, an additional low frequency receiver is required. Additionally, the two receivers need to be synchronized together for an accurate mitigation of the phase noise. This could potentially allow the use of higher order QAM, 256 or 512, with low cost lasers. Another application for this technique is to mitigate phase noise from a fast tunable lasers. The technique is especially useful because the phase noise generated after a wavelength transition is not Lorentzian, however, the measurement is agnostic the phase noise distribution. This was demonstrated with a burst mode receiver detecting 6 GBd PDM-16QAM [7], where without DCE it would not have been possible.

3.6 Summary

This chapter focused on modifying existing DSP techniques to enable some different next generation systems. The DSP techniques allow tighter frequency spacing, dynamic routing and higher order modulation formats. The techniques are applicable to PON, metro distance optical network and high spectral efficient system. The key results from this chapter are:

- Backreflections, which limit the sensitivity of Passive Optical Network (PON) are mitigated by spectrally shaping the optical channels.
- Delay skew caused by imperfections in the front end of digital coherent systems can lead to severe penalties for higher order QAM and when Nyquist filtering is employed. With a modified adaptive equaliser the delays can be fully compensated which alleviates constraints of the coherent receivers.
- Chromatic Dispersion (CD) needs to be known in advance for accurate compensation in dynamically routed networks. By adaptively compensating the CD, up to 88,000 ps/nm, network reconfigurability is enabled.
- The update algorithm for adaptive equalisers is modified to reduce computational

complexity. No loss of performance is observed even for a multiplier free update scheme.

- Interleaving the equaliser with Carrier Phase Estimation (CPE) can increase the phase noise tolerance of higher order QAM. Another approach is to utilise Digital Coherence Enhancement (DCE) to detect the phase noise of the LO and remove it digitally from the signal, which can dramatically improve the phase noise tolerance.

4

Wavelength Division Multiplexed (WDM) subsystems

In the previous chapter, although there was an implicit assumption that the subsystems can be applied to WDM systems, the focus was mainly on single channel systems. In this chapter the focal point will be subsystems for WDM systems, starting with how they can be generated utilising optical frequency combs and how different optical frequency combs differ, afterwards, WDM transmission is evaluated in simulations and experimentally. Finally, a joint channel DSP technique is investigated for compensating phase noise.

4.1 Optical frequency combs

An optical frequency comb (hereafter comb) is a series of optical carriers at a fixed frequency spacing generated from a single laser source. Because the generated carriers

are copies of the seed laser all the carriers are frequency and phase locked together. Depending on the generation technique the frequency spacing is specified by an external frequency source or by the characteristics of the device generating the comb. Additionally, there is a fixed phase relationship between the carriers, which depends on the generation technique. Assuming that a single carrier can be represented with the delta function, $\delta(\omega)$, then the amplitude of a comb can be represented with equation (4.1); where N is the number of sub-carriers, a_n is the amplitude of the nth sub-carrier and $\Delta\omega$ is the frequency spacing of the sub-carriers.

$$F(\omega) = \sum_{n=-N/2}^{N/2} a_n \delta(\omega \pm n\Delta\omega) \tag{4.1}$$

An alternative way to achieve multiple sub-carriers is to use multiple lasers, however, there are several disadvantages to this approach. Because they are individual sources there is no phase relationship between the carriers. Additionally, although the spacing might be fixed the wavelength of the lasers drifts over time leading to uneven spacing. The OIF recommendation, for tunable lasers on 50 GHz and 25 GHz grids, is a drift less than $\pm$2.5 GHz and $\pm$1.25 GHz respectively [64]. Although this is sufficient for large channel spacing, moving to smaller channel spacing, potentially at the Nyquist rate, can lead to significant performance degradation caused by crosstalk between adjacent channels. Additionally, as systems scale to more channels with smaller spacing, using individual lasers might be unrealisable due to cost constraints.

4.1.1 Applications

In telecommunication systems, optical frequency combs are used to generate optical sub-carriers. The frequency spacing is the key feature, because it provides the transmission system with a stable frequency grid. Any fluctuation in the seed laser will result in frequency drift of the whole comb, but not between individual sub-carriers avoiding potential crosstalk. The use of combs for transmission system has been demonstrated numerously in the literature [9; 10; 65; 66]. Sub-carriers with a narrow linewidth are of particular interest, because they are able to support higher order modulation formats such as M-QAM to further increase the bandwidth utilisation [11; 67; 68]. Furthermore, the phase synchronization between the sub-carriers can be utilised for spectral stitching.

This can be done at the transmitter to generate signals with bandwidths larger than what can be achieved with electronics [69; 70]. The high bandwidth channel is generated digitally and split into frequency bands, then each band is modulated onto separate sub-carriers of a comb. Alternatively, each sub-carrier can modulated with separate but correlated channel, for example non-linear pre-compensation across multiple channels, where the phase synchronization is vital [71; 72]. Another approach is to apply spectral stitching at the receiver, where each comb line is used as a LO for a different receiver. By matching the frequency spacing of the sub-carriers and the bandwidth of the receivers a larger optical bandwidth can be detected. Subsequently, the bandwidth can be stitched together in the digital domain for joint DSP [73; 74].

Although in this work combs are only used for data communications there are other potential applications which have further increased the interest in the field. By generating a large number of sub-carriers and shaping their amplitude and phases separately it is possible to achieve an arbitrary time domain pulse [75]. Another time domain application of a comb is to generate short and high power pulses, which can be represented as a comb in the frequency domain; by spacing and shaping the amplitudes of a comb a desired pulse can be generated. Yet another application of a combs in combination with high bandwidth photodiodes is for terahertz generation. Filtering two lines from a comb and beating them together on a photodiode, a RF signal is generated with a frequency dependent on the separation of the two lines [76]. If the phase noise of the comb lines is low the resulting RF tone would then also have low phase noise.

4.1.2 Fibre loop

When a RF sine wave is applied to a phase modulator (section 2.2.1) additional frequencies are generated, if this process it repeated multiple times a comb with a large bandwidth can be generated. A schematic of such technique utilising a fibre loop design is illustrated in figure 4.1 [77]. Using equation (2.8), where the applied voltage is a sine wave, with an amplitude A and a frequency ω_m, equation (4.2) is derived. It describes the behaviour of a single pass through the phase modulator, where $\mathbf{E}_{In}$ and $\mathbf{E}_{Out}$ represent the input and output of the modulator respectively.

$$\mathbf{E}_{Out}(t) = \mathbf{E}_{In}(t)\exp\left(j\frac{\pi}{V_\pi}Asin(\omega_m t)\right) = \mathbf{E}_{In}(t)\exp\left(j\beta\sin(\omega_m t)\right) \tag{4.2}$$

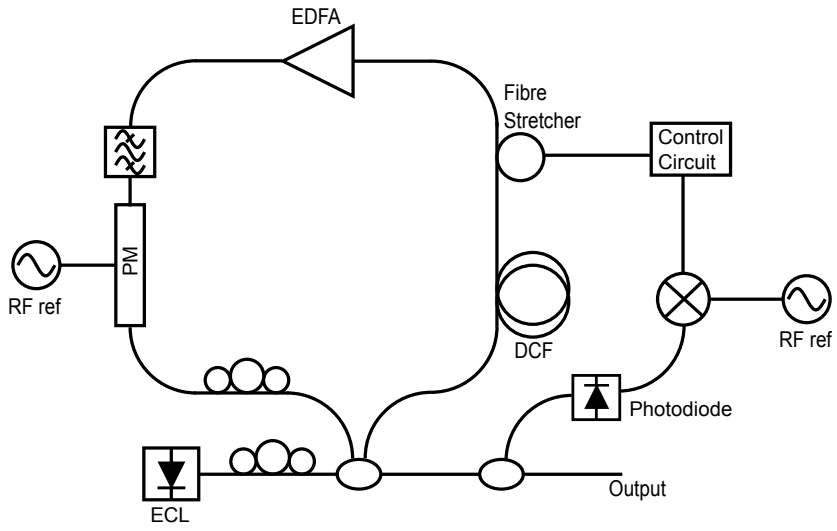

Figure 4.1: Comb generation technique using a fibre loop.

The frequency domain representation of a single pass through the phase modulator is described with equation (4.3). The Fourier transform of $\exp(j\beta sin(\omega_m t))$ is a series of delta functions with amplitude corresponding to Bessel functions of n$^{\text{th}}$ order.

$$\begin{aligned} \mathfrak{F}\left[\exp\left(j\beta\sin(\omega_m t)\right)\right] &\propto \sum_N \delta(\omega - n\omega_m) J_{-n}(\beta) = \mathbf{M}(\omega) \\ \mathbf{E}_{Out}(\omega) &= \mathbf{E}_{In}(\omega) * \mathbf{M}(\omega) \end{aligned} \tag{4.3}$$

The number of sub-carriers and their amplitude dependent on the modulation depth β, which is dependent on the amplitude A of the sine wave driving the modulator. With a higher modulation depth additional sub-carriers are generated, however, their respective amplitudes are lower. Additionally, the total power of the comb is limited by the EDFA in the loop, it is distributed between all the sub-carriers, therefore as the bandwidth of the comb is increased the power of individual sub-carriers is decreased.

The polarisation controller, bandpass filter and EDFA are used to maintain the polarisation alignment and a flat power by limiting the total bandwidth of the comb. The phase modulator will keep introducing new sub-carriers each loop iteration as long as they are within the optical bandwidth of the components. The Dispersion Compensating Fibre (DCF) is used to compensate the dispersion caused when the optical signal continuously passes through the loop. By maintaining zero dispersion there is no walk off between sub-carrier and phase alignment can be maintain. However, if the length of the loop is not kept constant the comb can become unstable leading to discontinuous

power profile or a noisy comb where newly generated frequencies interfere destructively. The length of the loop varies over time due to ambient temperature fluctuation resulting in expansion or compression of the fibre. To maintain an equilibrium a control circuit together with fibre stretcher can be utilised. This can be achieved by measuring the amplitude of the beat signal of the comb spacing and changing the length accordingly [78]. To maintain a stable comb the control circuit has to have a large operating range while continuously fine tuning of the fibre length.

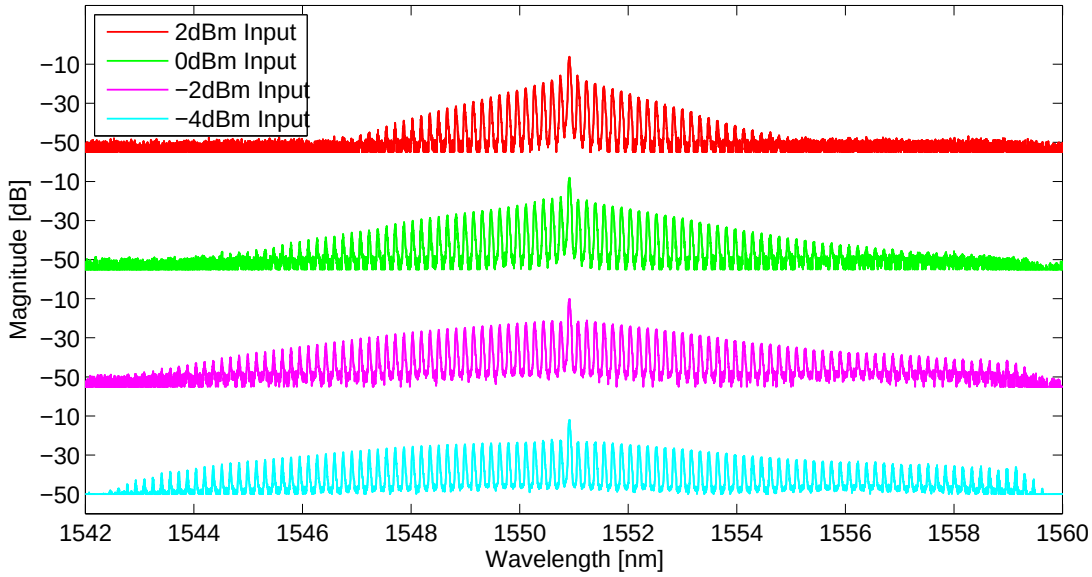

Figure 4.2: Example comb spectrum generated using the fibre loop technique, 20 GHz spacing.

Figure 4.2 illustrates experimental spectra of combs generated with this technique, with a pre-existing configuration. Although large bandwidth combs with a hundred sub-carriers are achieved the inherent stability of the amplitudes proved that the technique was not suitable as a WDM optical source.

4.1.3 Gain switching

One possible technique for generation of an optical frequency comb is by utilising a discrete-mode laser [79]. By applying an oscillating RF signal to the gain section of the mode laser it can be switched on and off rapidly. If the switching RF signal has the appropriate frequency the photon density would not be able to reach a steady state before the gain section is turned off; this effect leads to pulse generation based on the RF frequency. The repetition rate of the pulses is inversely proportional to the sub-carrier

spacing of the corresponding comb spectrum. The higher linewidth often associated with gain switched laser is offset by seeding the laser with a master laser with low linewidth. The mode locked laser can then be driven by the high speed RF signal; while the phase noise characteristics of the master laser will mapped onto the generated comb. Figure figure 4.3(a) illustrates a potential configuration (other configurations [79]) and figure 4.3(b) shows a sample spectrum with 10 filtered sub-carriers.

Although not detailed in this work, this techniques was used generate result for the following publications: [10; 11; 12].

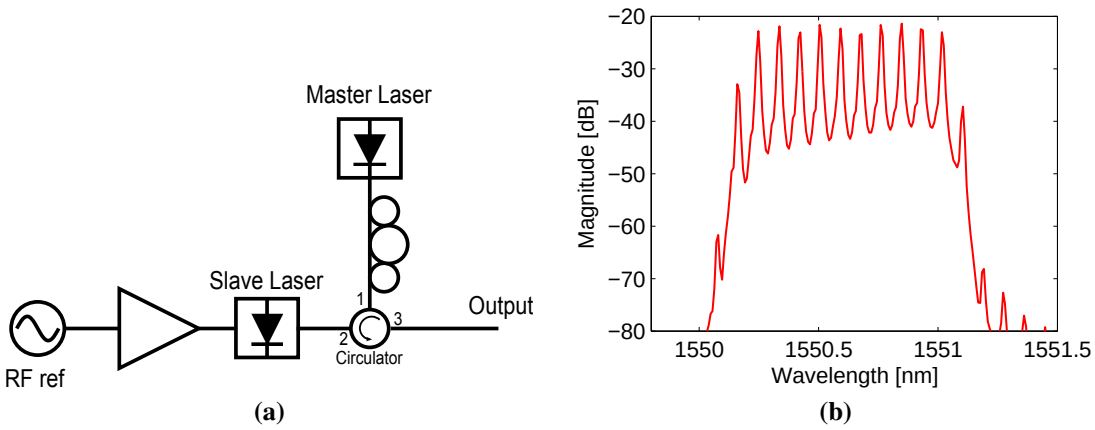

Figure 4.3: a) Comb generation technique using externally injected gain-switched laser. **b)** Example comb spectrum generated using the gain switching technique, 10 GHz spacing.

4.1.4 Dual-Drive Mach-Zehnder modulator (DD-MZM)

Another technique to generate a comb is to utilise a Dual-Drive Mach-Zehnder Modulator (DD-MZM) [80], a schematic of the technique is shown in figure 4.4(a). A DD-MZM is a MZM in a push-pull configuration (section 2.2.1) with two independent electrical driving signals, which is equivalent to two parallel phase modulators. By extending equation (4.2) to include the parallel structure the behaviour of the DD-MZM can be described with equation (4.4), where A_1 and A_2 represent the amplitude of the two RF signals while θ_1 and θ_2 are their respective phase.

$$\mathbf{E}_{Out}(t) = \mathbf{E}_{In}(t)\left[\exp\left(j\frac{\pi}{V_\pi}A_1\sin(\omega_m t+\theta_1)\right) + \exp\left(j\frac{\pi}{V_\pi}A_2\sin(\omega_m t+\theta_2)\right)\right] \tag{4.4}$$

By configuring the amplitudes and the relative phase of the two RF signals it is possible to tailor the output optical signal to achieve a flat comb [80]. Unlike the fibre loop configuration, discussed previously, the optical signal is modulated only once, therefore a large RF power or a low V_π is required to achieve a large bandwidth comb. However, the total input power to the DD-MZM is limited to avoid overheating of the device.

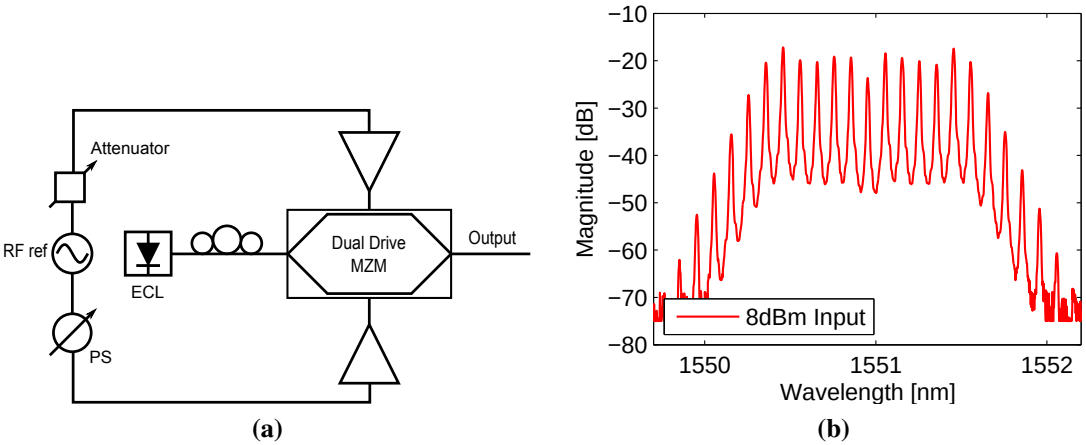

Figure 4.4: a) Comb generation technique using a DD-MZM. **b)** Sample comb spectrum generated using DD-MZM, 10 GHz spacing.

Figure 4.4(b) illustrates a sample comb spectrum generated with a DD-MZM modulator. This technique was used in section 4.5 for WDM transmission.

4.1.5 Cascaded modulators

An alternative technique to achieve a wide bandwidth comb, instead of using a single modulator in a loop or a DD-MZM with high RF power, is to use multiple cascaded modulators. Similar performance is achieved with different configurations and combinations of modulators [81; 82]. The approach used in this work is two cascaded intensity modulators and one phase modulator [83], as illustrated in figure 4.5(a). This technique promises wide bandwidth due to multiple modulators, while flatness is achieved by tailoring the RF waveforms. By applying the second harmonic to the phase modulator with a 180° phase shift and an amplitude of 1/16 (24 dB difference) a better approximation to a quadratic temporal phase can be achieved which leads to a comb with a flat power spectrum [83].

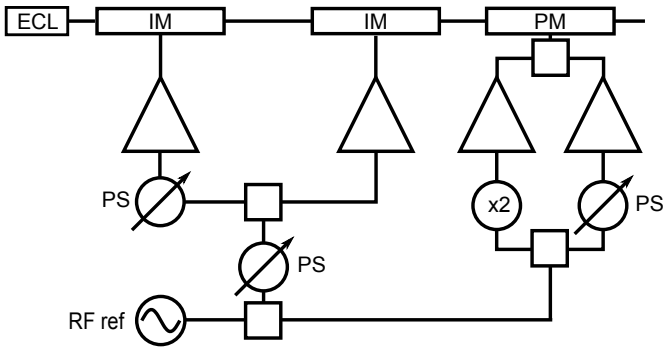

(a)

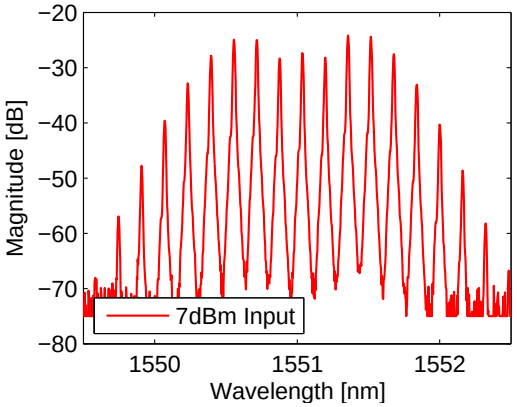

(b)

Figure 4.5: a) Comb generation technique using cascaded modulators. IM: Intensity modulator, PM: Phase modulator, PS: Phase shifter. **b)** Example comb spectrum generated using cascaded modulators, 10 GHz spacing.

The behaviour of the system can be expressed using equation (4.5). Where A_1, A_2, A_3, A_4 represent the amplitude of individual RF signals and $\theta_1, \theta_2, \theta_3, \theta_4$ are their respective phases.

$$\begin{aligned}\mathbf{E}_{Out}(t) = \mathbf{E}_{In}(t) \Bigg[& \cos\left(\frac{\pi}{V_\pi}\left(V_{Bias1} + A_1 \sin(\omega_m t + \theta_1)\right)\right) \\ & \cos\left(\frac{\pi}{V_\pi}\left(V_{Bias2} + A_2 \sin(\omega_m t + \theta_2)\right)\right) \\ & \exp\left(j\frac{\pi}{V_\pi}\left(A_3 \sin(\omega_m t + \theta_3) + A_4 \sin(2\omega_m t + \theta_4)\right)\right)\Bigg]\end{aligned} \tag{4.5}$$

Because the amplitudes and phases of the RF signal can be configured separately using attenuators and phase shifters, this technique offers high flexibly, during configuration, to achieve the desired power profile. Additionally, unlike DD-MZM, the low V_π requirement is alleviated as RF power can be spread over multiple modulators. Although, it has been reported that this technique can achieve a comb with up to 30 sub-

carriers [83], the configuration used in this work was able to generate only 9 sub-carriers within 2 dB power variation mainly due to the higher V_π of the available modulators, figure 4.5(b) illustrates a sample spectrum. This technique was used through this work, sections 4.3 and 4.5, due to easy configuration and flexibility while offering a good temporal stability.

4.2 System design

A group of sub-channels, spaced close to the Nyquist rate, which is routed and managed through the network as a single entity is called a 'superchannel'. Because optical frequency combs generate narrow and evenly spaced sub-carriers, they are ideal for superchannels. An overview of the transmitter system considered in this work is presented in figure 4.6. A single low linewidth laser is used to generate an optical frequency comb. Each sub-carrier is then separated using an arrayed wavelength grating, interleaver or optical filters and is modulated separately. The data stream is split between each sub-carrier and is feed into each modulator. The optical sub-channels are then combined in a single superchannel entity, before multiplexing with other superchannels and transmitted through the optical fibre.

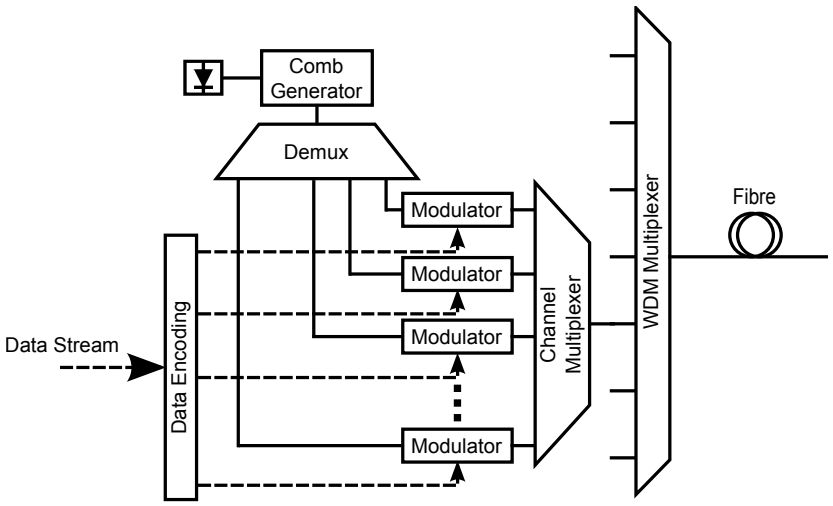

Figure 4.6: Superchannel transmitter.

Two different configurations can be utilised to detect the incoming superchannel. The first approach is to use a single, high bandwidth, receiver to detect the full superchannel, figure 4.7(a); the approach used in this work. Afterwards, each sub-channel

can be digitally filtered and processed independently or joint DSP can be applied. An alternative method is to generate an optical frequency comb at the receiver, separate each sub-carrier to individual low bandwidth receivers, each detecting a single sub-channel figure 4.7(b). Processing can then be applied to each sub-channel separately or the signals from each receiver can be stitched together in the digital domain to recover the full superchannel simultaneously [74].

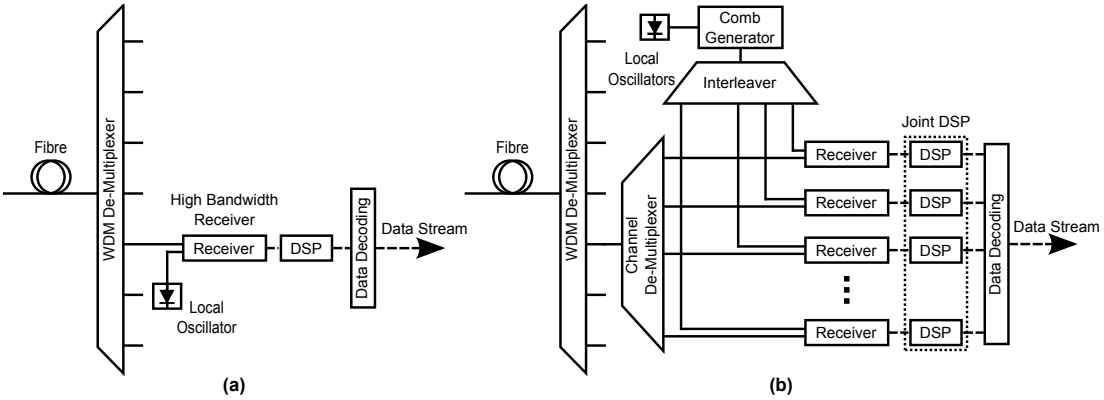

Figure 4.7: Superchannel receivers: **a)** Single high bandwidth receiver . **b)** Multi channel, low bandwidth, receivers.

4.3 Modulation of comb

In this section data modulation with PDM-16QAM and 64QAM at 3 GBd is used to verify and demonstrate the narrow linewidth of an optical frequency comb. These modulation formats greatly increase the constraint on the linewidth, sections 2.3.3 and 2.4.3. The required linewidth for 16QAM at 3 GBd is 420 kHz and 120 kHz for 64QAM to achieve a penalty of less than 1 dB at a BER of 3.8×10^{-3} [26].

Comb generation

The comb was generated using the scheme detailed in section 4.1.5, with a frequency spacing of 10 GHz. Each of the modulators had a V_π of about 7 V while the total loss through the system was approximately 18 dB. The RF power going into each intensity modulator was set to 21 dBm in order to match V_π, which improved the stability. The bias point of the modulators drifts away from optimal position, however, as they are operated in the non-linear region this effect is minimized. The RF power into the phase

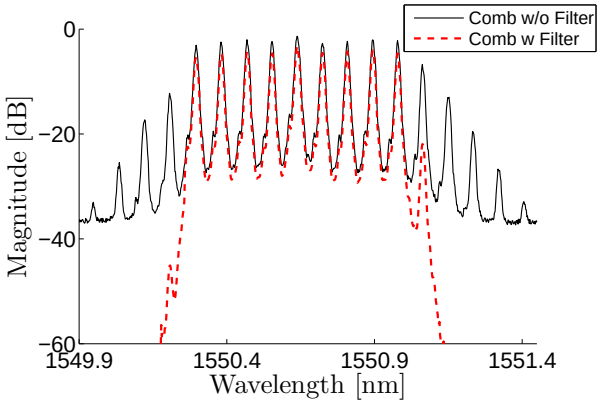

Figure 4.8: Generated comb spectra for experiment, 10 GHz spacing.

modulator was set as high as equipment allowed, 29 dBm, while still maintaining 24 dB relationship between the harmonics. The seed laser was a ECL with a linewidth of $<$15 kHz, which gives rise to sub-carriers with an estimated linewidth of 25 kHz or less. After passing through the modulators the comb is amplified to compensate the accumulated loss and filtered to remove unused sub-carriers. Figure 4.8 illustrates a sample of the generated and filtered spectrum.

Experimental configuration

The transmitter and receiver system are displayed in figure 4.9. To avoid constructive crosstalk from adjacent channels modulated with the same data, after the comb was generated the channels were separated by a two stage interleaver into two groups, odd and even, achieving an extinction ratio of at least 35 dB. Each sub group was modulated by an independent IQ modulator with decorrelated data. The data streams were pre-generated offline using decorrelated 2^{15} De Bruijn sequences. The electrical signals were generated from two pairs of Field-Programmable Gate Array (FPGA) and DAC operating at 12 GSample/s, 4 Sa/symbol, with a hardware resolution of 6 bits, to produce 3 GBd 16-QAM. They were then amplified using linear amplifiers and filtered using fifth order Bessel low pass filters with a cut off frequency of 7 GHz to minimize side bands which can interfere with adjacent channels. After the modulation the channels were combined with an optical coupler and PDM was emulated by passing the signal through a polarisation multiplexing stage.

At the receiver the sub-carriers were noise loaded before being detected by a phase- and polarisation-diverse coherent receiver. The LO was a tunable ECL with a linewidth

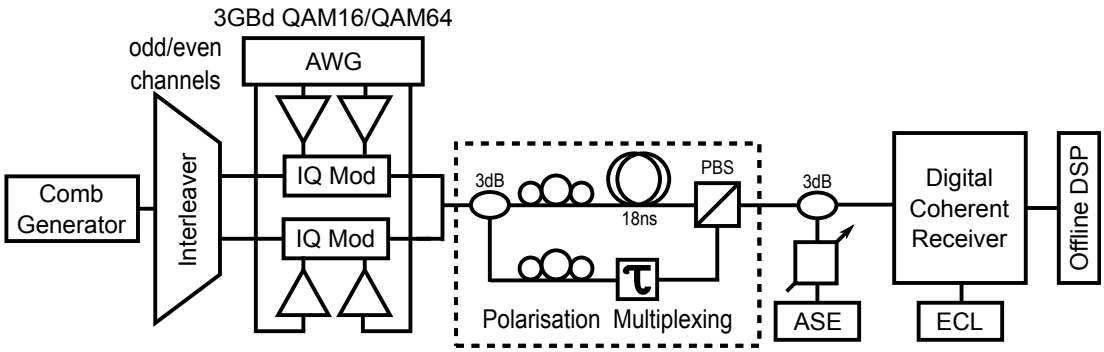

Figure 4.9: Experimental configuration used to modulate the comb.

of 100 kHz. The detected signals were then sampled at 50 GSample/s. Correction due to imperfections in the front-end and normalisation were applied before down sampling to 2 Sa/symbol. The equaliser was pre-converged using CMA before switching to a MMA [84] (section 2.4.2). Frequency offset compensation was then applied before a DD-CPE [26] (section 2.4.3). Finally maximum likelihood hard decisions were made using k-means clustering [43] and BER estimation over 2^{18} symbols.

Experiment results

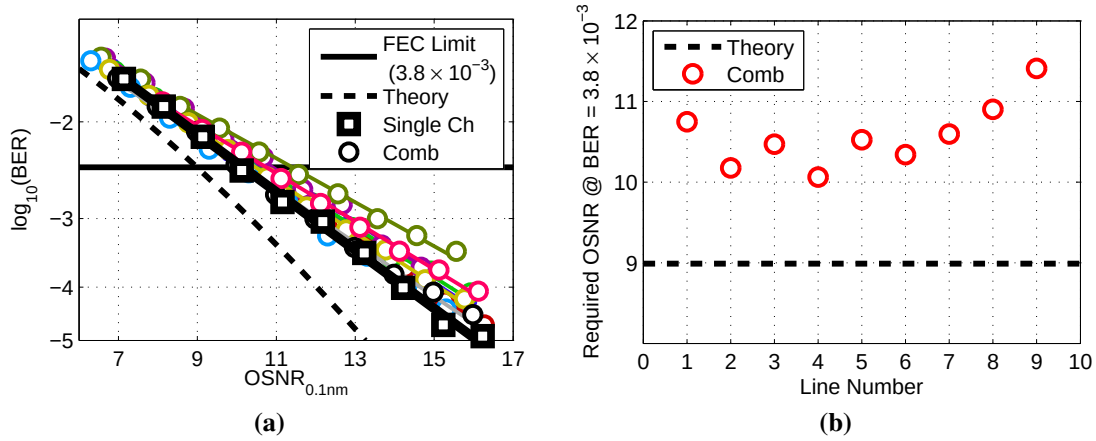

Figure 4.10: a) BER vs OSNR for single channel and each sub-carrier using 3 GBd PDM-16QAM **b)** Required OSNR of 3 GBd PDM-16QAM

The receiver noise sensitivity for PDM-16QAM was measured for each sub-carrier, by tuning the LO to the channel of interest, and compared to single channel using the seed laser, figure 4.10(a). At a hard decision FEC, with 7% overhead, and a BER limit of 3.8×10^{-3} [44] the required OSNR of a single channel is $<$10 dB, with an implementation penalty of about 0.8 dB. The performance of the sub-carriers did not

vary significantly and most of the lines have less than 2 dB implementation penalty, figure 4.10(b).

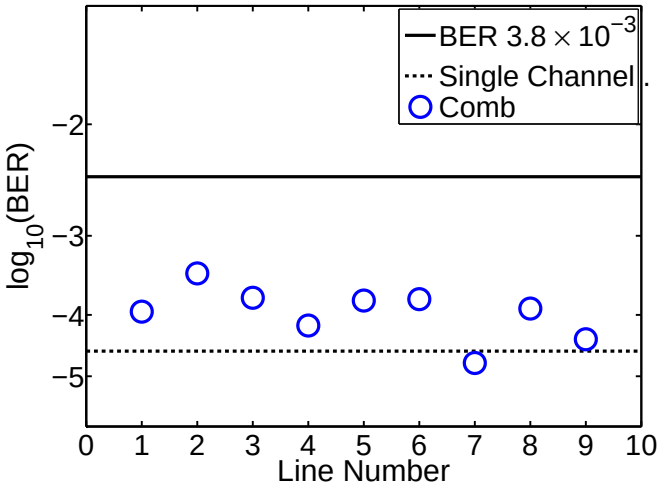

Figure 4.11: BER floor for 3 GBd 64QAM for single channel and each sub-carrier.

Additionally the performance of a single channel and each sub-carrier with 64QAM was measured, the results are displayed in figure 4.11. An error floor is present for both the single channel and the comb, however, the performance consistently around a BER 10^{-4}, which is below the FEC limit. The error floor is attributed to a sub-optimal receiver DSP in combination with the total linewidth of 125 kHz, which at a symbol rate of 3 GBd incurs at least 1 dB penalty [26] (section 2.4.3). These results indicated that a comb source generated using cascaded modulators and a narrow linewidth seed laser is able support high order modulation formats and is suitable to further transmission experiments.

4.4 Transmission simulations of optical frequency combs

The use of optical frequency combs as sub-carriers has been used extensively in recent years [85; 86; 65]. However, the impact of phase and frequency locked carriers on the transmission performance has not been evaluated or compared to independently generated carriers. This section investigates these effects on a transmission system in simulations.

In simulations nine sub-channels spaced at 10 GHz are generated, to create a

superchannel. Each channel was modulated with a 6 GBd PDM-16QAM carrying a gross bit rate of 48 Gbit/s. Assuming the use of a 7% FEC [44], with a BER limit of 3.8×10^{-3}, results in a total bit rate of 403 Gbit/s for the full superchannel.

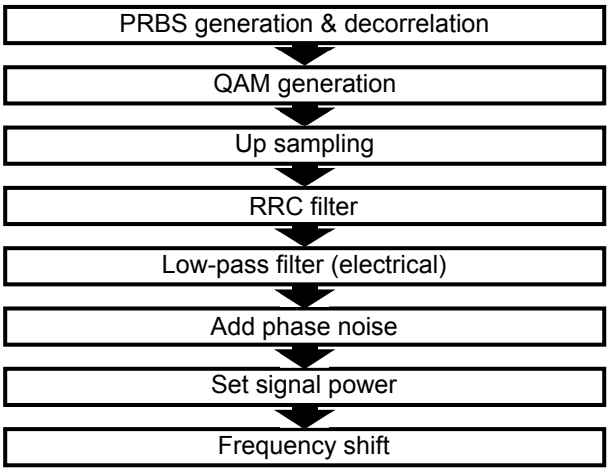

Figure 4.12: Transmitter steps used for simulations.

4.4.1 Simulation configurations

Figure 4.12 illustrates each of the step used to emulate the transmitter. Firstly, a $2^{15} - 1$ PRBS was generated and decorrelated for each of the 8 bits of PDM-16QAM. The main processes of bandwidth expansion in the transmission system is Four Wave Mixing (FWM), however, as the CD, in the fibre, counteracts FWM the expansion is restricted. To accurately capture the transmission effects the simulation bandwidth was set to be at least twice the total bandwidth of the superchannel [87]. Although, the total superchannel bandwidth is 86 GHz, the simulation bandwidth was set to 174 GHz to maintain an integer oversampling of each sub-channel, 29 Sa/symbol. Afterwards the sub-channels were filtered using a RRC filter to limit the bandwidth of the channel and to avoid crosstalk between adjacent channels. The sub-channels were then low pass filtered with a fifth order Bessel filter at 70% of the symbol rate, to emulate limited electronic bandwidth. The phase noise was added in two different ways: when simulating a superchannel with a comb each of the sub-carriers received the exact same phase noise, while when simulating independent sub-carriers the phase noise was generated separately for each sub-carrier. The optical power of each sub-channel was then set before frequency shifting to corresponding frequency slot in the

overall superchannel. This processes was then repeated for each of sub-channels of the superchannel before combining them together.

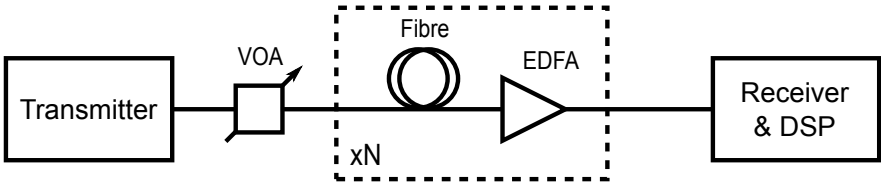

Figure 4.13: The simulated transmission consists of cascaded single fibre span followed by an EDFA.

Parameter	Value
Attenuation coefficient (α)	0.2 dB/km
Dispersion parameter (D)	17 ps/km/nm
Nonlinear coefficient (γ)	1.2 $W^{-1}km^{-1}$
PMD	0.1 $ps/\sqrt{km}$
Span length	80 km
Number of spans	50
EDFA noise figure	4.5 dB
Simulation bandwidth	174 GHz
Simulation step	100 m

Table 4.1: Transmission simulation parameters.

A multi span transmission system was emulated as illustrated in figure 4.13. The fibre was simulated using the well known technique of symmetric Split Step Fourier (SSF) [20; 88]. In each of the 100 m steps half of dispersion was applied followed by a non-linear rotation and second half of the dispersion to fully capture the non-linear effect of the transmission. After 80 km of fibre a single EDFA was used to fully compensating for the loss of the span. The simulated fibre was SMF with 0.2 dB/km attenuation, 17 ps/km/nm dispersion and non-linear parameter of 1.2 $W^{-1}km^{-1}$, the full parameters of the simulations are summarised in table 4.1.

After transmission the full superchannel was detected using a single phase- and polarisation-diverse coherent receiver. The LO was an independently generated laser with the same linewidth and a 200 MHz frequency offset. The signal was then quantised to 6 bits of resolution, which together with the laser linewidth emulates laboratory conditions. Afterwards, each sub-channel was processed independently, by first normalising the signal and frequency shifting the signal to the desired sub-channel. The

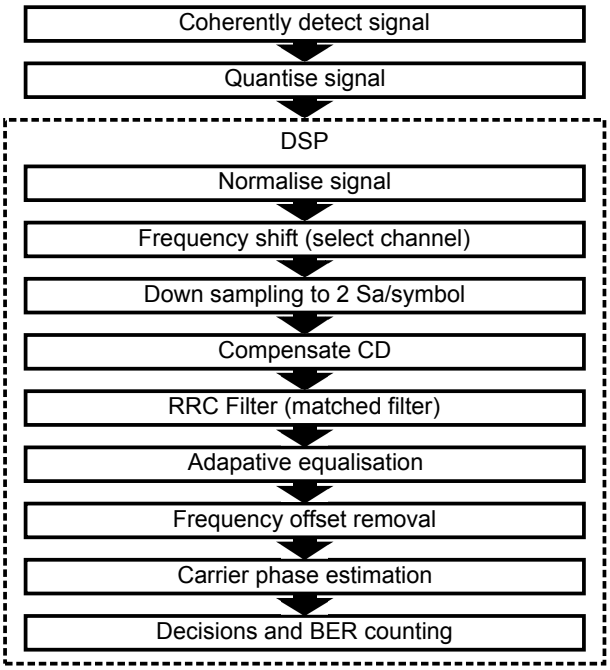

Figure 4.14: Emulation of digital coherent receiver followed by a DSP chain.

signal was down sampled to 2 Sa/symbol and CD was compensated before a matched RRC filter was applied. Timing and PMD are compensated using an adaptive 2×2 equaliser (no delay skew was considered so the 4×4 equaliser was not required). The frequency offset was estimated using a 4^{th} power algorithm before DD-CPE was used to compensate the phase noise [26] (section 2.4.3). Symbol decision was made with k-means clustering [43] followed by BER estimation.

4.4.2 Simulation results

Firstly, the single channel performance was verified with and without the required RRC filter. Figure 4.15 illustrates that a RRC filter with a rolloff of 0.1 provides sufficient channel isolation to mitigate linear crosstalk (overlap) between adjacent channels. Additionally, the performance of the single channel without filtering is equivalent to when a RRC is applied to a WDM system.

Afterwards the transmission performance of a single channel was investigated to verify the simulator. The results are shown in figure 4.16, where single channel 6 GBd PDM-16QAM is compared with and without a RRC filter. The maximum distance was achieved at a launch power of -6 dB, 4,320 km and 4,000 km for the non-filtered and the RRC filtered channels respectively. The performance in the linear region, at launch

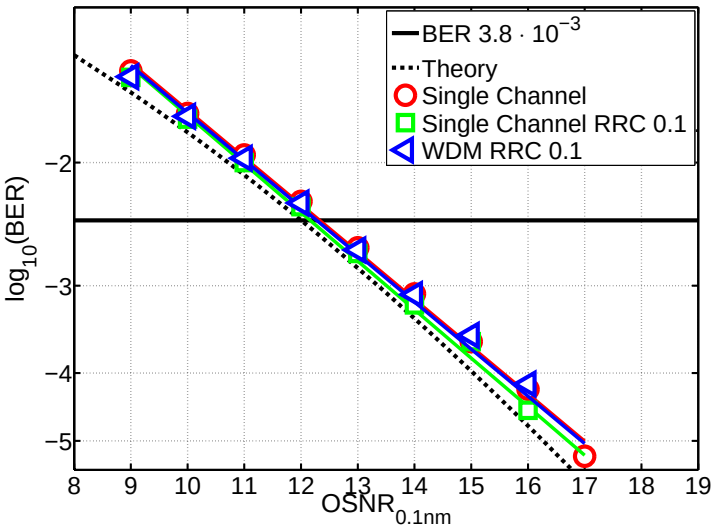

Figure 4.15: Simulations of single channel and WDM, BER vs OSNR with 6 GBd PDM-16QAM in a back-to-back configuration.

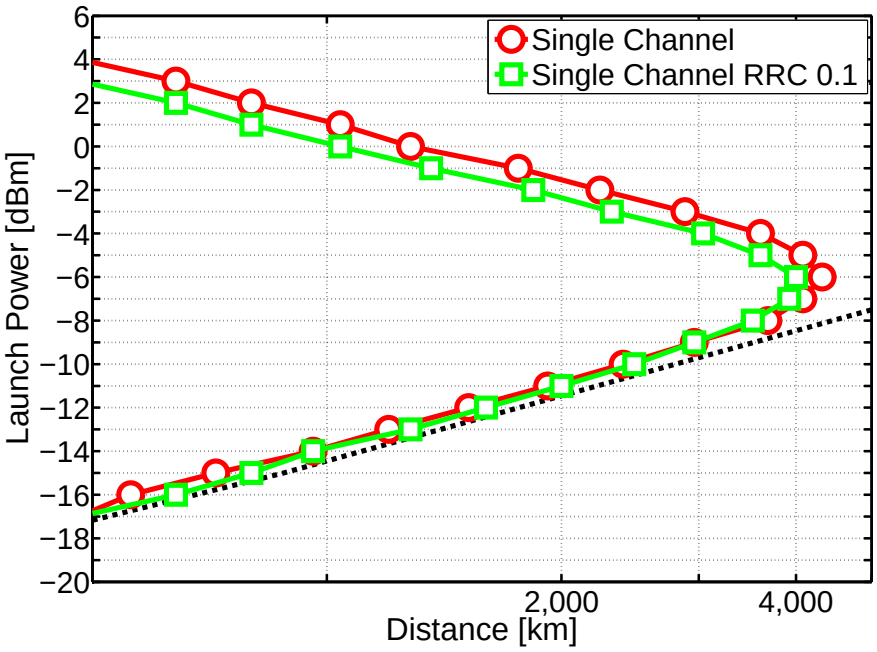

Figure 4.16: Simulations of single channel transmission performance of 6 GBd PDM-16QAM with and without RRC filtering.

powers less than -8 dB, is equivalent between the configurations, as expected from figure 4.15. However, in the non-linear region the performance of the RRC filtered channel is worse. Even though the optimum launch power was the same for the two configuration, the filtered channel has a constrained bandwidth resulting in higher power spectral density, which leads to greater non-linear effects.

Once the single channel performance was established, as base line, multichannel simulations were carried out. The goal of this investigation was to determine if phase

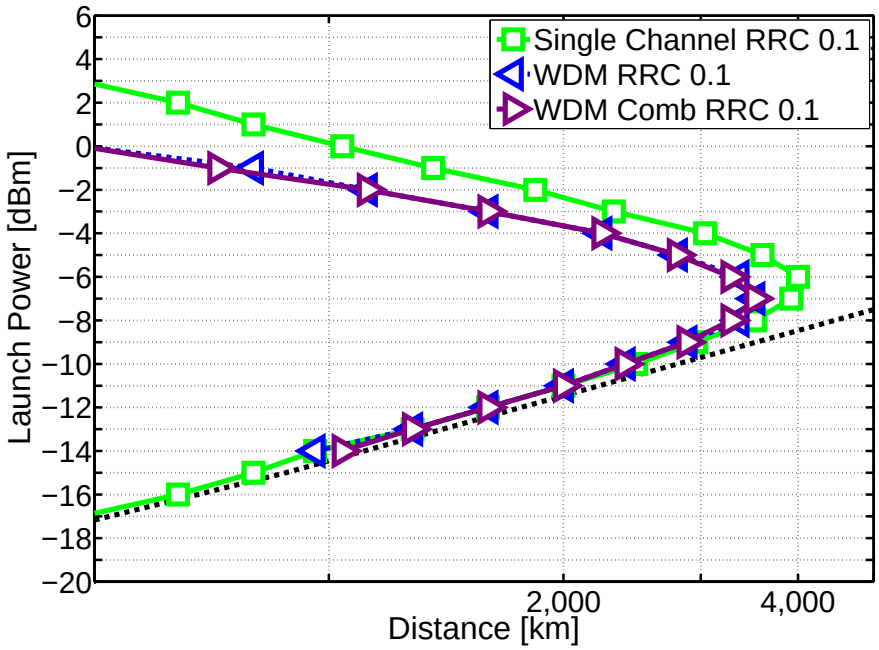

Figure 4.17: Simulations of WDM transmission performance of 6 GBd PDM-16QAM with phase synchronous sub-carriers.

locked sub-carriers (comb) have an effect on transmission performance. The emulating of the comb was implemented as previously described, by applying the same phase noise onto each sub-carrier. The results are shown in figure 4.17 together with the single channel for comparison. It is clear that the performance of the two WDM systems is identical and they are able to reach the same distance for all launch powers. The maximum distance of 3,520 km is achieved with a launch power of -7 dB, which is only 1 dB lower than the single channel system, this is, due to the additional non-linearities in a WDM system; cross phase modulation between sub-channels.

These results indicate that there is no performance degradation or improvement in transmission when using phase synchronous sub-carriers without additional processing or special system configurations. This implies that optical frequency combs could be used in DWDM systems with minimal guardbands to mitigate linear crosstalk from drifting sub-carriers. Although, additional simulations and experiments would need to be carried out with different system configurations to verify that there are no consequences of the phase synchronous sub-carriers. For example multi-channel pre-compensation, for non-linearity, has recently been investigated [71] were the phase synchronous sub-carriers are essential for an accurate compensation, however, the effect on post-compensation are unknown.

4.5 Transmission experiment with optical frequency combs

Although techniques for generating optical frequency combs have been analysed, most commonly that has been done in terms of spectral flatness and number of sub-carriers. Additionally, the phase noise behaviour has been investigated for some techniques [89; 65]. However, the comparison between optical frequency combs has been limited to only minor modifications of the proposed systems [90; 91; 92]. Although, these analysis and comparisons provide insights of the performance it is not possible to predict the full system behaviour. In this section the use of two different combs is compared experimentally in a transmission system implementing a 400 Gbit/s superchannel utilising PDM-16QAM.

4.5.1 Experiment configurations

The same system configuration used for the simulation in the previous section was utilised in this experiment. Nine sub-carriers spaced at 10 GHz are generated using two different techniques, DD-MZM (section 4.1.4) and cascaded modulators (section 4.1.5). First 16QAM signal was generated offline at 2 Sa/symbol and filtered with RRC filter with a rolloff of 0.1. The electrical signals were generated by an AWG operating at 12 GSa/s to produce a 6 GBd signal. The RF signal was then filtered with a low pass filter to eliminate aliases from the AWG before being applied to the modulator. The optical frequency comb was first filtered with a bandpass filter to eliminate unused sub-carriers before being split into odd and even using an interleaver achieving a minimum of 25 dB extinction ratio. The odd and even channels were then combined passively before PMD was emulated by passing the signal through a polarisation multiplexing stage. Because odd and even channels are modulated separately the phase synchronous is not maintained in this configuration. The full transmitter configuration is shown in figure 4.18.

The transmission was emulated using a single span recirculating loop as illustrated in figure 4.19. The loop consists of 80.7 km of SMF with 0.2 dB/km attenuation, 16.7 ps/km/nm dispersion and a non-linear parameter of 1.2 $W^{-1}km^{-1}$. Two EDFAs with noise figures of 5 dB were used, one to set the launch power into each span and the

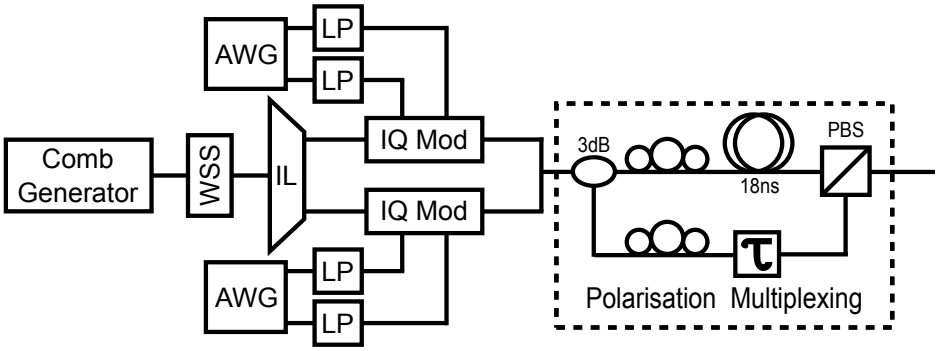

Figure 4.18: Experimental configuration of a WDM transmitter.

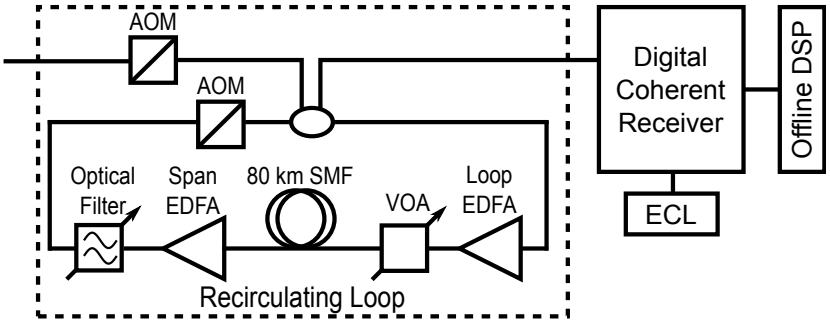

Figure 4.19: Experimental configuration used for transmission and detection of the signal.

other to compensate the loss through connecting components. A polarisation scrambler was used to introduce random polarisation rotations for each span and tunable optical filter was used to reject out of band noise, while Acoustic Optic Modulators (AOMs) were used to gate the signal. At the receiver the superchannel was detected by a wideband phase- and polarisation-diverse coherent receiver. The LO laser was an ECL with a 15 kHz linewidth. After sampling the signal at 160 GSa/s, the signal was processed as described in the previous simulations sections.

4.5.2 Experiment results

Similar to the simulations, firstly, the system was tested in a back-to-back configuration. The performance of the single channel PDM-16QAM from the odd and even IQ modulators is displayed in figure 4.20. The two modulators exhibit the same performance with an additional penalty of 0.7 dB observed when RRC filtering is applied to the signal, this is attributed to the higher digital resolution requirement both at the transmitter and receiver.

Subsequently the transmission performance was investigated for a single channel

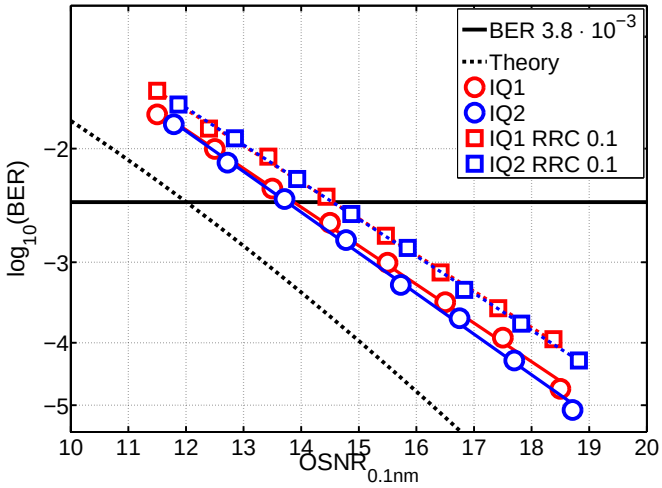

Figure 4.20: Experimental single channel from the two IQ modulators with and without RRC filtering, BER vs OSNR with 6 GBd PDM-16QAM in a back-to-back configuration.

over 1,200 km and compared to the simulation results of the same system, figure 4.21. The simulations results are consistent with the previous transmission results in figure 4.16 where in the linear region (up to -8 dB) the performance is the same with and without filtering and only in the non-linear region does the filtered signal performance drop. The same trend is observed in the experimental results which exhibit a lower performance due to the experimental implementation penalty illustrated in figure 4.20.

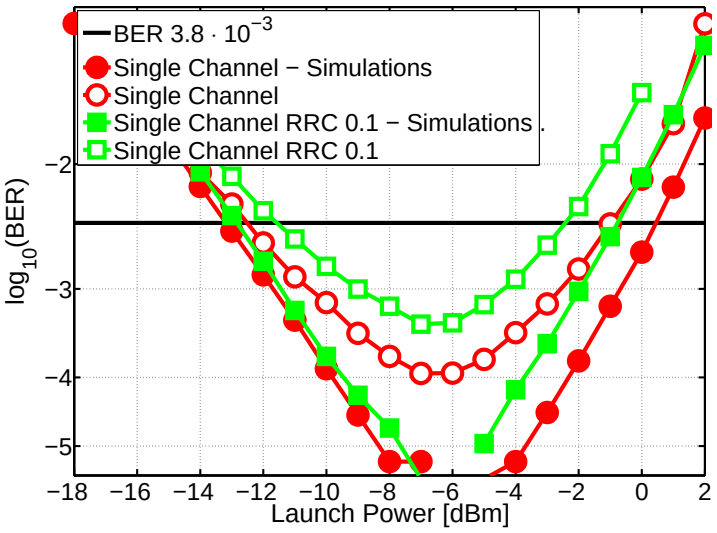

Figure 4.21: Simulation and experimental results for single channel transmission over 1200 km with and without RRC filtering, BER vs launch power per sub-carrier.

Once the single channel performance was established as a base the optical frequency combs were used to implement a WDM system. Although, the generation techniques were able to achieve a power variation less than 0.5 dB after separating odd and even

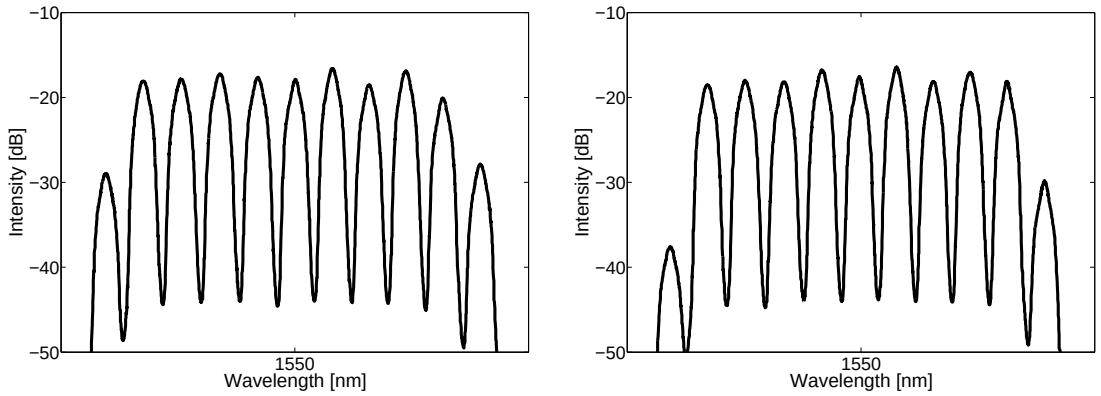

Figure 4.22: Transmitted optical spectra of the full superchannel; **a)** Cascaded modulators comb **b)** DD-MZM comb.

channels, modulating and combining them the resulting power variation was less than 2 dB, as illustrated in figure 4.22. The launch power per channel was calculated by averaging the launch power across the superchannel. The LO was tuned to three different locations along the full optical superchannel to capture and process the sub-channels in groups of three. Each of the sub-channels were processed with the DSP step described in previous simulation section.

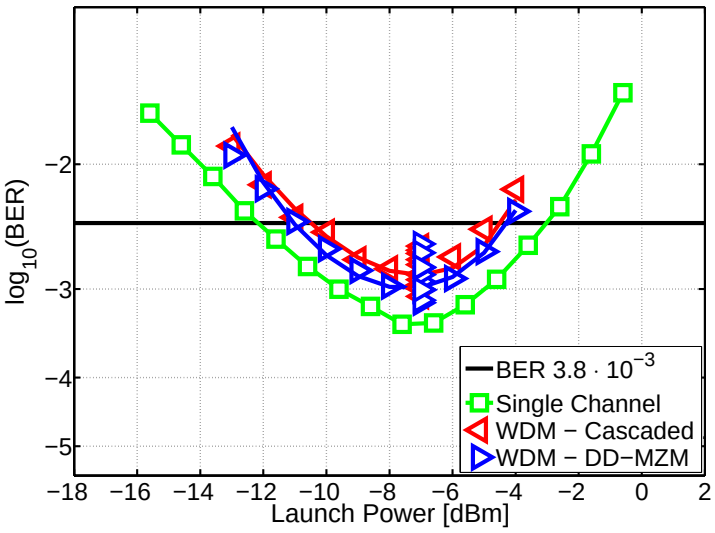

Figure 4.23: Experimental comparison between optical frequency combs in transmission over 1200 km, BER vs launch power per sub-carrier.

The transmission results for the superchannel after 1,200 km using the two different combs is illustrated and compared with the single channel in figure 4.23. The performance of the comb is calculated by averaging the BER across all nine sub-channels. Additionally, at the optimal launch power of -7 dB the individual BER for each sub-

channel in the superchannel is plotted. Although performance variations were observed between sub-channels due to the variation in the initial launch power, once the performance was averaged no significant difference was found between the two generation techniques. These results indicate that any fluctuations in the power spectrum of the superchannel could be negated and absorbed if the data stream is processed jointly by the FEC decoder. Although this would require data synchronisation between sub-channels it could mitigate sub-channel errors that exceed the BER limit.

4.6 Joint Digital Signal Processing (DSP)

In the previous sections optical frequency combs were used as sub- carriers for superchannels, however, each of the sub-channels was processed independently, without utilising the knowledge that the sub-carrier are frequency and phase synchronous. This section will investigate how the DSP can be modified to utilise this additional information.

In DWDM where the guardbands between sub-channels are reduced to achieve Nyquist spacing, crosstalk can be observed. In particular if there is no frequency locking between sub-carriers or if the channels rolloff is not sufficiently sharp, this is known as Inter-Channel Interference (ICI). It has been demonstrated that joint equalisation between adjacent channels can be used to mitigate the incurred penalty [93; 94]. The technique involves an additional equalisation step, after CPE, operating on multiple sub-channels. Although ICI can become problem when the guardbands are reduced to zero, if the sub-carriers are frequency locked and RRC filtering is applied to the sub-channels, the penalty can be significantly reduced.

If the optical frequency comb is used as a sub-carrier source its phase synchronous property can be utilised. So far joint CPE has only been investigated for PDM-QPSK systems using the Viterbi & Viterbi algorithm [93]. This section will focus on extending that work by utilising a DD-CPE for 16QAM to investigate the feasibility and advantages. The conventional DD-CPE algorithm, for a single channel, is presented in section 2.4.3 and shown again in equation (4.6). The phase, at a sample point k, is calculated by making a decision, D, on the symbol and extracting the phase difference compared to the detected symbol, this is then averaged over a window of $2w+1$ symbols

as phase noise is a time varying effect.

$$\phi(k) = \angle \left(\sum_{n=k-w}^{k+w} D[\mathbf{x}(n)]\mathbf{x}(n) \right) \tag{4.6}$$

$$\phi(k) = \angle \left(\sum_{m=0}^{N-1} \left[\sum_{n=k-w}^{k+w} D[\mathbf{x}_m(n)]\mathbf{x}_m(n) \right] \right) \tag{4.7}$$

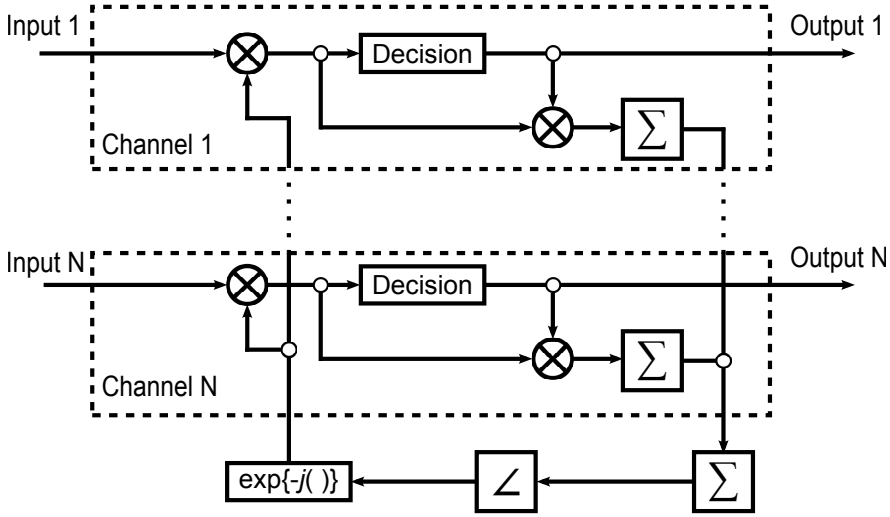

Figure 4.24: Schematic diagram of the joint DD-CPE algorithm operating on multiple channels.

Because the phase of all sub-carriers is the same the principle can be extended to averaging the phase across multiple sub-channels. The schematic of the algorithm is illustrated in figure 4.24 and the mathematical description is presented in equation (4.7). Where N channels are processed together and $\mathbf{x}_m$ is input stream of the m-th channel. Because symbol decisions are made based on the modulation formats, rather than exploiting a symmetry like the Viterbi & Viterbi phase estimator (section 2.4.3), the algorithm suitable for different formats.

4.6.1 Simulation results

The simulation configuration described in section 4.4 was used to generate superchannels with PDM-16QAM. Similarly to the previous sections a nine sub-channel spaced at 10 GHz was modulated with 6 GBd signals and filtered by a RRC filter with a roll-off of 0.1. The phase noise was added synchronously to all sub-carriers to emulate an optical frequency comb.

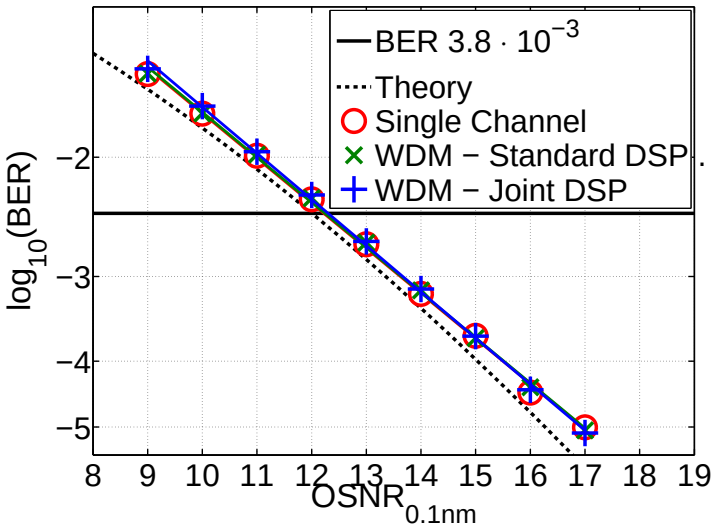

Figure 4.25: Simulations comparing independent and joint DD-CPE compensating for 100 kHz of linewidth, BER vs OSNR with 6 GBd PDM-16QAM in a back-to-back configuration.

Firstly, to verify that the joint CPE algorithm was functioning it was tested on a low phase noise signal, 100 kHz, and compared to the performance of independent CPE. Figure 4.25 illustrates that the performance of algorithm is identical to the conventional algorithm. Because the joint CPE algorithm uses symbols from multiple sub-channels a smaller window length can be utilised to achieve the same performance. The conventional CPE used a window of 32 symbols to estimate the phase, while the joint CPE a window of 3 symbols (27 symbols across all nine sub-channels) could be used. When the phase varies slowly (the phase noise is low) a larger window length can be used to average out the additive noise and improve the SNR tolerance. However, with large window fast phase variation cannot be tracked; requiring smaller averaging windows with lower SNR tolerance. Although the joint CPE estimates the phase variation over a smaller window, by averaging over different realizations of the additive noise the SNR tolerance is preserved. The algorithm was tested by varying the phase noise and optimising the averaging window w for both the independent and the joint CPE. Figure 4.26 demonstrates that the joint CPE algorithm (for nine channels) is able to tolerate linewidths five times larger, for the same OSNR, penalty compared to the independent CPE algorithm. The additional OSNR penalty is plotted against (linewidth) $\times$ (symbol period) product ($\Delta\nu \times T$) to make the results independent of the symbol period. Although both algorithms were tested with even larger phase noise reliable BER was not obtainable due to frequent cycle slips.

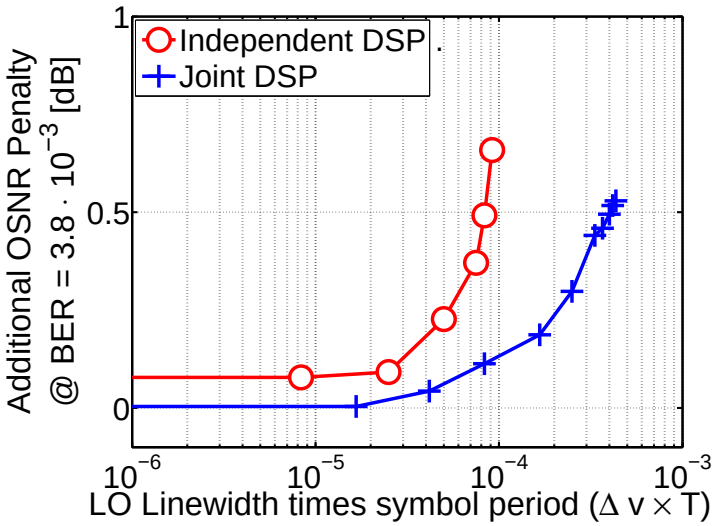

Figure 4.26: Simulations comparing independent and joint DD-CPE, (linewidth) $\times$ (symbol period) product ($\Delta v \times T$) vs additional OSNR penalty at a BER of $3.8 \cdot 10^{-3}$, with 6 GBd PDM-16QAM.

Although significant improvement in linewidth tolerance is achieved in simulations the phase noise in an experiment might not be symbol synchronised between sub-channels. Therefore, to utilise the technique training symbols would have to be inserted periodically to maintain phase synchronisation between sub-channels. An additional advantage would then be that phase can also be estimated on the training symbols resulting in a more robust estimation suitable for higher order modulation formats such as 64 and 256QAM [95; 96].

So far joint CPE has only been investigated and demonstrated in a back- to-back configuration, without fibre transmission which would introduces an additional challenge with CD. The walk-off between frequencies, caused by CD, will result in un-synchronised phase noise at the end of the transmission link. If CD is compensated on a sub-channel basis the frequencies within a channel will be synchronised, however, there will be a time delay between sub-channels. Compensating CD across the full superchannel bandwidth is possible, however, it will introduce equaliser enhanced phase noise, which is an additional amplitude noise, limiting the performance [60; 97]. A future direction would be to investigate if CD can be compensated on a sub-channel basis, to avoid enhanced noise, but to synchronise the sub-channels before applying the joint CPE.

4.7 Summary

This chapter investigated generation techniques of optical frequency combs for optical data communications. Some of the techniques were verified experimentally in a back-to-back configuration and fibre transmission systems. Additionally, the effects of the phase synchronous superchannel were studied and a joint DSP technique, that utilises the additional information, was proposed. The key results from this chapter are:

- Several techniques, such as gain switching and modulator based methods, are able generate suitable combs for data communications. Configurations with optical modulators offer stable and very flexible comb sources at the expense of lower bandwidth, compared to other investigated techniques.

- The linewidth of comb generated from cascaded modulators, was verified by modulating a low symbol rate PDM-16 and 64QAM to exacerbate the impact of phase noise.

- Simulations indicate that phase and frequency synchronisation does not effect the overall performance of a transmission system, without the use of additional optical or digital processing.

- Experimentally two techniques for comb generation ware utilised in implementing a 400 Gb/s superchannel over a transmission system of 1,200 km. Although variation between individual channels was observed the averaged performance of the two combs was identical. The performance variations were caused by the variation in launch power induced by the non-flat power profile of the comb and the modulation process.

- By averaging the phase noise estimator across phase synchronous sub-channels the tolerance was improved by a factor of 5 for the nine sub-channel system that was considered. However implementing this technique in an experimental system requires training symbols to synchronise the phase within a symbol period.

5

Future work

THIS chapter presents future directions to extend the work presented in the previous chapters. In chapter 3 equalisation techniques used to tackle specific problems, such as RRC filtering, receiver delay skew, CD and phase noise, were presented. In this chapter another technique for equalising higher order modulation formats is explored. In chapter 4 techniques for optical frequency comb generation were presented and their performance was tested. As the main impediment was the flatness and the total bandwidth of the comb this chapter looks into an alternative generation technique that overcomes those obstacles. Afterwards, how the inherent multi-dimensional property of superchannels can be utilised is discussed. Finally, future investigations of phase synchronous transmission are reviewed.

5.1 Equalisation of higher order QAM

Although this work has used equaliser for higher order QAM, their design has not been investigated in detail. Additionally, these equalisers have been used extensively

in the literature; 64, 512 1024 and even 2048 QAM [57; 98; 99; 100]. Analysis of equalisers for PDM-16QAM have been carried out using MMA and DD schemes [84; 101], however, mathematical analysis for higher order QAM has not been carefully studied.

Section 2.4.2 discussed the basic concepts of equalisation and acknowledged that DD schemes can sometimes be unsuitable, because frequency offset and phase noise need to be compensated jointly or before equalisation. Additional complications arise when RRC filtering and delay skews are present, resulting in performance penalty (section 3.2). It is more desirable to use blind equalisers such as the MMA which can be carried out independently and prior to frequency offset and phase noise compensation. Therefore this section will explore tailoring the MMA to give better performance with higher order QAM.

5.1.1 Decision boundaries

The first part in updating a MMA equaliser is to determine to which ring amplitude a symbol belongs to after applying the adaptive filter. Intuitively this can be done by selecting the closest ring amplitude to the received constellation point, similar to the following pseudocode[1]:

```
x_out := output value of the equaliser
radii := a vector with all possible radii
minLoc = 1
deviation = abs(abs(x_out)-radii(1))
for n = 1:length(radii)
    temp_deviation = abs(abs(x_out)-radii(n))
    if(temp_deviation < deviation)
        deviation = temp_deviation
        minLoc = n
    end
end
return radii(minLoc)
```

[1]Note that the vectors, arrays, start from index 1.

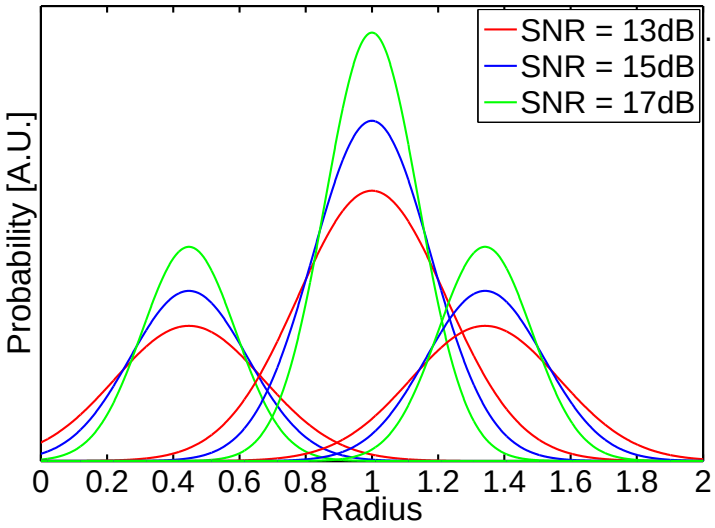

Figure 5.1: Ring amplitude probability distribution of 16QAM for different SNR values.

However, this approach does not utilise the full information about the modulation format. An important aspect of 16QAM is that not all ring amplitudes are equally probably; there are 3 ring amplitudes, the inner and outer rings have a 4 symbols each while the middle ring has 8 symbols. This applies similarly for higher order modulation formats and the probabilistic distributions could be taken into account. Figure 5.1 illustrates the absolute value of a 16QAM constellation with different amounts of AWGN. The optimal decision threshold is not, as might naively be expected, halfway between two amplitude levels, as implicitly assumed above, it actually depends on the SNR.

Considering two radii with Gaussian distributions[2] P_1 and P_2, where μ_1 and μ_2 are the mean radii and σ^2 (SNR = $1/\sigma^2$) is the variance:

$$P_1 = A\frac{1}{\sqrt{2\pi\sigma^2}}\exp\left(\frac{-(r-\mu_1)^2}{2\sigma^2}\right) \qquad P_2 = B\frac{1}{\sqrt{2\pi\sigma^2}}\exp\left(\frac{-(r-\mu_2)^2}{2\sigma^2}\right) \tag{5.2}$$

[2]Note that the actual distribution for the absolute value of complex (two dimensional) Gaussian distribution has a Rician distribution. It is described by equation (5.1), where $I_0(x)$ is the modified Bessel function of the first kind with order zero. However, for large values of r it converges to a Gaussian distribution, which is easier to work in this initial investigation.

$$f(r \mid \nu, \sigma) = \frac{r}{\sigma^2}\exp\left(\frac{-(r^2+\nu^2)}{2\sigma^2}\right) I_0\left(\frac{r\nu}{\sigma^2}\right) \tag{5.1}$$

If they are equally probable ($B/A = 1$) then the decision threshold can be calculated as follows:

$$\begin{aligned} P_1 &= P_2 \\ \frac{1}{\sqrt{2\pi\sigma^2}}\exp\left(\frac{-(r-\mu_1)^2}{2\sigma^2}\right) &= \frac{1}{\sqrt{2\pi\sigma^2}}\exp\left(\frac{-(r-\mu_2)^2}{2\sigma^2}\right) \\ \frac{-(r-\mu_1)^2}{2\sigma^2} &= \frac{-(r-\mu_2)^2}{2\sigma^2} \\ r^2 - 2r\mu_1 + \mu_1^2 &= r^2 - 2r\mu_2 + \mu_2^2 \\ 2r(\mu_2-\mu_1) &= \mu_2^2 - \mu_1^2 \\ r_{Threshold} &= \frac{\mu_2^2-\mu_1^2}{2(\mu_2-\mu_1)} = \frac{(\mu_2+\mu_1)}{2} \end{aligned} \tag{5.3}$$

Which is equivalent to the closest ring calculation discussed above. However, if the P_1 and P_2 are not equally probable[3], $A \neq B$. Note that if $A = B$ the threshold reduces to the previous equation:

$$\begin{aligned} P_1 &= P_2 \\ \frac{1}{\sqrt{2\pi\sigma^2}}\exp\left(\frac{-(r-\mu_1)^2}{2\sigma^2}\right) &= B\frac{1}{\sqrt{2\pi\sigma^2}}\exp\left(\frac{-(r-\mu_2)^2}{2\sigma^2}\right) \\ \frac{-(r-\mu_1)^2}{2\sigma^2} &= \ln(B) - \frac{-(r-\mu_2)^2}{2\sigma^2} \\ -r^2 + 2r\mu_1 - \mu_1^2 &= 2\sigma^2\ln(B) - r^2 + 2r\mu_2 - \mu_2^2 \\ 2r(\mu_1-\mu_2) &= 2\sigma^2\ln(B) - \mu_2^2 + \mu_1^2 \\ r_{Threshold} &= \frac{2\sigma^2\ln(B)+\mu_1^2-\mu_2^2}{2(\mu_1-\mu_2)} \end{aligned} \tag{5.4}$$

In this scenario the threshold is shifted towards the ring with smaller probability and a different logic for determining the ring amplitude is required:

```
x_out := output value of the equaliser
radii := a vector with all possible radii
thresholds := a vector with pre-calculated
              threshold values based on SNR
for n = 1:length(thresholds)
    temp_deviation = abs(abs(x_out)-radii(n))
```

[3]It is possible to set $A = 1$ without losing any generality.

```
    if(thresholds(n) < abs(x_out))
        return radii(n)
    end
end
return radii(length(radii))
```

This becomes more important as higher order QAM are utilised and ring amplitudes have a different probability to adjacent ring amplitudes.

5.1.2 Probabilistic error functions

Another key aspect of an equaliser is how the error term is computed. The error term for the MMA is computed by a Least Mean Squares (LMS) method, equation (5.5), where a discrete decision is made on the radius R. By plotting the error term as a function of the radius, figure 5.2, it is clear that there are discontinuities in the error function. Around the discontinuities, the confidence about the ring amplitude is the lowest. Yet, counterintuitively that is where the largest error values are present, resulting the largest update. Additionally, as the OSNR, or the SNR, is decreased wrong decisions around the discontinuities become more likely, which could lead performance penalty or equaliser divergence.

$$\varepsilon \leftarrow R^2 - |\mathrm{X}_{out}|^2 \tag{5.5}$$

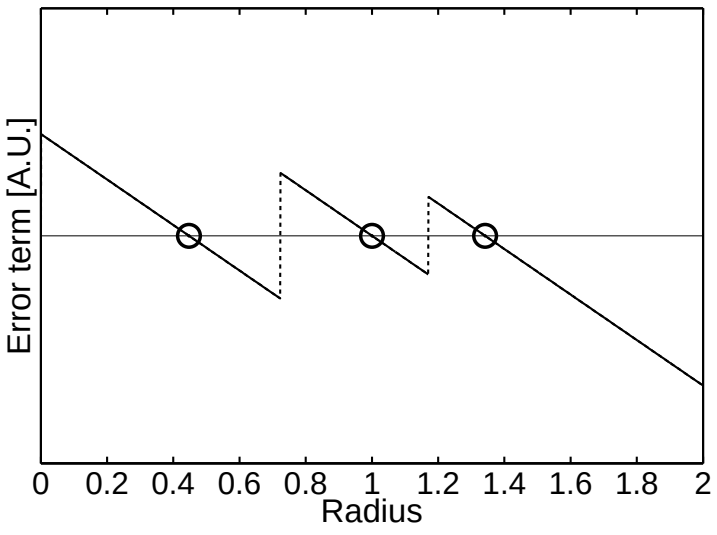

Figure 5.2: Error term as a function radii for 16QAM MMA.

Another approach instead of making a decision on the ring, is to scale the error from each radius, R, by the probability of a symbol having that radius. This is essentially an update algorithm that utilises Maximum *a posteriori* Probability (MAP).

$$\varepsilon \leftarrow \sum_{R} p(x_{out} \mid R) g(x_{out}, R) \tag{5.6}$$

Where R is the set of all possible radii for the modulation format and x_{out} is the output of the equaliser. The first part of the equation, $p(x_{out} \mid R)$[4], is the probability that the output, of the equaliser, x_{out} belongs to radius R and the second part, $g(x_{out}, R)$, represents the error function. These are calculated using equations (5.7), in this preliminary derivation the $g_2(x, R)$ was used. The error term is plotted as a function of the radius in figure 5.3, note that for lower SNR values the error term does not go to zero as expected, instead there is still a large uncertainty about the accuracy of that point.

$$\begin{aligned} p(R \mid x_{out}) &= \frac{1}{\sqrt{2\pi\sigma^2}} \exp\left(\frac{-(R - |x_{out}|)^2}{2\sigma^2}\right) \\ g_1(x_{out}, R) &= R^2 - |x_{out}|^2 \\ g_2(x_{out}, R) &= R - |x_{out}| \end{aligned} \tag{5.7}$$

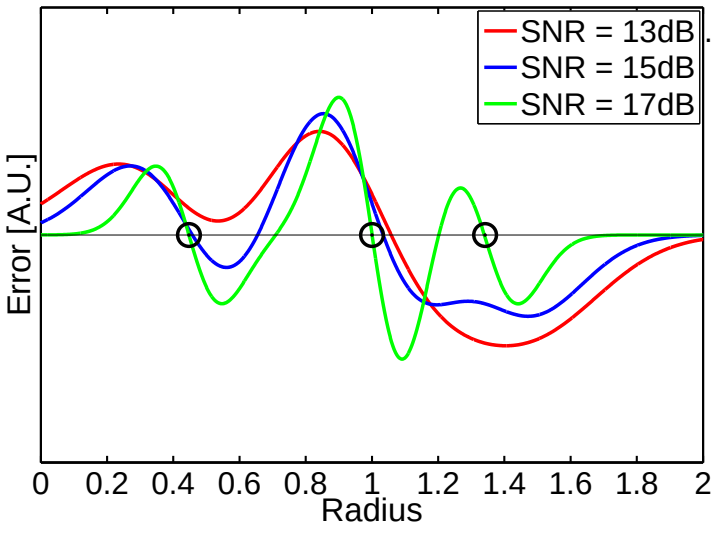

Figure 5.3: Error term as a function radii for 16QAM with the developed MAP equaliser.

[4]Note that $p(x_{out} \mid R) = p(R \mid x_{out})$ due to the symmetry of the Gaussian distribution.

To calculate the update, the gradient of the squared error with respect to the equaliser taps are set to 0. This is equivalent to finding the minimum error with respect to the filter.

$$\begin{aligned} \mathbf{h} &\leftarrow \mathbf{h} - \mu \frac{d\left(\varepsilon^2\right)}{d\mathbf{h}^*} \\ \mathbf{h} &\leftarrow \mathbf{h} - \mu 2\varepsilon \frac{d\left(\varepsilon\right)}{d\mathbf{h}^*} \end{aligned} \tag{5.8}$$

$$\frac{d\left(\varepsilon\right)}{d\mathbf{h}^*} = \frac{x_{in}^* |x_{out}|}{2x_{out}^*} \sum_R p(R \mid x_{out}) \left(\frac{(R - |x_{out}|)^2}{\sigma^2} - 1 \right) \tag{5.9}$$

The final update can then be expressed as follows:

$$\mathbf{h} \leftarrow \mathbf{h} - \mu\varepsilon \frac{x_{in}^* |x_{out}|}{2x_{out}^*} \sum_R p(R \mid x_{out}) \left(\frac{(R - |x_{out}|)^2}{\sigma^2} - 1 \right) \tag{5.10}$$

To verify the equaliser, initially it was then tested and compared to conventional MMA on a simulated 6 GBd PDM-64QAM signal. The results for that are illustrated in figure 5.4. Due to the various effects such as polarisation rotations and low pass filtering the effective SNR, which determines the σ^2 in equation (5.10), needs to be optimised for the specific system. However, the initial simulations of a simplified system show that the performance of the MAP equaliser is identical to the MMA equaliser.

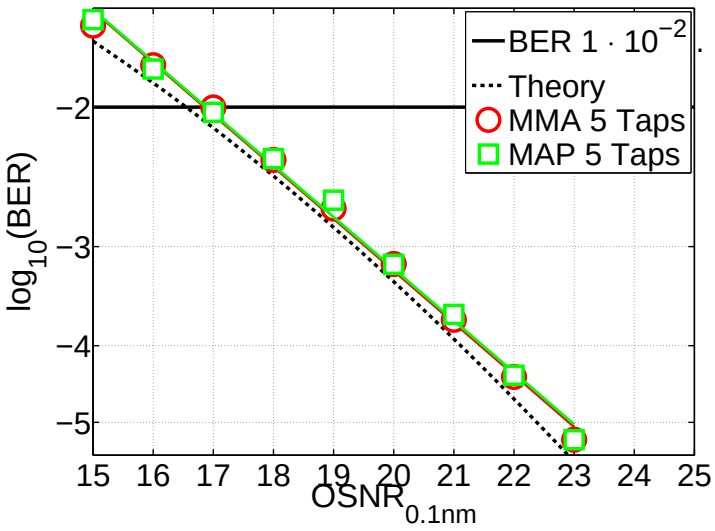

Figure 5.4: Simulations of PDM-64QAM comparing MMA and MAP equalisers.

A simplified version of the concept developed here is to scale the update base on the ring amplitude probability of the current symbol. That technique allowed for higher tolerance of polarisation rotations [102]. However, to fully analyse this equaliser additional simulations and experiments are required.

5.2 Non-linear optical frequency comb generation

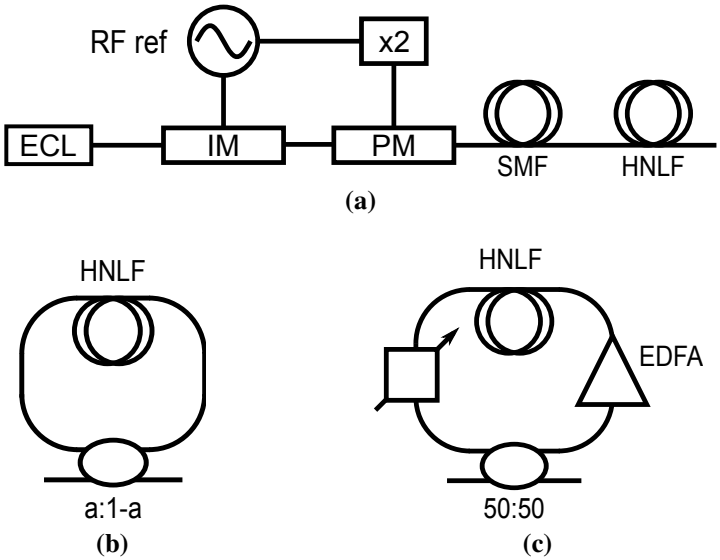

Figure 5.5: a) Basic parametric comb generator. IM: Intensity modulator, PM: Phase modulator. **b)** Pulse compressor Non-linear Optical Loop Mirror (NOLM). **c)** Pulse compressor Non-linear Amplified Loop Mirror (NALM)

Section 4.1 discussed different techniques for optical frequency comb generation, however, all techniques, except for the fibre loop (section 4.1.2), generate combs with up to 30 sub-carriers. Although that is sufficient for a single superchannel it would require multiple generators to fill the optical bandwidth (C-band). Recently, comb generators that are suitable for data communications and span the full C-band have been reported [91; 92]. Instead of using modulators to generate new frequencies the non-linear properties, FWM specifically, of the fibre are utilised. When any two frequencies interact in the non-linear optical fibre they produce two new frequencies as described by equations (5.11), where f_1 and f_2 represent the original frequencies. As the signal propagates through the fibre both additional frequencies are generated and existing frequencies, if f_3 and f_4 have already been generated, are amplified, this process is called parametric amplification. Figure 5.5(a) illustrates a basic example of a parametric comb generator. The intensity and phase modulators are utilised to generate the initial phase-synchronous frequencies. The phase modulator applies a linear chirp to the signal, so SMF is used to compress the time pulse and achieve a higher peak power more suitable for parametric amplification. The signal is then launched through Highly

Non-Linear Fibre (HNLF), where new frequencies are generated.

$$f_3 = f_1 - (f_2 - f_1) = 2f_1 - f_2 \qquad f_4 = f_2 + (f_2 - f_1) = 2f_2 - f_1 \tag{5.11}$$

The efficiency of the FWM process is a function of the power of the original frequencies (P_1 and P_2) and the non-linear parameter of the fibre γ [20; 103]. Additionally, the FWM process requires phase matching between frequencies, which is normally counteracted in SMF as CD decorrelats the frequencies. Therefore, it is advantageous to use non-linear fibres with low or no CD to fully utilise the FWM process. To increase the efficiency of the FWM process the time domain pulse can be compressed additionally, to increase the peak power of the signal before launching into the non-linear fibre. Two different compression techniques have been proposed [92], the use of Non-linear Optical Loop Mirror (NOLM) and Non-linear Amplified Loop Mirror (NALM), which are illustrated in figure 5.5(b) and (c). Both of these devices have a non-linear transfer function expressed with equations (5.12) and (5.14) respectively, where P is the power of the input signal and L is the length of the HNLF loop. They are designed to pass through or amplify the peak power of the signal while attenuating lower powers to achieve a compressed pulse. Their transfer functions oscillate from a blocking state to a transparent state, $T = 1 - 4a(1-a)$ to $T = 1$ for the NOLM and $T = 0$ to $T = GA$ for the NALM. However, achieving transparency requires either large initial peak powers or long fibre loops, as dictated by equations (5.13) and (5.15) for the NOLM and NALM respectively.

$$T = 1 - 2a(1-a)(1 + \cos(\gamma PL(1-2a)) \tag{5.12}$$

$$PL = \frac{\pi}{\gamma(1-2a)} \tag{5.13}$$

$$T = \frac{GA}{2}\left(1 - \cos\left(\gamma PL\frac{G-A}{2}\right)\right) \tag{5.14}$$

$$PL = \frac{2\pi}{\gamma(G-A)} \tag{5.15}$$

Although it is challenging to fulfil all the requirements for the parametric comb it promises enormous bandwidth with a flat power spectrum something that is not achieved with the other techniques investigated in this work. It would allow experimental

investigation of frequency and phase synchronization across the full channel bandwidth rather than a portion of the bandwidth. A superchannel was defined as a group of sub-channels that is routed through the network a single entity, and as such does not usually occupy the full C-band. However, with a sub-carrier source spanning the C-band, it would be possible to generate multiple superchannels which are split through the network as separate entities.

5.3 Multi-dimensional processing

At the end of the previous chapter, section 4.6, joint CPE for a phase synchronous optical frequency combs was investigated. In essence that is a DSP algorithm that operates on multiple dimensions of the optical field, time and frequency. That is only one example of multi-dimensional processing, this section presents a different approach, applicable to single channel system but also extendible to WDM systems, especially if superchannels are utilised.

Although the optical field supports 4 dimensions (4D), which are fully captured by a digital phase- and polarisation-diverse coherent receiver, all of the modulation formats used herein are 2 dimensional (2D). Each polarisation of the optical field is modulated with a separate 2D-format. It has been shown, however, that optimising the modulation format in 4D can achieve a better performance than the two independent formats [18]. If each symbol is represented by a sphere the design of a modulation formats can be visualised as sphere-packing. The optimisation can be carried out on different parameters, such as total power or, the most common metric, SNR performance.

To achieve better SNR tolerance it is desirable for symbols (spheres) to have a large separation, Euclidean distance. The underlying assumption for this optimisation is that the dominant noise source is AWGN which is equally spread in each dimension. The performance of a modulation format is then characterized by the smallest Euclidean distance d_{min} among all symbol pairs, the most likely symbol error. The distance d between any two N-dimensional symbols, p and q, is calculated with equation (5.16). An additional assumption is that the SNR is very high, tends to infinity, because when the SNR is very low a symbol errors are not only caused by the nearest symbol (d_{min}), but rather all possible symbol errors. A more practical approach would be to design the

modulation formats for the SNR region where they are going to used, around the region for of a FEC limit.

$$d = \sum_{k=1}^{N} (p_k - q_k)^2 \tag{5.16}$$

Furthermore, it is possible to utilise other dimensions of the optical signal such as; time, spatial modes and frequency, to design even higher dimensional modulation formats. Cross phase modulation is a non-linear effect which causes interference between frequency channels, when combined with CD results leads to interaction across time, this is then known as channel memory. A similar interaction is also present multi-mode fibres where mode coupling and mode delays are present. If the actual interaction is known in advance, if there is a complete channel model, this should be considered in the design process to achieve a channel aware modulation format.

A closely related alternative approach is to use coded modulation, which is a method for adding redundancy to the data stream. By design some multi-dimensional symbols are unused, which increases the minimum Euclidean distance d_{min} and increases the SNR tolerance at the expense of lower spectral efficiency [104; 105]. Similarly coding can be applied across different dimension and the interaction between those dimensions should be considered. One example of this particular technique was to designing a 6D code across in-phase and quadrature components to achieve larger phase noise tolerance [106]. By applying coding across different dimension it could be possible to mitigate some of the interactions between those dimensions, such non-linear crosstalk between sub-channels. Additionally, coding across dimensions can mitigate error burst, in a single dimension, by averaging the performance across dimensions, as discussed in section 4.5.2.

Designing an optimal modulation format and a coding scheme for the optical channel is an open problem. A potential aspect of the solution would be to apply joint processing across all interacting dimensions of the optical signal.

These techniques are very suitable for WDM utilising combs, because the sub-channels propagate and interact together as single entity. Additionally, if equalisation and CPE is applied jointly across the superchannel, an extension to multi-dimensional modulation formats or coding is convenient next step.

5.4 Phase synchronous transmission

In the previous chapter optical frequency combs were utilised in transmission systems. Additionally, the effects of the phase synchronous nature of combs were investigated in section 4.4. In those simulations, however, no additional optical or digital processing was applied, resulting identical performance with and without phase synchronous sub-carriers. Recently, the phase synchronous of the sub-carrier has been utilised for high bandwidth applications, as discussed in section 4.1.1, which is essentially another form of multi-dimensional processing. Additionally, optical frequency comb in combination with multiple receivers has been used to detect and digitally stitch a large optical bandwidth [73; 74]. The phase synchronisation is important to accomplish a continuous stitching off the sub-bands, otherwise discontinuities would result in performance degradation. Another approach is to utilise a comb to generate a large bandwidth synchronous signal. In a recent work [71; 72] multi-channel pre-compensation for non-linearity has been implement with a comb, which allowed for an improvement in non-linear performance. The individual channels were pre-processed jointly, assuming phase synchronisation, and are therefore no longer independent; requiring a phase synchronous sub-carrier source. In a future work the interaction between phase synchronous sub-carriers and additional specialised processing should be investigated in detail. One specific study would be to analyse the effects of phase synchronous sub-carriers when a more traditional non-linear post-compensation, digital back-propagation, is applied.

6

Conclusions

OPTICAL fibre communication systems will have to be maintained and upgraded as demand for data transfer continues to increase. This has to be done for all parts of the optical infrastructure from transatlantic links to access networks. Each of these areas imposes different specific requirements and faces distinct challenges, but a common requirement is, higher capacity. In this work subsystems and DSP techniques, that alleviate and tackle some of the system constraints, have been proposed. Additionally, with modifications they can be applied to different optical systems.

In section 3.1 for PONs a WDM digital coherent system, which can deliver 10 Gbit/s per user for up to 1024 users, was considered. Although each user would have to be supplied with a digital coherent receiver, a cost challenge on its own, it would offer significant improvements over existing commercial systems that utilise TDM and offer data rates of several 100 Mbit/s. One specific challenge that arises in the system due to bi-directional transmission is backreflections. This effect can causes a severe crosstalk

penalty which would ultimately limit the number of users. This was tackled by spectrally shaping the signal with RRC filters to limit the bandwidth of the signal and minimise the overlap between channels. As DSP resources are scarce at the receiver no matched filter was applied which lead to a small fixed penalty. However, the spectral shaping allowed for greater tolerance to reflected power which subsequently enabled more users.

Section 3.2 discussed an equalisation technique to dynamically compensate for receiver impairments. When spectral shaping is applied, especially with higher order modulation formats and high symbol rates, the time alignment between in-phase and quadrature components becomes critical. A modification to the equaliser structure enabled adaptive compensation of delay skews while also implementing a matched filter for the channel with no additional computational complexity. Although this technique is primarily for systems utilising higher order modulation formats, it can also be used to relax the manufacturing requirements in cost sensitive applications, like PON and metro networks.

The following section 3.3 developed a different modification to the equaliser to adaptively compensate CD. In this scenario additional constraints were added to the equaliser structure to increase the stability and allow easier convergence. A dynamic compensation of 88,000 ps/nm worth of CD, equivalent to 5,200 km at 10.7 GBd or 770 km at 28 GBd, is demonstrated. Dynamic compensation of CD can be utilised in medium ranged metro networks with dynamic routing, where the receiving node has no prior knowledge about the signal source. This would enable the routing algorithms to distribute signals through the network more freely.

To tackle some of the DSP computational complexity, in section 3.4, multiplier free updates were investigated. Half of the equaliser complexity is in the update scheme and by making them multiplier free the computational complexity is substantially reduced. This is especially attractive for low power, low cost systems like PONs and metro networks. Additionally it was demonstrated that although the complexity was reduced the performance was not diminished for the considered systems.

After investigating DSP algorithms for single channel systems the focus was shifted towards WDM systems. Multi channel systems are required to utilise the full optical fibre bandwidth. There are two main approaches to maximise the capacity of a WDM system; use higher order modulation formats which are able to carry more data or to

minimise the guardbands between channels. By applying RRC filtering to each channel their spectral bandwidths are reduced which enables DWDM systems, superchannels. When the guardbands are reduced, it is critical that each individual channel's central frequency does not fluctuate otherwise this will incur severe crosstalk penalty. Optical frequency combs were investigated in this work as a sub-carrier source, with fixed frequency spacing and synchronised phase, to mitigate channel frequency variations. Several generation techniques were studied for the application of data communications. Subsequently the generated comb were modulated with PDM-16 and 64QAM implementing full superchannels. While frequency stability and phase noise did not limit the performance, variation between sub-channels of the superchannel were observed due to the non-flat power spectrum of the launched signal. Additionally, the effects of phase synchronisation between sub-channels was investigated and no performance deviation was observed when no additional optical or digital processing was applied.

Finally, to enable higher order modulation formats, with lower phase margin, different compensation techniques were studied. An equaliser interleaved with a CPE algorithm proposed, achieving only a small increase in phase noise tolerance. Another approach, where the linewidth of the LO was measured using with a low bandwidth coherent receiver, and inversely applied to the optical signal, achieved a significant reduction in the effective linewidth. The technique showed one order of magnitude increase in in phase noise tolerance and was demonstrated with PDM-64QAM and high linewidth laser and was later used to enable burstmode transmission with PDM-16QAM. Additionally the phase synchronous nature of the optical frequency comb was utilised for multi channel joint phase estimation. Averaging the phase estimation across nine sub-channel of the superchannel allowed for a factor of 5 increase in phase noise tolerance.

As more computational resources are becoming available at the digital transmitter and receiver many impairments and challenges are tackled with DSP. As the understanding of the optical channel is refined those techniques are further improved and adapted to fit the system of interest. This work studied different parts of the DSP chain and offers insight into separate subsystems. The next step will be to try and combine this knowledge and optimise the optical transmission system as a single entity.

A

Appendix

A.1 Relationship between 2×2 and 4×4 equalisers

This section will step through and derive equations (3.1).

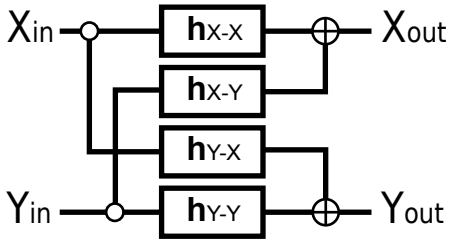

Figure A.1: Equaliser structure for 2×2 MIMO.

For simplicity only the X polarisation is considered, but an equivalent derivation can be done for Y polarisation.

The output of the 2×2 equaliser structure can be expressed using equation (A.1),

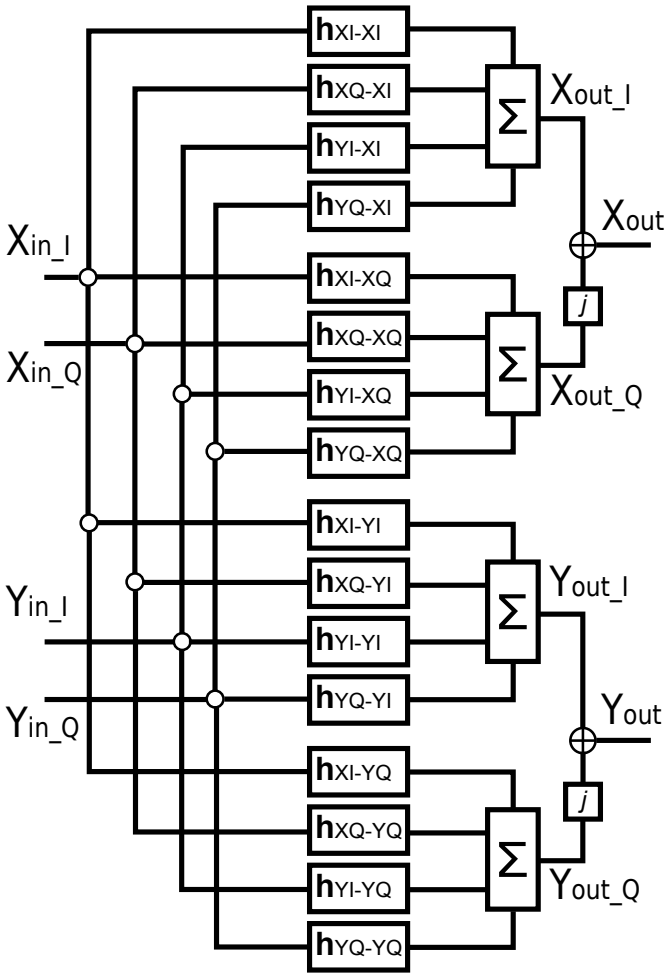

Figure A.2: Equaliser structure for 4×4 MIMO.

with respect to figure A.1.

$$\begin{aligned} \mathrm{X}_{out} &= \mathbf{h}_{XX}(\mathbf{X}_{in\_I} + i\mathbf{X}_{in\_Q}) + \mathbf{h}_{XY}(\mathbf{Y}_{in\_I} + i\mathbf{Y}_{in\_Q}) \\ &= \mathbf{h}_{XX}\mathbf{X}_{in\_I} + i\mathbf{h}_{XX}\mathbf{X}_{in\_Q} + \mathbf{h}_{XY}\mathbf{Y}_{in\_I} + i\mathbf{h}_{XY}\mathbf{Y}_{in\_Q} \end{aligned} \tag{A.1}$$

Similarly the output of the 4×4 equaliser structure can be expressed using equation (A.2), with respect to figure A.2 [1].

$$\begin{aligned} \mathrm{X}_{out} =& (\mathbf{h}_{XI\_XI}X_{in\_I} + \mathbf{h}_{XQ\_XI}X_{in\_Q} + \mathbf{h}_{YI\_XI}Y_{in\_I} + \mathbf{h}_{YQ\_XI}Y_{in\_Q}) + \\ & i(\mathbf{h}_{XI\_XQ}X_{in\_I} + \mathbf{h}_{XQ\_XQ}X_{in\_Q} + \mathbf{h}_{YI\_XQ}Y_{in\_I} + \mathbf{h}_{YQ\_XQ}Y_{in\_Q}) \\ =& (\mathbf{h}_{XI\_XI} + i\mathbf{h}_{XI\_XQ})X_{in\_I} + (\mathbf{h}_{XQ\_XI} + i\mathbf{h}_{XQ\_XQ})X_{in\_Q} + \\ & (\mathbf{h}_{YI\_XI} + i\mathbf{h}_{YI\_XQ})Y_{in\_I} + (\mathbf{h}_{YQ\_XI} + i\mathbf{h}_{YQ\_XQ})Y_{in\_Q} \end{aligned} \tag{A.2}$$

[1] Note that the convention for naming the filter is different; 2×2 $\mathbf{h}_{OutputInput}$ vs 4×4 $\mathbf{h}_{InputOutput}$. This change allows easier reading of the equaliser structures.

By equating equations (A.1) and (A.2), the relationship in equations (A.3) can be extracted.

$$\begin{aligned}
\mathbf{h}_{XX} &= \mathbf{h}_{XI_XI} + i\mathbf{h}_{XI_XQ} \\
i\mathbf{h}_{XX} &= \mathbf{h}_{XQ_XI} + i\mathbf{h}_{XQ_XQ} \\
\mathbf{h}_{XY} &= \mathbf{h}_{YI_XI} + \mathbf{h}_{YI_XQ} \\
i\mathbf{h}_{YX} &= \mathbf{h}_{YQ_XI} + i\mathbf{h}_{YQ_XQ}
\end{aligned} \tag{A.3}$$

Now by translating all the filters in the same form, equation (A.4).

$$\begin{aligned}
\mathbf{h}_{XX} = \mathbf{h}_{XI_XI} + i\mathbf{h}_{XI_XQ} = \mathbf{h}_{XQ_XQ} - i\mathbf{h}_{XQ_XI} \\
\mathbf{h}_{XY} = \mathbf{h}_{YI_XI} + i\mathbf{h}_{YI_XQ} = \mathbf{h}_{YQ_XQ} - i\mathbf{h}_{YQ_XI}
\end{aligned} \tag{A.4}$$

This leads to the constraints in equations (A.5), which include both polarisations.

$$\begin{aligned}
\Re\{\mathbf{h}_{XX}\} &\implies \mathbf{h}_{XI_XI} = \mathbf{h}_{XQ_XQ} \\
\Im\{\mathbf{h}_{XX}\} &\implies \mathbf{h}_{XI_XQ} = -\mathbf{h}_{XQ_XI} \\
\Re\{\mathbf{h}_{XY}\} &\implies \mathbf{h}_{YI_XI} = \mathbf{h}_{YQ_XQ} \\
\Im\{\mathbf{h}_{XY}\} &\implies \mathbf{h}_{YI_XQ} = -\mathbf{h}_{YQ_XI} \\
\Re\{\mathbf{h}_{YX}\} &\implies \mathbf{h}_{XI_YI} = \mathbf{h}_{XQ_YQ} \\
\Im\{\mathbf{h}_{YX}\} &\implies \mathbf{h}_{XI_YQ} = -\mathbf{h}_{XQ_YI} \\
\Re\{\mathbf{h}_{YY}\} &\implies \mathbf{h}_{YI_YI} = \mathbf{h}_{YQ_YQ} \\
\Im\{\mathbf{h}_{YY}\} &\implies \mathbf{h}_{YI_YQ} = -\mathbf{h}_{YQ_YI}
\end{aligned} \tag{A.5}$$

The same equations can be derived by expanding and restructuring the structure from figure A.1; this is done in figure A.3.

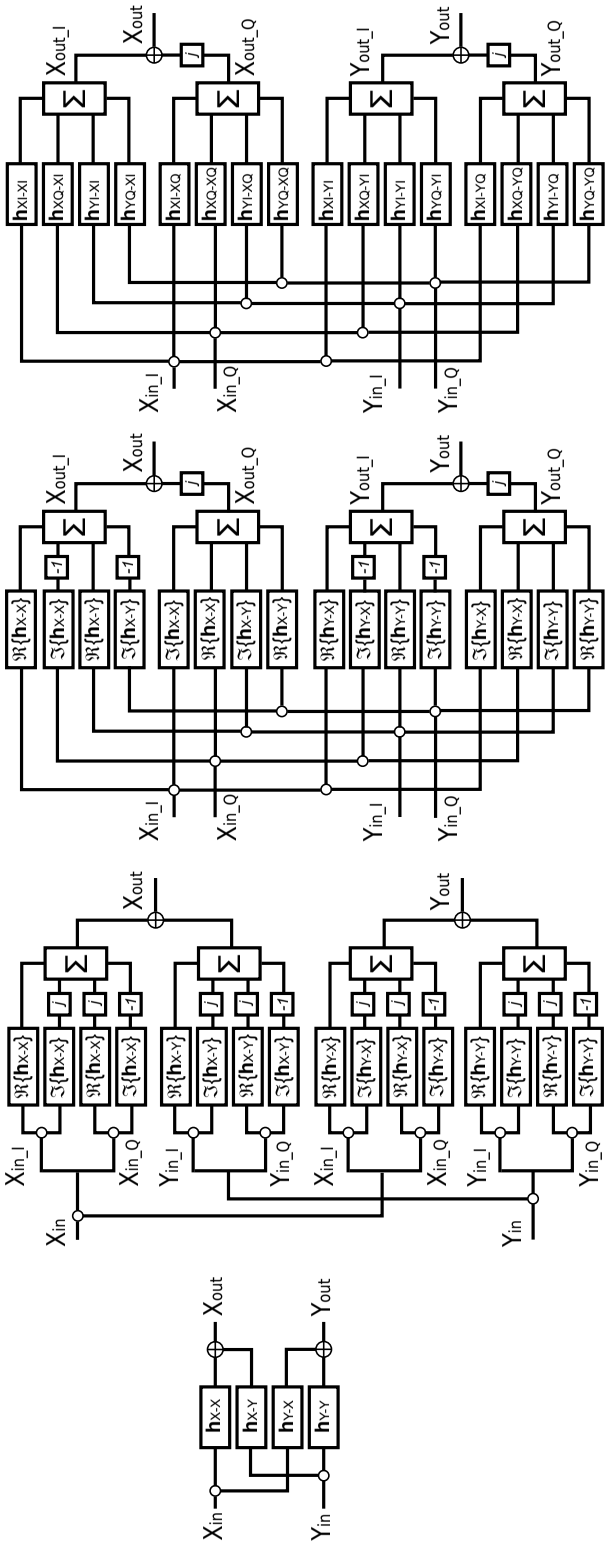

Figure A.3: Relationship between 2×2 and 4×4 equalisers.

A.2 Average update for adaptive CD equalisation

The Constant Modulus Algorithm (CMA) assumes that the modulus (absolute value) of the signal is constant and tries to update the filter taps of an equaliser to achieve that. In the presence of polarisation rotations that is not valid, as illustrated in in figure A.4 where a rotation $\pi/8$ (22.5°) is included. In the CMA that is reflected in the cross polarisation filters $\mathbf{h}_{XY}$ and $\mathbf{h}_{YX}$, and the polarisations rotations are corrected. However, for the pre-convergence stage in the adaptive CD equalisation the cross polarisations filters are not updated. This will then result in an error which cannot be compensated during pre-convergence. An alternative is to use a modified update scheme which does not try to correct the absolute value of the signal per polarisation, but tries to conserve a constant total power.

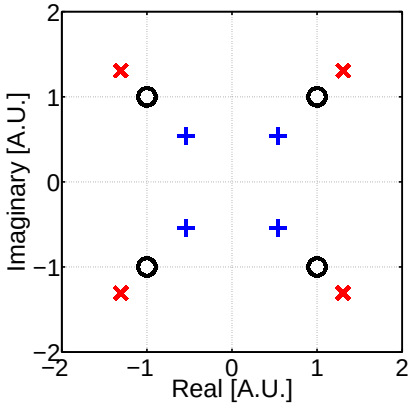

Figure A.4: Polarisation rotation of QPSK, $\Theta = 22.5°$; black are the original points while red and blue represent X and Y polarisations respectively.

The equaliser filters are applied to the input signal as follows, equation (A.6). Where $\mathbf{h}_{CD}$ is the adaptive CD filter, which is the same for both X and Y polarisations and T denotes the transpose. For convenience the inner product notation in equation (A.7) will be used.

$$\mathrm{X}_{out} = \mathbf{h}_{CD}^{T}\mathbf{X}_{in} \qquad \mathrm{Y}_{out} = \mathbf{h}_{CD}^{T}\mathbf{Y}_{in} \tag{A.6}$$

$$\mathrm{X}_{out} = \mathbf{h}_{CD} \cdot \mathbf{X}_{in} \qquad \mathrm{Y}_{out} = \mathbf{h}_{CD} \cdot \mathbf{Y}_{in} \tag{A.7}$$

The error terms are the same per polarisation, equation (A.8), however, instead of

averaging the updated filters the errors are averaged.

$$\begin{aligned} \varepsilon_x &\leftarrow 1-|\mathrm{X}_{out}|^2 \qquad \varepsilon_y \leftarrow 1-|\mathrm{Y}_{out}|^2 \\ \varepsilon &= \frac{\varepsilon_x+\varepsilon_y}{2} = \frac{2-|\mathrm{X}_{out}|^2-|\mathrm{Y}_{out}|^2}{2} \end{aligned} \tag{A.8}$$

Similar to CMA the update is derived based on minimizing the gradient of the squared error, equation (A.9).

$$\mathbf{h}_{CD} \leftarrow \mathbf{h}_{CD} - \mu \frac{d\left(\varepsilon^2\right)}{d\mathbf{h}_{CD}^*} \tag{A.9}$$

Setting the gradient to 0 to solving the equation the increment in the taps is derived in equations (A.10), (A.11), (A.12).

$$0 = \frac{d\left(\varepsilon^2\right)}{d\mathbf{h}_{CD}^*} = 2\varepsilon \frac{d\varepsilon}{d\mathbf{h}_{CD}^*} \tag{A.10}$$

$$\begin{aligned} \frac{d\varepsilon}{d\mathbf{h}_{CD}^*} &= \frac{d\left(\left(2-|\mathrm{X}_{out}|^2-|\mathrm{Y}_{out}|^2\right)/2\right)}{d\mathbf{h}_{CD}^*} \\ &= \frac{1}{2}\frac{d\left(2-|\mathbf{h}_{CD}\cdot\mathbf{X}_{in}|^2-|\mathbf{h}_{CD}\cdot\mathbf{Y}_{in}|^2\right)}{d\mathbf{h}_{CD}^*} \\ &= \frac{1}{2}\frac{d\left(2-\left(\mathbf{h}_{CD}^T\cdot\mathbf{X}_{in}\right)\left(\mathbf{h}_{CD}^*\cdot\mathbf{X}_{in}^*\right)-\left(\mathbf{h}_{CD}\cdot\mathbf{Y}_{in}\right)\left(\mathbf{h}_{CD}^*\cdot\mathbf{Y}_{in}^*\right)\right)}{d\mathbf{h}_{CD}^*} \\ &= \frac{-\left(\mathbf{h}_{CD}^T\cdot\mathbf{X}_{in}\right)\mathbf{X}_{in}^*-\left(\mathbf{h}_{CD}\cdot\mathbf{Y}_{in}\right)\mathbf{Y}_{in}^*}{2} \\ &= \frac{-\mathrm{X}_{out}\mathbf{X}_{in}^*-\mathrm{Y}_{out}\mathbf{Y}_{in}^*}{2} \end{aligned} \tag{A.11}$$

$$\frac{d\left(\varepsilon^2\right)}{d\mathbf{h}_{CD}^*} = -\left(\varepsilon_x+\varepsilon_y\right)\frac{\left(\mathrm{X}_{out}\mathbf{X}_{in}^*+\mathrm{Y}_{out}\mathbf{Y}_{in}^*\right)}{2} \tag{A.12}$$

The final updates are shown in equation (A.13), where μ is the convergence parameter.

$$\mathbf{h}_{CD} \leftarrow \mathbf{h}_{CD} + \frac{\mu}{2}(\varepsilon_x+\varepsilon_y)(\mathrm{X}_{out}\mathbf{X}_{in}^*+\mathrm{Y}_{out}\mathbf{Y}_{in}^*) \tag{A.13}$$

This update algorithm is agnostic to polarisation rotations, meaning that even if there are polarisation rotations the sum of ε_x and ε_y will result in 0 and the equaliser will reach a stable state.

A.3 Computational complexity calculations

In chapter 3, section 3.2, a 4×4 equaliser was introduced, subsequently a lower complexity version was discussed in section 3.4. This section will discuss the assumptions and detail the computational complexity calculations.

All the calculations will be broken down into basic components such as multiplications, additions, inverters, bit shifters and comparators. The first assumption is that multiplications have the highest computational complexity followed by additions. Therefore the complexity calculations are often compared by the total number of multiplications. In hardware, however, the complexity and ultimately the power consumption is highly dependent on the precision of the calculations, the number of bits used to represent the each number. In some scenarios it might even mean that multiplications and additions have comparable power consumption [54]. The precision of the calculations will not be considered in the following calculations. Additionally the complexity calculations will be done for the time domain applications, although implementing some parts in the frequency domain would potentially lower the complexity in terms of multiplications and power consumption.

One of the main assumptions throughout the analysis in this section is that complex multiplications require four real-valued multiplications (hereafter real multiplications). There are several known methods to implement complex multiplications with only three real multiplications but they require extra additions [42]. If w and v are two complex numbers ($w = a + jb$, $v = c + jd$) the multiplications can be performed either using four multiplications, two additions and 1 inverter, equation (A.14), or using three multiplications, five additions and 2 inverters, equation (A.15).

$$wv = (a + jb)(c + jd) = (ac - bd) + j(ad + bc) \tag{A.14}$$

$$wv = [d(a-b) + a(c-d)] + j\,[d(a-b) + b(c+d)] \tag{A.15}$$

Calculating the output samples for each filter is done using equation (A.16), independent of the update scheme for the filter coefficient. For the 2×2 equaliser the filter coefficients $\mathbf{h}$ and the input signal $\mathbf{X}$ are both complex resulting in complex multiplications. For all the 4×4 equaliser, however, both $\mathbf{h}$ and $\mathbf{X}$ are real-valued, resulting in real

multiplications.

$$\mathbf{h}^T \mathbf{X}_{in} = \sum_{n=0}^{N-1} \mathbf{h}(n)\, \mathbf{X}_{in}(k-n) \tag{A.16}$$

	Real Multiplications	Real Additions	Inverters
2×2	16N	16N-4	4N
4×4	16N	16N-4	0

Table A.1: Computational implementation complexity for applying the equaliser filters.

Each complex filter requires, N complex multiplications and (N-1) complex additions, where N is the number of taps of the filter. Converting those into real multiplications and additions results in 4N multiplications and 2N + 2(N-1) additions, as well as N inverters. The real filters require N real multiplications and (N-1) real additions. The 2×2 equaliser has four complex filters while the 4×4 equaliser has 16 real-valued filters, whose outputs are summed up in groups, the total complexity is shown in table A.1. This shows that the equaliser structures have the same complexity both in terms of multiplications and additions.

$$\begin{aligned}
\mathbf{h}_{XX} &\leftarrow \mathbf{h}_{XX} + \mu\varepsilon_x \mathrm{X}_{out} \mathbf{X}_{in}^* \\
\mathbf{h}_{XY} &\leftarrow \mathbf{h}_{XY} + \mu\varepsilon_x \mathrm{X}_{out} \mathbf{Y}_{in}^* \\
\mathbf{h}_{YX} &\leftarrow \mathbf{h}_{YX} + \mu\varepsilon_y \mathrm{Y}_{out} \mathbf{X}_{in}^* \\
\mathbf{h}_{YY} &\leftarrow \mathbf{h}_{YY} + \mu\varepsilon_y \mathrm{Y}_{out} \mathbf{Y}_{in}^*
\end{aligned} \tag{A.17}$$

The updates for the conventional 2×2 equaliser are shown in equation (A.17). If the μ is of the form 2^{-k} for a k-integer then it can easily be implemented as a bit shifter rather than multiplication, which saves hardware resources. The terms $(\mu\varepsilon_x)\mathrm{X}_{out}$ and $(\mu\varepsilon_y)\mathrm{Y}_{out}$ need to be calculated only once. Because X_{out} and Y_{out} are complex, while μ and ε are real, this can be done with 1 bit shifter and 2 real multiplication each, for a total of 2 bit shifters and 4 real multiplications. Afterwards the following terms are calculated $(\mu\varepsilon_x \mathrm{X}_{out})\mathbf{X}_{in}^*$, $(\mu\varepsilon_x \mathrm{X}_{out})\mathbf{Y}_{in}^*$, $(\mu\varepsilon_x \mathrm{Y}_{out})\mathbf{X}_{in}^*$, $(\mu\varepsilon_x \mathrm{Y}_{out})\mathbf{Y}_{in}^*$ each requiring 4 real multiplications, 2 additions and 1 inverter per tap (1 complex multiplication per tap). The conjugations $\mathbf{X}_{in}^*$ and $\mathbf{Y}_{in}^*$ can be done once and requires a total of 2N inverters. Those terms are subsequently added to the previous filter coefficients using 2N real

additions per filter.

$$\left.\begin{aligned}
\mathbf{h}_{mn} &\leftarrow \mathbf{h}_{mn} + \mu\, \varepsilon_k\, \mathrm{n}_{out}\, \mathbf{m}_{in} \\
\mathbf{h}_{mn} &\leftarrow \mathbf{h}_{mn} + \mu\, \varepsilon_k\, \mathrm{sgn}(\mathrm{n}_{out})\, \mathbf{m}_{in} \\
\mathbf{h}_{mn} &\leftarrow \mathbf{h}_{mn} + \mu\, \mathrm{sgn}(\varepsilon_k)\, \mathrm{sgn}(\mathrm{n}_{out})\, \mathbf{m}_{in}
\end{aligned}\right\} \quad m,n \in \{XI,XQ,YI,YQ\} \tag{A.18}$$

The updates for the 4×4 equaliser, with and without the simplified updates are all summarized in equations (A.18). All the values in the 4×4 equaliser are real resulting in real multiplications and additions. The terms $\mu\varepsilon_x$ and $\mu\varepsilon_y$ are calculated only once, requiring only 2 bit shifters. Next the terms $(\mu\varepsilon_x)\mathrm{XI}_{out}$, $(\mu\varepsilon_x)\mathrm{XQ}_{out}$, $(\mu\varepsilon_y)\mathrm{YI}_{out}$ and $(\mu\varepsilon_y)\mathrm{YQ}_{out}$ are calculated for a total of 4 multiplications. Each of those four terms is then multiplied with each of $\mathbf{XI}_{in}$, $\mathbf{XQ}_{in}$, $\mathbf{YI}_{in}$ and $\mathbf{YQ}_{in}$ requiring 16N multiplications. The results of those multiplications are added to previous filter coefficients using N additions for each of the 16 filters.

	Real Multiplications	Real Additions	Inverters	Bit Shifter
2×2 Conventional	16N + 4	16N	6N	2
4×4 Conventional	16N + 4	16N	0	2
4×4 Sign-Data	8N	16N	16N	2
4×4 Sign-Sign	0	16N	16N+4	2

Table A.2: Computational implementation complexity for different update schemes.

For the Sign-Data algorithm the signum function is applied to the output of the equaliser XI_{out}, XQ_{out}, YI_{out} and YQ_{out}, requiring 4 comparators. The terms $\mu\varepsilon_x$ and $\mu\varepsilon_y$ are again calculated only once, requiring only 2 bit shifters. Next, the terms $(\mu\varepsilon)\mathbf{XI}_{in}$, $(\mu\varepsilon)\mathbf{XQ}_{in}$, $(\mu\varepsilon)\mathbf{YI}_{in}$ and $(\mu\varepsilon)\mathbf{YQ}_{in}$ for each polarisation are calculated using a total of 8N multiplications. Afterwards, multiplications with the $\mathrm{sgn}(XI_{out})$, $\mathrm{sgn}(XQ_{out})$, $\mathrm{sgn}(YI_{out})$ and $\mathrm{sgn}(YQ_{out})$, which have values[2] of ± 1 are simplified to N inverters per filter. The update to the previous filter coefficients is then performed with 16N additions.

In the Sign-Sign algorithm the signum is also applied to the ε_x and ε_y using 2 additional comparators. Following that the terms $\mu\mathrm{sgn}(\varepsilon_x)\mathrm{sgn}(\mathrm{XI}_{out})$, $\mu\mathrm{sgn}(\varepsilon_x)\mathrm{sgn}(\mathrm{XQ}_{out})$, $\mu\mathrm{sgn}(\varepsilon_y)\mathrm{sgn}(\mathrm{YI}_{out})$ and $\mu\mathrm{sgn}(\varepsilon_y)\mathrm{sgn}(\mathrm{YQ}_{out})$ are calculated using 2 bit shifters and 4

[2]The zero value of the sgn-function can be discarded for simplified implementation.

inverters. The subsequent multiplications with $\mathbf{XI}_{in}$, $\mathbf{XQ}_{in}$, $\mathbf{YI}_{in}$ and $\mathbf{YQ}_{in}$ requires only N inverters for each of the 16 filters. Again the update to the previous filter coefficients is then performed with 16N additions.

The computational complexity for all update schemes are summarised in table A.2.

References

[1] Cisco, "Cisco visual networking index: Forecast and methodology, 2012-2017," Cisco, Technical Report, May 2013. [Online]. Available: http://www.cisco.com/en/US/solutions/collateral/ns341/ns525/ns537/ns705/ns827/white_paper_c11-481360_ns827_Networking_Solutions_White_Paper.html 16

[2] G. Gilder, *TELECOSM: How Infinite Bandwidth will Revolutionize Our World*, 1st ed. Simon & Schuster, Jun 2000. 16

[3] O. Tonguz and R. Wagner, "Equivalence between preamplified direct detection and heterodyne receivers," *Photonics Technology Letters, IEEE*, vol. 3, no. 9, pp. 835–837, Sep 1991. 17

[4] M. Paskov, D. Lavery, and S. Savory, "Blind Equalization of Receiver In-Phase/Quadrature Skew in the Presence of Nyquist Filtering," *Photonics Technology Letters, IEEE*, vol. 25, no. 24, pp. 2446–2449, 2013. 19

[5] M. Paskov, D. Lavery, B. C. Thomsen, and S. J. Savory, "Blind adaptive equalization of chromatic dispersion for PDM-QPSK," in *Optical Fibre Technology, 2014 OptoElectronics and Communication Conference and Australian Conference on*, Jul 2014, pp. 947–949. 19

[6] D. Lavery, R. Maher, M. Paskov, B. Thomsen, P. Bayvel, and S. Savory, "Digital Coherence Enhancement Enabling 6-GBd DP-64QAM Using a 1.4-MHz Linewidth Laser," *Photonics Technology Letters, IEEE*, vol. 25, no. 22, pp. 2213–2216, 2013. 19

[7] R. Maher, D. Lavery, M. Paskov, P. Bayvel, S. Savory, and B. Thomsen, "Fast

Wavelength Switching 6 GBd Dual Polarization 16QAM Digital Coherent Burst Mode Receiver," *Photonics Technology Letters, IEEE*, vol. 26, no. 3, pp. 297–300, Feb 2014. 19, 75

[8] R. Killey, M. Sezer Erkilinc, R. Maher, M. Paskov, S. Kilmurray, R. Bouziane, B. Thomsen, S. Savory, and P. Bayvel, "Nyquist-WDM-based system performance evaluation," in *Transparent Optical Networks (ICTON), 2013 15th International Conference on*, 2013, pp. 1–4. 19

[9] M. Erkilinc, R. Maher, M. Paskov, S. Kilmurray, S. Pachnicke, H. Griesser, B. Thomsen, P. Bayvel, and R. Killey, "Spectrally-efficient single-sideband subcarrier-multiplexed quasi-Nyquist QPSK with direct detection," in *Proceedings of European Conference on Optical Communication (ECOC)*, 2013, pp. 1–3. 19, 78

[10] P. M. Anandarajah, R. Zhou, R. Maher, D. Lavery, M. Paskov, B. Thomsen, S. Savory, and L. P. Barry, "Gain-switched multicarrier transmitter in a long-reach UDWDM PON with a digital coherent receiver," *Optics Letters*, vol. 38, no. 22, pp. 4797–4800, Nov 2013. 19, 78, 82

[11] R. Zhou, P. Anandarajah, R. Maher, M. Paskov, D. Lavery, B. Thomsen, S. Savory, and L. Barry, "80-km Coherent DWDM-PON on 20-GHz Grid With Injected Gain Switched Comb Source," *Photonics Technology Letters, IEEE*, vol. 26, no. 4, pp. 364–367, Feb 2014. 19, 78, 82

[12] P. M. Anandarajah, R. Zhou, V. Vujicic, M. Deseada Gutierrez Pascual, R. Maher, D. Lavery, M. Paskov, B. Thomsen, S. Savory, and L. P. Barry, "Long reach UDWDM PON with direct and coherent detection," in *Transparent Optical Networks (ICTON), 2014 16th International Conference on*, Jul 2014, pp. 1–1. 19, 82

[13] P. Rosa, M. Erkilinc, R. Maher, M. Paskov, S. Kilmurray, M. Tan, P. Harper, I. Philips, A. Ellis, J.-D. Ania-Castanon, B. Thomsen, S. Savory, R. Killey, and P. Bayvel, "Nyquist-WDM PDM-QPSK transmission over SMF-28 fibre using URFL amplification," in *Transparent Optical Networks (ICTON), 2014 16th International Conference on*, Jul 2014, pp. 1–3. 19

[14] M. S. Erkilinç, S. Kilmurray, R. Maher, M. Paskov, R. Bouziane, S. Pachnicke, H. Griesser, B. C. Thomsen, P. Bayvel, and R. I. Killey, "Nyquist-shaped dispersion-precompensated subcarrier modulation with direct detection for spectrally-efficient WDM transmission," *Optics Express*, vol. 22, no. 8, pp. 9420–9431, Apr 2014. 19

[15] K. Kikuchi, T. Okoshi, and J. Kitano, "Measurement of bit-error rate of heterodyne-type optical communication system - a simulation experiment," *Quantum Electronics, IEEE Journal of*, vol. 17, no. 12, pp. 2266–2267, 1981. 24

[16] R. Mears, L. Reekie, I. Jauncey, and D. Payne, "Low-noise erbium-doped fibre amplifier operating at 1.54 μ m," *Electronics Letters*, vol. 23, no. 19, pp. 1026–1028, 1987. 24

[17] B. Widrow, I. Kollar, and M.-C. Liu, "Statistical theory of quantization," *Instrumentation and Measurement, IEEE Transactions on*, vol. 45, no. 2, pp. 353–361, 1996. 27

[18] M. Karlsson and E. Agrell, "Four-dimensional optimized constellations for coherent optical transmission systems," in *Proceedings of European Conference on Optical Communication (ECOC)*, Sep 2010, pp. 1–6. 27, 113

[19] D. Lavery, C. Behrens, and S. J. Savory, "A comparison of modulation formats for passive optical networks," *Optics Express*, vol. 19, no. 26, pp. B836–B841, Dec 2011. 28

[20] G. P. Agrawal, *Nonlinear fiber optics*, 4th ed. Academic Press, 2007. 32, 91, 112

[21] M. Taylor, "Phase estimation methods for optical coherent detection using digital signal processing," *Lightwave Technology, Journal of*, vol. 27, no. 7, pp. 901 –914, Apr 2009. 33

[22] S. J. Savory, "Digital filters for coherent optical receivers," *Optics Express*, vol. 16, no. 2, pp. 804–817, Jan 2008. 35, 57, 58, 59

[23] D. Godard, "Self-Recovering Equalization and Carrier Tracking in Two-Dimensional Data Communication Systems," *Communications, IEEE Transactions on*, vol. 28, no. 11, pp. 1867–1875, Nov 1980. 37

[24] D. Rife and R. Boorstyn, "Single tone parameter estimation from discrete-time observations," *Information Theory, IEEE Transactions on*, vol. 20, no. 5, pp. 591–598, Sep 1974. 39

[25] A. Viterbi and A. Viterbi, "Nonlinear estimation of PSK-modulated carrier phase with application to burst digital transmission," *Information Theory, IEEE Transactions on*, vol. 29, no. 4, pp. 543 – 551, Jul 1983. 39, 54, 59

[26] T. Pfau, S. Hoffmann, and R. Noe, "Hardware-efficient coherent digital receiver concept with feedforward carrier recovery for m -qam constellations," *Lightwave Technology, Journal of*, vol. 27, no. 8, pp. 989 –999, Apr 2009. 39, 40, 53, 65, 86, 88, 89, 92

[27] OFCOM, "Fibre capacity limitations in access networks," OFCOM, Tech. Rep., 2010. [Online]. Available: http://stakeholders.ofcom.org.uk/market-data-research/other/technology-research/research/emerging-tech/fibre/ 42

[28] ITU, "Gigabit-capable passive optical networks (GPON): General characteristics, recommendation G. 984.1," Iternation Telecommunication Union (ITU), Tech. Rep., 2008. [Online]. Available: http://www.itu.int/rec/T-REC-G.984.1/en 42

[29] ——, "10-Gigabit-capable passive optical networks (XG-PON): General requirements, recommendation G. 987.1," Iternation Telecommunication Union (ITU), Tech. Rep., 2010. [Online]. Available: http://www.itu.int/rec/T-REC-G.987.1/en 42

[30] ——, "40-Gigabit-capable passive optical networks (NG-PON2): General requirements, recommendation G. 989.1," Iternation Telecommunication Union (ITU), Tech. Rep., 2013. [Online]. Available: http://www.itu.int/rec/T-REC-G.989.1/en 42

[31] H. Rohde, S. Smolorz, E. Gottwald, and K. Kloppe, "Next generation optical access: 1 Gbit/s for everyone," in *Proceedings of European Conference on Optical Communication (ECOC)*, Sep 2009, pp. 1–3. 42

[32] D. Lavery, M. Ionescu, S. Makovejs, E. Torrengo, and S. J. Savory, "A long-reach ultra-dense 10 Gbit/s WDM-PON using a digital coherent receiver," *Optics Express*, vol. 18, no. 25, pp. 25 855–25 860, Dec 2010. 42

[33] D. Lavery, R. Maher, D. Millar, B. Thomsen, P. Bayvel, and S. Savory, "Digital Coherent Receivers for Long-Reach Optical Access Networks," *Lightwave Technology, Journal of*, no. 99, p. 1, Feb 2013. 42, 43

[34] A. Shahpari, J. Reis, R. Ferreira, D. Neves, M. Lima, and A. Teixeira, "Terabit+ (192x10 Gb/s) Nyquist shaped UDWDM coherent PON with upstream and downstream over a 12.8 nm band," in *Proceedings of Optical Fiber Communications Conference and Exhibition (OFC)*, Mar 2013, pp. 1–3. 43, 47

[35] F. Chang, K. Onohara, and T. Mizuochi, "Forward error correction for 100 G transport networks," *Communications Magazine, IEEE*, vol. 48, no. 3, pp. S48–S55, 2010. 44, 65, 67

[36] D. Lavery, M. Paskov, and S. Savory, "Spectral shaping for mitigating backreflections in a bidirectional 10 Gbit/s coherent WDM-PON," in *Proceedings of Optical Fiber Communications Conference and Exhibition (OFC)*, 2013, pp. 1–3. 47

[37] *OIF-DPC-RX-01.1 - Implementation Agreement for Integrated Dual Polarization Intradyne Coherent Receivers*, Optical Internetwork Forum (OIF) Std., Sep 2011. [Online]. Available: http://www.oiforum.com/documents/implementation-agreements/ 48

[38] A. Beling, N. Ebel, A. Matiss, G. Unterborsch, M. Nolle, J. K. Fischer, J. Hilt, L. Molle, C. Schubert, F. Verluise, and L. Fulop, "Fully-integrated polarization-diversity coherent receiver module for 100G DP-QPSK," in *Proceedings of Optical Fiber Communications Conference and Exhibition (OFC)*, Mar 2011, pp. 1–3. 48

[39] B. Reyes, V. Gopinathan, P. Mandolesi, and M. Hueda, "Joint sampling-time error and channel skew calibration of time-interleaved adc in multichannel fiber optic receivers," in *Circuits and Systems (ISCAS), 2012 IEEE International Symposium on*, May 2012, pp. 2981–2984. 48

[40] M. Faruk and K. Kikuchi, "Compensation for in-phase/quadrature imbalance in coherent-receiver front end for optical quadrature amplitude modulation," *Photonics Journal, IEEE*, vol. 5, no. 2, pp. 7 800 110–7 800 110, 2013. 48

[41] P. Winzer, A. Gnauck, S. Chandrasekhar, S. Draving, J. Evangelista, and B. Zhu, "Generation and 1,200-km transmission of 448-Gb/s ETDM 56-Gbaud PDM 16-QAM using a single I/Q modulator," in *Proceedings of European Conference on Optical Communication (ECOC)*, 2010, pp. 1–3. 48

[42] A. Wenzler and E. Luder, "New structures for complex multipliers and their noise analysis," in *Circuits and Systems, 1995. ISCAS '95., 1995 IEEE International Symposium on*, vol. 2, 1995, pp. 1432–1435 vol.2. 52, 125

[43] S. Lloyd, "Least squares quantization in PCM," *Information Theory, IEEE Transactions on*, vol. 28, no. 2, pp. 129 – 137, Mar 1982. 53, 66, 88, 92

[44] ITU, "Forward error correction for high bit-rate DWDM submarine systems, recommendation G. 975.1," Iternation Telecommunication Union (ITU), Tech. Rep., 2004. [Online]. Available: http://www.itu.int/rec/T-REC-G.975.1-200402-I/en 54, 88, 90

[45] M. Kuschnerov, F. Hauske, K. Piyawanno, B. Spinnler, M. Alfiad, A. Napoli, and B. Lankl, "DSP for Coherent Single-Carrier Receivers," *Lightwave Technology, Journal of*, vol. 27, no. 16, pp. 3614–3622, 2009. 57

[46] D. Wang, C. Lu, A. P. T. Lau, and S. He, "Adaptive chromatic dispersion compensation for coherent communication systems using delay-tap sampling technique," *Photonics Technology Letters, IEEE*, vol. 23, no. 14, pp. 1016–1018, 2011. 57

[47] K. Ishihara, T. Kobayashi, R. Kudo, Y. Takatori, A. Sano, E. Yamada, H. Masuda, and Y. Miyamoto, "Coherent optical transmission with frequency-domain equal-

ization," in *Proceedings of European Conference on Optical Communication (ECOC)*, 2008, pp. 1–2. 57

[48] R. Corsini, A. Peracchi, E. Matarazzo, T. Foggi, J. Nijhof, G. Meloni, L. Poti, R. Magri, and E. Ciaramella, "Blind Adaptive Chromatic Dispersion Compensation and Estimation for DSP-Based Coherent Optical Systems," *Lightwave Technology, Journal of*, vol. 31, no. 13, pp. 2131–2139, 2013. 57

[49] M. S. Faruk and K. Kikuchi, "Adaptive frequency-domain equalization in digital coherent optical receivers," *Optics Express*, vol. 19, no. 13, pp. 12 789–12 798, Jun 2011. 59

[50] D. Millar, S. Makovejs, V. Mikhailov, R. Killey, P. Bayvel, and S. Savory, "Experimental comparison of nonlinear compensation in long-haul PDM-QPSK transmission at 42.7 and 85.4 Gb/s," in *Proceedings of European Conference on Optical Communication (ECOC)*, 2009, pp. 1–2. 59

[51] B. C. Thomsen, R. Maher, D. S. Millar, and S. J. Savory, "Burst Mode Receiver for 112 Gb/s DP-QPSK with parallel DSP," *Optics Express*, vol. 19, no. 26, pp. B770–B776, Dec 2011. 60

[52] F. Hauske, M. Kuschnerov, B. Spinnler, and B. Lankl, "Optical performance monitoring in digital coherent receivers," *Lightwave Technology, Journal of*, vol. 27, no. 16, pp. 3623–3631, 2009. 60

[53] D. J. Ives, P. Bayvel, and S. J. Savory, "Routing, modulation, spectrum and launch power assignment to maximize the traffic throughput of a nonlinear optical mesh network," *Photonic Network Communications*, vol. 29, no. 3, pp. 244–256, 2015. 61

[54] D. Cardenas, D. Lavery, P. Watts, and S. Savory, "Reducing the power consumption of the CMA equalizer update for a digital coherent receiver," in *Proceedings of Optical Fiber Communications Conference and Exhibition (OFC)*, Mar 2014, pp. 1–3. 62, 63, 125

[55] D. Lavery, B. Thomsen, P. Bayvel, and S. Savory, "Reduced complexity equalization for coherent long-reach passive optical networks [invited]," *Optical Com-*

munications and Networking, IEEE/OSA Journal of, vol. 7, no. 1, pp. A16–A27, Jan 2015. 63, 68

[56] A. Poularikas and Z. Ramadan, *Adaptive Filtering Primer with MATLAB*, ser. Electrical Engineering Primer Series. Taylor & Francis, 2006. [Online]. Available: http://books.google.co.uk/books?id=one-Na3QMW0C 64

[57] X. Zhou, L. Nelson, P. Magill, R. Isaac, B. Zhu, D. Peckham, P. Borel, and K. Carlson, "High Spectral Efficiency 400 Gb/s Transmission Using PDM Time-Domain Hybrid 32-64 QAM and Training-Assisted Carrier Recovery," *Lightwave Technology, Journal of*, vol. 31, no. 7, pp. 999–1005, 2013. 68, 105

[58] A. Gnauck, P. Winzer, A. Konczykowska, F. Jorge, J. Dupuy, M. Riet, G. Charlet, B. Zhu, and D. Peckham, "Generation and Transmission of 21.4-Gbaud PDM 64-QAM Using a Novel High-Power DAC Driving a Single I/Q Modulator," *Lightwave Technology, Journal of*, vol. 30, no. 4, pp. 532 –536, feb 2012. 69

[59] I. Kim, O. Vassilieva, P. Palacharla, and M. Sekiya, "Feed-forward optical carrier phase noise compensation in m-qam transmitter," in *Opto-Electronics and Communications Conference (OECC), 2012 17th*, 2012, pp. 148–149. 71

[60] I. Fatadin and S. J. Savory, "Impact of phase to amplitude noise conversion in coherent optical systems with digital dispersion compensation," *Optics Express*, vol. 18, no. 15, pp. 16 273–16 278, Jul 2010. 71, 102

[61] M. Secondini, G. Meloni, T. Foggi, G. Colavolpe, L. Poti, and E. Forestieri, "Phase noise cancellation in coherent optical receivers by digital coherence enhancement," in *Proceedings of European Conference on Optical Communication (ECOC)*, 2010, pp. 1–3. 71

[62] Z. Zan and A. J. Lowery, "Experimental demonstration of a flexible and stable semiconductor laser linewidth emulator," *Optics Express*, vol. 18, no. 13, pp. 13 880–13 885, Jun 2010. 72

[63] A. Sano, T. Kobayashi, S. Yamanaka, A. Matsuura, H. Kawakami, Y. Miyamoto, K. Ishihara, and H. Masuda, "102.3-Tb/s (224 x 548-Gb/s) C- and extended L-band all-Raman transmission over 240 km using PDM-64QAM single carrier

FDM with digital pilot tone," in *Proceedings of Optical Fiber Communications Conference and Exhibition (OFC)*, 2012, pp. 1–3. 9, 74, 75

[64] *OIF-ITLA-MSA-01.2 - Integrable Tunable Laser Assembly Multi Source Agreement*, Optical Internetwork Forum (OIF) Std., Jun 2008. [Online]. Available: http://www.oiforum.com/documents/implementation-agreements/ 78

[65] A. Gnauck, B. Kuo, E. Myslivets, R. Jopson, M. Dinu, J. Simsarian, P. Winzer, and S. Radic, "Comb-Based 16-QAM Transmitter Spanning the C and L Bands," *Photonics Technology Letters, IEEE*, vol. 26, no. 8, pp. 821–824, Apr 2014. 78, 89, 95

[66] E. Temprana, V. Ataie, B. P.-P. Kuo, E. Myslivets, N. Alic, and S. Radic, "Low-noise parametric frequency comb for continuous C-plus-L-band 16-QAM channels generation," *Optics Express*, vol. 22, no. 6, pp. 6822–6828, Mar 2014. 78

[67] X. Zhou and L. E. Nelson, "400G WDM Transmission on the 50 GHz Grid for Future Optical Networks," *Lightwave Technology, Journal of*, vol. 30, no. 24, pp. 3779 –3792, Dec 2012. 78

[68] Y.-K. Huang, E. Ip, T. Xia, G. Wellbrock, M.-F. Huang, Y. Aono, T. Tajima, and M. Cvijetic, "Mixed Line-Rate Transmission (112-Gb/s, 450-Gb/s, and 1.15-Tb/s) Over 3560 km of Field-Installed Fiber With Filterless Coherent Receiver," *Lightwave Technology, Journal of*, vol. 30, no. 4, pp. 609 –617, Feb 2012. 78

[69] D. J. Geisler, N. K. Fontaine, R. P. Scott, T. He, L. Paraschis, O. Gerstel, J. P. Heritage, and S. J. B. Yoo, "Bandwidth scalable, coherent transmitter based on the parallel synthesis of multiple spectral slices using optical arbitrary waveform generation," *Optics Express*, vol. 19, no. 9, pp. 8242–8253, Apr 2011. 79

[70] H. Mardoyan, R. Rios-Müller, M. A. Mestre, P. Jennevé, L. Schmalen, A. Ghazisaeidi, P. Tran, S. Bigo, and J. Renaudier, "Transmission of Single-Carrier Nyquist-Shaped 1-Tb/s Line-Rate Signal over 3,000 km," in *Proceedings of Optical Fiber Communications Conference and Exhibition (OFC)*. Optical Society of America, Mar 2015, p. W3G.2. 79

[71] N. Alic, E. Myslivets, E. Temprana, B.-P. Kuo, and S. Radic, "Nonlinearity Cancellation in Fiber Optic Links Based on Frequency Referenced Carriers," *Lightwave Technology, Journal of*, vol. 32, no. 15, pp. 2690–2698, Aug 2014. 79, 94, 115

[72] E. Temprana, E. Myslivets, B.-P. Kuo, L. Liu, V. Ataie, N. Alic, and S. Radic, "Overcoming Kerr-induced capacity limit in optical fiber transmission," *Science*, vol. 348, no. 6242, pp. 1445–1448, Jun 2015. 79, 115

[73] N. K. Fontaine, R. P. Scott, L. Zhou, F. M. Soares, J. P. Heritage, and S. J. B. Yoo, "Real-time full-field arbitrary optical waveform measurement," *Nature Photonics*, vol. 4, no. 4, pp. 248–254, Apr 2010. 79, 115

[74] N. Fontaine, "Spectrally-sliced coherent receivers for THz bandwidth optical communications," in *Electrical Electronics Engineers in Israel (IEEEI), 2012 IEEE 27th Convention of*, 2012, pp. 1–4. 79, 86, 115

[75] Z. Jiang, D. Leaird, C.-B. Huang, H. Miao, M. Kourogi, K. Imai, and A. Weiner, "Spectral line-by-line pulse shaping on an optical frequency comb generator," *Quantum Electronics, IEEE Journal of*, vol. 43, no. 12, pp. 1163 –1174, Dec 2007. 79

[76] A. J. Seeds, M. J. Fice, K. Balakier, M. Natrella, O. Mitrofanov, M. Lamponi, M. Chtioui, F. van Dijk, M. Pepper, G. Aeppli, A. G. Davies, P. Dean, E. Linfield, and C. C. Renaud, "Coherent terahertz photonics," *Optics Express*, vol. 21, no. 19, pp. 22 988–23 000, Sep 2013. 79

[77] S. Bennett, B. Cai, E. Burr, O. Gough, and A. Seeds, "1.8-thz bandwidth, zero-frequency error, tunable optical comb generator for dwdm applications," *Photonics Technology Letters, IEEE*, vol. 11, no. 5, pp. 551 –553, May 1999. 79

[78] P. Shen, N. Gomes, P. Davies, P. Huggard, and B. Ellison, "Analysis and demonstration of a fast tunable fiber-ring-based optical frequency comb generator," *Lightwave Technology, Journal of*, vol. 25, no. 11, pp. 3257 –3264, Nov 2007. 81

[79] P. M. Anandarajah, R. Maher, Y. Xu, S. Latkowski, J. O'Carroll, S. G. Murdoch, R. Phelan, J. O'Gorman, and L. Barry, "Generation of Coherent Multicarrier

Signals by Gain Switching of Discrete Mode Lasers," *Photonics Journal, IEEE*, vol. 3, no. 1, pp. 112–122, 2011. 81, 82

[80] T. Sakamoto, T. Kawanishi, and M. Izutsu, "Asymptotic formalism for ultraflat optical frequency comb generation using a Mach-Zehnder modulator," *Optics Letters*, vol. 32, no. 11, pp. 1515–1517, Jun 2007. 82, 83

[81] T. Healy, F. C. G. Gunning, A. D. Ellis, and J. D. Bull, "Multi-wavelength source using low drive-voltage amplitude modulators for optical communications," *Optics Express*, vol. 15, no. 6, pp. 2981–2986, Mar 2007. 83

[82] Y. Dou, H. Zhang, and M. Yao, "Generation of flat optical-frequency comb using cascaded intensity and phase modulators," *Photonics Technology Letters, IEEE*, vol. 24, no. 9, pp. 727 –729, May 2012. 83

[83] R. Wu, V. R. Supradeepa, C. M. Long, D. E. Leaird, and A. M. Weiner, "Generation of very flat optical frequency combs from continuous-wave lasers using cascaded intensity and phase modulators driven by tailored radio frequency waveforms," *Optics Letters*, vol. 35, no. 19, pp. 3234–3236, Oct 2010. 83, 85

[84] I. Fatadin, D. Ives, and S. Savory, "Blind Equalization and Carrier Phase Recovery in a 16-QAM Optical Coherent System," *Lightwave Technology, Journal of*, vol. 27, no. 15, pp. 3042 –3049, Aug 2009. 88, 105

[85] A. Ellis and F. Gunning, "Spectral density enhancement using coherent WDM," *Photonics Technology Letters, IEEE*, vol. 17, no. 2, pp. 504 –506, Feb 2005. 89

[86] T. Ohara, H. Takara, T. Yamamoto, H. Masuda, T. Morioka, M. Abe, and H. Takahashi, "Over-1000-channel ultradense WDM transmission with supercontinuum multicarrier source," *Lightwave Technology, Journal of*, vol. 24, no. 6, pp. 2311–2317, Jun 2006. 89

[87] G. Bosco, A. Carena, V. Curri, R. Gaudino, P. Poggiolini, and S. Benedetto, "Suppression of spurious tones induced by the split-step method in fiber systems simulation," *Photonics Technology Letters, IEEE*, vol. 12, no. 5, pp. 489–491, May 2000. 90

[88] O. V. Sinkin, R. Holzlöhner, J. Zweck, and C. R. Menyuk, "Optimization of the Split-Step Fourier Method in Modeling Optical-Fiber Communications Systems," *Lightwave Technology, Journal of*, vol. 21, no. 1, p. 61, Jan 2003. 91

[89] A. Ishizawa, T. Nishikawa, A. Mizutori, H. Takara, A. Takada, T. Sogawa, and M. Koga, "Phase-noise characteristics of a 25-GHz-spaced optical frequency comb based on a phase- and intensity-modulated laser," *Optics Express*, vol. 21, no. 24, pp. 29 186–29 194, Dec 2013. 95

[90] X. Zhou, X. Zheng, H. Wen, H. Zhang, and B. Zhou, "Generation of broadband optical frequency comb with rectangular envelope using cascaded intensity and dual-parallel modulators," *Optics Communications*, no. 0, 2013. 95

[91] T. Yang, J. Dong, S. Liao, D. Huang, and X. Zhang, "Comparison analysis of optical frequency comb generation with nonlinear effects in highly nonlinear fibers," *Optics Express*, vol. 21, no. 7, pp. 8508–8520, Apr 2013. 95, 111

[92] V. Ataie, E. Myslivets, B.-P. Kuo, N. Alic, and S. Radic, "Spectrally Equalized Frequency Comb Generation in Multistage Parametric Mixer With Nonlinear Pulse Shaping," *Lightwave Technology, Journal of*, vol. 32, no. 4, pp. 840–846, Feb 2014. 95, 111, 112

[93] C. Liu, J. Pan, T. Detwiler, A. Stark, Y.-T. Hsueh, G.-K. Chang, and S. E. Ralph, "Joint digital signal processing for superchannel coherent optical communication systems," *Optics Express*, vol. 21, no. 7, pp. 8342–8356, Apr 2013. 99

[94] M. Xiang, S. Fu, H. Tang, M. Tang, P. Shum, and D. Liu, "Linewidth-Tolerant Joint Digital Signal Processing for 16QAM Nyquist WDM Superchannel," *Photonics Technology Letters, IEEE*, vol. 27, no. 2, pp. 129–132, Jan 2015. 99

[95] D. S. Millar, R. Maher, D. Lavery, T. Koike-Akino, M. Pajovic, A. Alvarado, M. Paskov, K. Kojima, K. Parsons, B. C. Thomsen, S. J. Savory, and P. Bayvel, "Detection of a 1 Tb/s Superchannel with a Single Coherent Receiver," in *To be presented at European Conference on Optical Communication (ECOC)*, 2015. 102

[96] M. Pajovic, D. S. Millar, T. Koike-Akino, R. Maher, D. Lavery, A. Alvarado, M. Paskov, K. Kojima, K. Parsons, B. C. Thomsen, S. J. Savory, and P. Bayvel, "Experimental Demonstration of Multi-Pilot Aided Carrier Phase Estimation for DP-64QAM and DP-256QAM," in *To be presented at European Conference on Optical Communication (ECOC)*, 2015. 102

[97] A. Kakkar, R. Schatz, X. Pang, J. R. Navarro, H. Louchet, O. Ozolins, G. Jacobsen, and S. Popov, "Impact of local oscillator frequency noise on coherent optical systems with electronic dispersion compensation," *Optics Express*, vol. 23, no. 9, pp. 11 221–11 226, May 2015. 102

[98] Y. Koizumi, K. Toyoda, T. Omiya, M. Yoshida, T. Hirooka, and M. Nakazawa, "512 QAM transmission over 240 km using frequency-domain equalization in a digital coherent receiver," *Optics Express*, vol. 20, no. 21, pp. 23 383–23 389, Oct 2012. 105

[99] Y. Koizumi, K. Toyoda, M. Yoshida, and M. Nakazawa, "1024 QAM (60 Gbit/s) single-carrier coherent optical transmission over 150 km," *Optics Express*, vol. 20, no. 11, pp. 12 508–12 514, May 2012. 105

[100] S. Beppu, K. Kasai, M. Yoshida, and M. Nakazawa, "2048 QAM (66 Gbit/s) single-carrier coherent optical transmission over 150 km with a potential SE of 15.3 bit/s/Hz," *Optics Express*, vol. 23, no. 4, pp. 4960–4969, Feb 2015. 105

[101] S. Savory, "Digital coherent optical receivers: Algorithms and subsystems," *Selected Topics in Quantum Electronics, IEEE Journal of*, vol. 16, no. 5, pp. 1164 –1179, Sep 2010. 105

[102] D. Lavery, M. Paskov, R. Maher, S. J. Savory, and P. Bayvel, "Modified Radius Directed Equaliser for High Order QAM," in *To be presented at European Conference on Optical Communication (ECOC)*, 2015. 110

[103] K. O. Hill, D. C. Johnson, B. S. Kawasaki, and R. I. MacDonald, "CW three-wave mixing in single-mode optical fibers," *Journal of Applied Physics*, vol. 49, no. 10, pp. 5098–5106, 1978. 112

[104] D. Millar, T. Koike-Akino, R. Maher, D. Lavery, M. Paskov, K. Kojima, K. Parsons, B. Thomsen, S. J. Savory, and P. Bayvel, "Experimental Demonstration of 24-Dimensional Extended Golay Coded Modulation with LDPC," in *Proceedings of Optical Fiber Communications Conference and Exhibition (OFC)*. Optical Society of America, 2014, p. M3A.5. 114

[105] S. Ishimura and K. Kikuchi, "Multi-dimensional permutation-modulation format for coherent optical communications," *Optics Express*, vol. 23, no. 12, pp. 15 587–15 597, Jun 2015. 114

[106] H. Zhang, H. Batshon, C. Davidson, D. Foursa, and A. Pilipetskii, "Multi-dimensional coded modulation in long-haul fiber optic transmission," *Lightwave Technology, Journal of*, no. 99, pp. 1–1, 2015. 114